

EXPERIMENTAL ASSESSMENT OF THE EFFECT OF SODIUM CHLORIDE  
DEICING AND ANTI-ICING SOLUTIONS ON EXPOSED, COATED, AND  
REINFORCING STEEL IN HIGHWAY BRIDGES

by

Thanh-Tu Diep

A thesis submitted to the faculty of  
The University of North Carolina at Charlotte  
in partial fulfillment of the requirements  
for the degree of Master of Science in  
Civil Engineering

Charlotte

2014

Approved by:

---

Dr. Matthew J. Whelan

---

Dr. Brett Q. Tempest

---

Dr. Tara L. Cavalline

©2014  
Thanh-Tu Diep  
ALL RIGHTS RESERVED

## ABSTRACT

THANH-TU DIEP. Experimental assessment of the effect of sodium chloride deicing solutions on exposed, coated, and reinforcing steel in highway bridges. (Under direction of DR. MATTHEW J. WHELAN and DR. BRETT Q. TEMPEST).

In North Carolina, winter roadway maintenance strategies vary across the state, with some areas using brine for anti-icing pre-treatment, some using granular salts for deicing, and some using a mix of granular salts with traction enhancing materials, such as sand. An adverse effect of all of these treatment methods is the initiation and progression of corrosion-based deterioration in both reinforced concrete and steel components of these structures. In this study, chloride initiated corrosion rates associated with each treatment approach are quantitatively evaluated for different steel and reinforced concrete bridge components. Corrosion rates on uncoated steel specimens and undercutting of conventional coating strategies under cyclic exposure to solutions of various sodium chloride concentrations are assessed using a modified laboratory procedure. Transport of chlorides to steel superstructure elements below the bridge deck and spatial susceptibility to corrosive loss associated with the different anti-icing and deicing treatments are evaluated through a field study using installation of a large number of sacrificial steel coupons on nine representative bridges in the Ashville and Greensboro regions. Lastly, differences in chloride ingress rates between the winter maintenance strategies within reinforced concrete specimens are investigated through accelerated simulation of North Carolina weather and deicing applications within an environmental chamber. The results of laboratory testing of steel specimens demonstrate quantitative differences between the performance of different steel alloys under cyclic exposure as well as coating methods to blistering and undercutting. Field sampling of corrosive losses on bridges after one

winter season suggest that deicing treatments result in more accelerated corrosion of superstructure elements below the bridge deck than anti-icing treatments and provide plausible indications of additional factors that may affect corrosion rates that are supported by statistical regression of the field data. Lastly, controlled laboratory testing with reinforced concrete specimens strongly suggests that anti-icing brine treatments result in higher ingress of chlorides than deicing treatments per application rate, which is attributed to differences in absorption rates driven by the high chloride concentration used in brines.

## ACKNOWLEDGMENTS

I would like to thank Dr. Brett Q. Tempest and Dr. Matthew J. Whelan for their guidance and support throughout the project. A special thanks to Dr. Tara Cavalline for being a committee member. This project was conducted through the Civil and Environmental Engineering Department at University of North Carolina at Charlotte. I want show my appreciation to Mike Moss and the staffs at the laboratory for their assistance and the student research assistants for their help during the course of this project.

## TABLE OF CONTENTS

LIST OF TABLES	ix
LIST OF FIGURES	x
CHAPTER 1: INTRODUCTION	1
1.1 Introduction	1
1.2 Anticipated Contribution of the Research Effort	3
1.3 Organization of Thesis	4
CHAPTER 2: LITERATURE REVIEW	6
2.1 Corrosion of Structural Steel in Highway Bridges	9
2.2 Transport Mechanism of Chloride in Concrete	13
2.3 Protective Strategies used in Highway Bridges	15
2.4 Test Methods for Evaluation of Corrosive Effects of Deicing Chemical	21
CHAPTER 3: LABORATORY ASSESSMENT OF CORROSIVE EFFECTS ON BARE AND COATED METAL SPECIMENS	27
3.1 SHRP H-205.7 Test Method	28
3.1.1 Summary of Test Method	28
3.1.2 Details of Testing Materials and Equipment	29
3.1.3 Details of Test Procedure	31
3.1.4 Results from SHRP H-205.7 Test	36
3.1.5 Conclusion for SHRP H-205.7 Test	43
3.2 Modified SHRP H-205.7 Test Method: Cyclic Corrosion Test	44
3.2.1 Test Procedures	44
3.3 Results for Modified SHRP Test Method: Cyclic Corrosion Test	48
3.4 Modified SHRP: Scribe Test for Evaluation of Painted or Coated Specimens	59

3.4.1 Test Procedure	59
3.4.2 Results	64
CHAPTER 4: FIELD SAMPLING OF CORROSIVE LOSS ON BRIDGE GIRDERS	73
4.1 Details of Experimental Test Program	73
4.2 Corrosive Losses Measured by Location	77
4.3 Statistical Analysis of Probable Significant Factors	84
4.4 Conclusion	97
CHAPTER 5: LABORATORY EVALUATION OF THE EFFECT OF DEICING AND ANTI-ICING TREATMENTS ON CORROSION OF REINFORCED CONCRETE COMPONENTS	99
5.1 Method for Assessing Chloride Ingress and Corrosion in Reinforced Concrete Specimens	100
5.2 Preparation of Test Specimens	101
5.3 Experimental Test Program	106
5.4 Results	115
5.5 Conclusion	120
CHAPTER 6: SUMMARY	122
6.1 Concluding Remarks	122
6.2 Future Work	123
REFERENCES	125
APPENDIX 3.1: MASS DATA FROM CYCLIC TEST	129
APPENDIX 4.1: MINITAB OUTPUT FOR FIRST RUN	133
APPENDIX 4.2: MINITAB OUTPUT FOR SECOND RUN	135
APPENDIX 5.1: CONCRETE MIX-DESIGN	137

APPENDIX 5.2: CALCULATIONS OF APPLICATION RATE FOR REINFORCED CONCRETE TEST	139
APPENDIX 5.3: RCT RESULTS FOR CONCRETE SPECIMENS	140



## LIST OF TABLES

TABLE 3.1: Mass loss of test specimen due to cleaning only	34
TABLE 3.2: Results for A36 steel at 0%, 3%, 23% NaCl using SHRP	37
TABLE 3.3: Results for A572 steel at 0% and 23% NaCl using SHRP	39
TABLE 3.4: Results for A588 steel at 0% and 23% NaCl using SHRP	41
TABLE 3.5: Results for A36 steel at 23% NaCl	42
TABLE 3.6: Mass losses from cleaning of un-corroded specimens	47
TABLE 3.7: Corrosive mass loss after acid cleaning and sand-blasting	56
TABLE 3.8: Mean corrosion rate (mpy) and standard deviation	56
TABLE 3.9: Rating table used based on ASTM D1654	63
TABLE 3.10: Size and frequency rating for blistering of epoxied and painted specimens	66
TABLE 3.11: Result of scribe test for painted and epoxied specimens	72
TABLE 4.1: Deicing application data for all bridges	76
TABLE 4.2: Mass losses for field samples after adjusting for cleaning controls	81
TABLE 4.3: Average mass loss and loss as a percentage of original mass for all treatment types	81
TABLE 4.4: Predictor variables used in stepwise regression analysis	93
TABLE 5.1: Resistance values of thermistors	104
TABLE 5.2: Concrete mixture proportions used for cyclic test specimens	104
TABLE 5.3: Details of typical winter conditions for Asheville, NC (1991-2001)	108
TABLE 5.4: RCT results at 0.2" depth increments	116
TABLE 5.5: Calculated mass of salt for each treatment type and control	117
TABLE 5.6: Calculated salt concentration for each treatment type and control	118

## LIST OF FIGURES

FIGURE 2.1: Granular salt application with auger type spinner	7
FIGURE 2.2: Brine application by spraying	8
FIGURE 2.3: Surface corrosion of iron	10
FIGURE 2.4: Graph of corrosive for carbon and weathering steel in various environments (reproduced from (Kogler 2012))	16
FIGURE 2.5: Specimen setup for ASTM G109 test method	24
FIGURE 3.1: Test coupon layouts for each steel grade	29
FIGURE 3.2: SHRP test equipment: cleaner, air pump, flow meter, electrode, and meters	31
FIGURE 3.3: SHRP H-205.7 test setup with specimens submerged in solution	32
FIGURE 3.4: Corroded specimens after 8 weeks of exposure before and after cleaning	35
FIGURE 3.5: Results for A36 Steel using SHRP test method	38
FIGURE 3.6: Results for A572 Steel using SHRP test method	40
FIGURE 3.7: Results for A588 Steel using SHRP test method	40
FIGURE 3.8: Schematic of dunking apparatus	46
FIGURE 3.9: Fixtures used for dunking motion in cyclic corrosion test	47
FIGURE 3.10: Test specimens with 4 weeks exposure before cleaning	49
FIGURE 3.11: Percent loss of galvanized layer in NaCl solutions	50
FIGURE 3.12: Test specimens after acid cleaning	51
FIGURE 3.13: Test specimens with 8 weeks exposure after sand-blasting	51
FIGURE 3.14: Mass loss result for specimens after acid clean and sandblasting (sb), at 0% NaCl	52
FIGURE 3.15: Mass loss result for specimens after acid clean and sandblasting (sb), at 3% NaCl	53

FIGURE 3.16: Mass loss result for specimens after acid clean and sandblasting (sb), at 5% NaCl	54
FIGURE 3.17: Mass loss result for specimens after acid clean and sandblasting (sb), at 23% NaCl	55
FIGURE 3.18: Comparison of corrosive losses measured as a function of solution concentration	58
FIGURE 3.19: Scribed painted, epoxied, and galvanized specimens, from left to right	60
FIGURE 3.20: Scribe test set-up for cyclic wetting and drying corrosive exposure	61
FIGURE 3.21: Corroded area determination using microscope captured image	62
FIGURE 3.22: Weekly images of coated specimens in deionized water	64
FIGURE 3.23: Weekly images of coated specimens under 3% NaCl	65
FIGURE 3.24: Microscope images of galvanized specimens	68
FIGURE 3.25: Microscope images of painted A572 specimens	69
FIGURE 3.26: Microscope images of epoxied A572 specimens	70
FIGURE 3.27: Microscope images of epoxied A588 specimens	71
FIGURE 4.1: Steel specimens prepared prior to installation on bridge girders	74
FIGURE 4.2: Testing sites for atmospheric exposure of metal coupons	75
FIGURE 4.3: Coupons placement and location for atmospheric exposure	75
FIGURE 4.4: Corroded steel specimens for Greensboro bridges prior to cleaning	78
FIGURE 4.5: Corroded steel specimens for Asheville bridges prior to cleaning	79
FIGURE 4.6: Average percent losses for girder locations and treatment types	82
FIGURE 4.7: Main effects plots for explanatory factors on mean corrosive loss in grams	87
FIGURE 4.8: Interaction effects of explanatory factors on mean corrosive loss in grams	88
FIGURE 4.9: Plots for checking model assumptions	96

FIGURE 5.1: Schematic of testing setup for reinforced concrete block	101
FIGURE 5.2: Preparation of reinforced bars and wood molding	102
FIGURE 5.3: Schematic of thermistors placement for temperature measurements	103
FIGURE 5.4: Pouring of concrete specimens	105
FIGURE 5.5: Finished specimens with attached wires and resistors	106
FIGURE 5.6: Amount of snow precipitation per event for 1991-2011 in Asheville, NC	108
FIGURE 5.7: Environmental chamber setup for one cycle	110
FIGURE 5.8: Data logger used to record voltage readings	111
FIGURE 5.9: Schematic of thermistor circuit	112
FIGURE 5.10: Overview of temperature readings of one cycle	113
FIGURE 5.11: Temperature readings at brine, snow, and deicing application	113
FIGURE 5.12: Chloride concentrations at drilled depth for each treatment type	116
FIGURE 5.13: Plot of surface solution concentration and RCT chloride percent	119
FIGURE 5.14: Plot of Cl% per application at 0.2" depth vs application rate	120

## CHAPTER 1: INTRODUCTION

### 1.1 Introduction

During winter seasons, chemicals are applied in both solid and liquid form for anti-icing and deicing of roadways and bridges. In North Carolina, the primary chemical agent is sodium chloride-based salts which are applied to reduce the freezing point. Depending on the regional location, the maintenance strategy includes a proactive approach that pre-treat the deck surface with brine and/or a reactive approach that applies salt in granular form on top of ice and snow to aid in melting. During severe winter precipitation, the North Carolina Department of Transportation uses more than 210,000 tons of salt a year and allocates more than \$65 million for snow and ice removal operations (North Carolina Department of Transportation 2013). While the use of anti-icing and deicing treatments is essential for maintaining winter roadway safety, the introduction of sodium chloride can initiate and accelerate corrosion damage to bridge components, namely exposed structural and non-structural steel and steel reinforcing bars. Unlike exposed steel, embedded steel including prestressed strand use in prestressed concrete are a major concern since they are can be harder to inspect and maintain.

Structural steel will naturally corrode if left unprotected from the natural environment. Over time, corrosion can lead to deterioration of concrete and steel surfaces including cross-section reducing the strength, serviceability, and aesthetics of the structure. Approximately 15% of United States bridges are structurally deficient due to

corroded steel components and steel reinforcement (Koch, et al. 2002). Exposed steel surfaces have the potential to be directly affected by corrosive chemicals and environmental factors such as moisture, thermal cycling, and UV radiation. Deterioration of reinforced concrete generally begins with the ingress of chloride from deicing salt leading to corrosion of embedded steel reinforcement and ultimately cracking or spalling of the concrete cover around the reinforcement. This cracking only accelerates the deterioration process by allowing further penetration of corrosive chemicals to the steel and weakening the bond between reinforcement and concrete. Also, the cross-sectional area of the steel rebar decreases with corrosion, resulting in reduction of both strength and ductility (Imperatore and Rinaldi 2009). A study conducted for the U.S. National Cooperative Highway Research Program (NCHRP) indicates that state agencies were most concerned with the corrosion of concrete reinforcement followed by vehicles, concrete damage, structural steel, and roadside structures resulting from the use of ice control materials (Levelton Consultants Ltd 2007). According to NCDOT (2013), an estimated cost of \$11 billion is required to improve all current substandard bridges in the state. Included in this cost estimate are bridge preservation actions such as resurfacing of bridge decks, painting of structural steel, cleaning/painting of bearings, and repairing/replacing expansion joints, which all deteriorate due to corrosion from winter roadway maintenance practices.

Current maintenance strategies include applying protective coatings, using corrosion resistant metals, or installing anodic/cathodic protection. The cost for corrosion control options vary depending on the method and severity of the exposed environment. Common protective practices in highway bridges employ paint coating for

corrosion protection. In 2012 a full abrasive blast with 3-coat paint system costs about \$6.60 per square foot, while water blasting plus spot prime with two overcoats cost about \$3.70 per square foot (Kogler 2012). According to FHWA Steel Bridge Design Handbook: Corrosion Protection of Steel Bridges (2012), the estimated service life for a typical 3-coat paint system is 15 to 20 years under marine environment and about 25 years for less aggressive salt containing environments. Another option is to use weathering steel, which has the potential to eliminate the cost of initial painting and repainting. However, a limitation of weathering steel is in the ability to form a proper protective corrosion film. Weathering steel is observed to continue to corrode over their lifetime under leaking bridge joints (American Iron and Steel Institute 1995), which is a common problem across the national inventory of highway bridges.

## 1.2 Anticipated Contribution of the Research Effort

In North Carolina (NC), anti-icing and deicing treatments of brine, granular salt, and granular salt-sand mix on bridge are expected to have different exposure levels of chloride concentrations across bridge surfaces due to the nature of the different transport mechanisms and dilution characteristics associated with each treatment over time. These surfaces include the bridge decks, components above the deck such as parapet walls and guardrails, and the superstructure below deck including stringers, floor beams, diaphragms, and bearing surfaces. Anti-icing and deicing salts applied to the deck surface eventually penetrate through concrete cover to steel reinforcement and migrate below deck in solid or dissolved solution form through transport driven by vehicle traffic and environmental factors, such as precipitation, gravity directed flow, and wind. The potential for corrosion will depend on the salt concentration level of the exposed surface,

which can vary from direct brine application or saturated liquid concentration to significantly diluted concentrations following dispersion and precipitation.

This thesis specifically examines:

- The corrosive effect of cyclic exposure of bare steels used in NC bridges to various concentrations of sodium chloride solutions.
- The effectiveness of protective coatings against undercutting and blistering when subject to cyclic exposure to sodium chloride solutions. Coatings evaluated include painting, epoxy coating, and galvanization.
- Field measurement of corrosion rates of steel superstructure components on typical North Carolina bridges over the course of one winter weather season to examine the exposure differences between anti-icing and deicing treatments. Evaluation of the statistically significant factors affecting the transport of chlorides to steel components below the deck and corrosive losses on bridge girders.
- Evaluation of the relative rates of ingress of chlorides in reinforced concrete exposed to either anti-icing or deicing treatments under accelerated simulation of representative North Carolina winter weather conditions.

### 1.3 Organization of Thesis

- Chapter 1 provides an introduction to the problem statement and anticipated contribution of the research effort.
- Chapter 2 presents a literature review on the process of structural steel corrosion and the relative contributions of anti-icing and deicing applications to corrosion of highway bridges. The chapter also provides a



summary of protective strategies currently used in highway bridges. Some general test methods for evaluating corrosive effects of deicing chemicals on bridge components are also highlighted in the chapter.

- Chapter 3 presents the laboratory assessment of corrosion rate for bare and coated metal specimens subject to cyclic exposure to deicing chemical solutions. Results for bare steel coupons are based on mass loss, while coating methods are performance rated according to blistering and creepage around a scribe line on the coated surface.
- Chapter 4 presents a field test program to determine the impact of deicing and anti-icing application strategies on the transport of chlorides and associated corrosive losses on bridge girders. Included in the chapter are the methodology and experimental results obtained from field installation of sacrificial coupons and statistical regression analysis to identify significant factors affecting corrosion rates on different highway bridge components.
- Chapter 5 provides the methodology and results from a test program designed to evaluate the effect of deicing and anti-icing applications on reinforced concrete freeze-thaw cycles, wetting and drying, and simulated snow and deicing applications.
- Chapter 6 presents conclusions of the experiment results and provides recommendation for future research.

## CHAPTER 2: LITERATURE REVIEW

The use of anti-icing and deicing treatments for snow and ice removal is a major source of chlorides to concrete decks and exposed steel bridge components. Chlorides can be directly deposited on steel components during the treatment application or may ingress through the pores in concrete to steadily build up reaching embedded reinforcement. Conventional winter roadway treatments include the application of granular sodium chloride to aid in melting of accumulated ice and snow or surface pretreatment with brine to prevent accumulation. Granular salt is used for snow and ice control and is typically applied to roads and bridges using an auger type spinner (FIGURE 2.1). To aid in traction control, granular salts can be mixed with traction enhancing materials, such as sand. Although applied directly to the deck, granular salts can also spread to surfaces below the deck, especially when joint conditions are compromised. Deicing salt can also be transported to bridge components by vehicle traffic under the bridge. Heavy truck traffic can develop a plume of chloride laden mist to heights that can reach the surface of steel girders above traffic. According to American Iron & Steel Institute Corrosion Advisory Group case studies, the corrosion rate on the bottom flange of steel girders above truck traffic is four times higher than the ambient corrosion rate (Kogler 2012).



FIGURE 2.1: Granular salt application with auger type spinner

Brine is produced as the mixture of liquid and a freezing point depressant chemical such as sodium chloride, magnesium chloride, potassium chloride, or calcium chloride. The saturated concentration for sodium chloride-based brine is 23.3%, which achieves the lowest freezing temperature (Nixon, et al. 2007). Brine is typically applied by spraying a series of streams onto the deck surface (FIGURE 2.2). In bridge applications, brine may also be inadvertently applied to steel guard rails by the stream from nozzles directed to pretreat the curb or sidewalk of the bridge. Unlike granular salt applications, brine adheres to the surface when applied and is known to maintain a significant residual concentration until precipitation occurs.

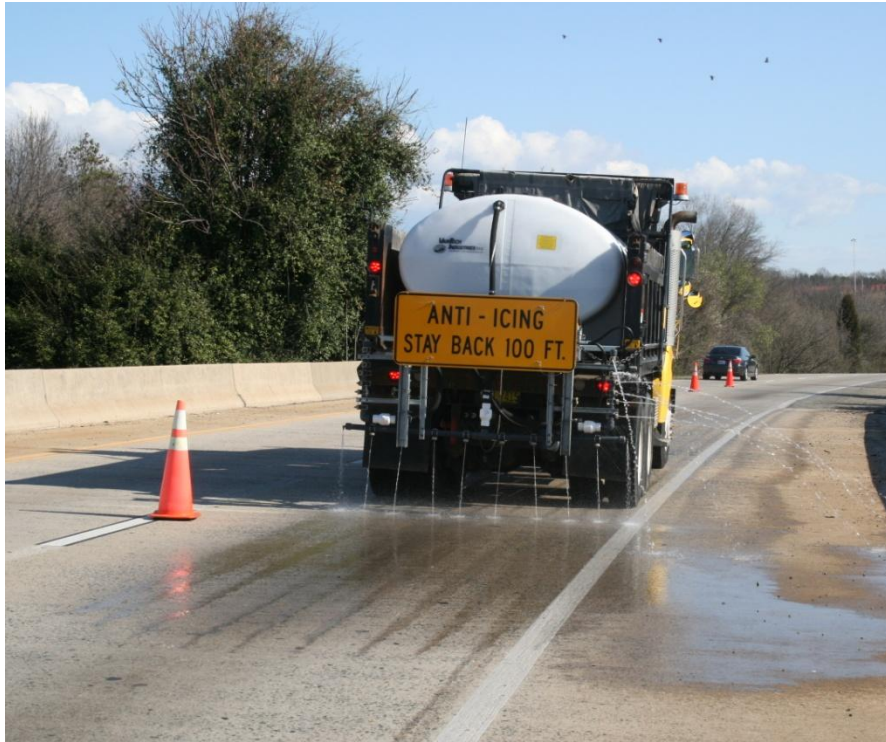


FIGURE 2.2: Brine application by spraying

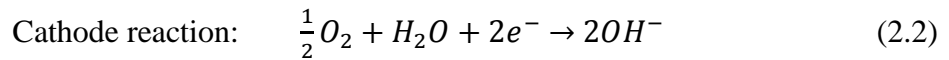
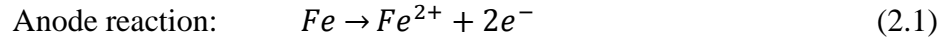
A study on the measurement of surface concentrations associated with anti-icing and deicing treatments on highway bridge was performed by Prah-Ennin (2013) using an X-ray fluorescence (XRF) handheld analyzer. The control field test measured the temporal and spatial distribution of chloride concentration for both above deck and below deck components for sodium chloride brine, granular, and granular sand-mix applications. Application rate used were typical for North Carolina winter maintenance strategy. Results from the study indicated that above deck surface concentrations prior to traffic and precipitation were highest for brine follow by granular then salt-sand mix. Even though the brine application exhibited the highest concentrations, the study mentioned that granular application were found to exhibit a more uniform concentration across the travel lane. Two main transport mechanism considered in the study were

vehicular traffic and precipitation in the form of rain. Effects of traffic induced transport were noted to be more significant for granular applications than for brine application (Prah-Ennin 2013). Specifically, accumulations of granular salt were observed at the expansion joint, which may present a more significant threat to steel components below the deck if joint conditions are compromised. In contrast, chloride concentrations associated with the brine treatment were found to remain high on the traffic lane, although noticeable reductions occurred in the wheel path. Measurements from the study obtained after a rain event show a drastic reduction in surface concentrations for all treatments, indicating that precipitation effectively reduces the surface concentrations of sodium chloride to nominal levels for all treatment strategies. Following the precipitation event, measurements taken on steel components below the deck indicated significant increases in sodium chloride concentrations on the girder and pier cap for granular salt application, while only a nominal increase was observed for the brine application. Aside from this limited field study, transport of chlorides from brine pretreatment to components below the bridge deck has not been extensively studied to date. Furthermore, the difference in corrosion rates associated with anti-icing and deicing treatments remains an unaddressed research area that is examined in this thesis.

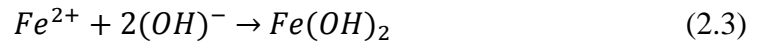
## 2.1 Corrosion of Structural Steel in Highway Bridges

Corrosion can be defined as the deterioration of material due to exposure from the natural environment, which is significantly accelerated by certain chemicals. The process consists of oxidation and reduction reactions at the surface of the material (Mindess, Young and Darwin 2002). The oxidation reaction generates metal ions and electrons, while the electrons are then consumed in the reduction process. In the case of the

corrosion of iron in structural steel, the two controlling agents are water and oxygen. Iron is oxidized producing electrons and ferrous ion at the anode (EQUATION 2.1). The electrons are then consumed by converting water and oxygen to hydroxide ions at the cathode (EQUATION 2.2).



Through movement of electrons and hydroxide ions migrating from the cathode to the anode, the produced hydroxide are then combined with iron ions to form ferrous hydroxide ( $Fe(OH)_2$ ) (EQUATION 2.3).



After subsequent reactions with oxygen and water, the ferrous hydroxide turns into hydrate ferric oxide, or rust (EQUATION 2.4). A schematic of the corrosion process for iron is shown in FIGURE 2.3.

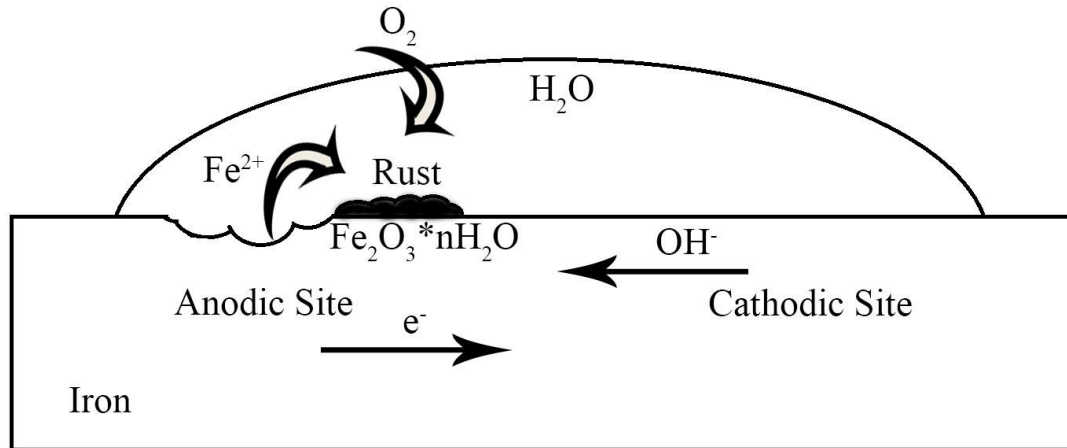
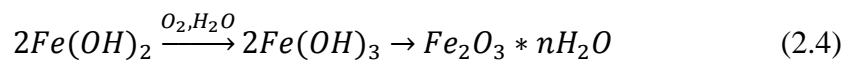
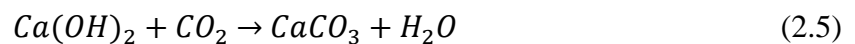


FIGURE 2.3: Surface corrosion of iron



The process occurs more rapidly with higher ionic conductivity (Guthrie, Battaat and Grethlein 2002), which is why the presence of electrolytes, such as salt in water can increase the rate of the corrosion process. Within concrete, ferric rust at the surface of the reinforcing steel can result in cracking due to the large volumetric increase associated with the formation of the corrosion byproduct.

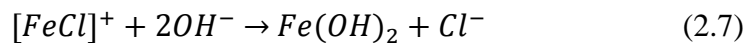
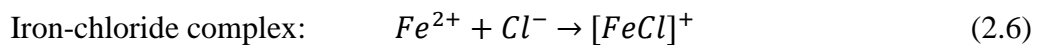
According to Mindes, Young, and Darwin (2002), reinforcing steel in concrete does not initially corrode due to the protection of concrete cover. The alkaline environment from the concrete results in the oxidation of  $\text{Fe}(\text{OH})_2$  to ferric hydroxide. Ferric hydroxide serves as a protective film that can limit the supply of oxygen and moisture to the metal thereby inhibiting corrosion. However, this occurs only at relative high pH, generally greater than 13. Once the pH level drops below 11.5, the oxide film is destroyed and corrosion can initiate. This reduction in pH level occurs naturally as concrete is exposed to atmospheric carbon dioxide ( $\text{CO}_2$ ). The  $\text{CO}_2$  can diffuse into porous concrete and react with alkaline substances in the pore solution. This carbonation process consumes calcium hydroxide according to the reaction:



The pH of pore water in hardened Portland cement paste can be reduced from as high as 13.5 to about 8.3 when all  $\text{Ca}(\text{OH})_2$  is converted to  $\text{CaCO}_3$  (Bioubakhsh 2011). The carbonated zone in normal concrete is within 1 inch and could be higher with increased severity of exposure conditions, such as the presence of cracks due to internal and external stress and carbonate shrinkage.

Even under low pH conditions, the corrosion process can be limited by controlling the availability of oxygen and moisture (Mindess, Young and Darwin 2002). For concrete with low permeability or in a condition when the pores are filled with water, the diffusion of oxygen is greatly reduced, thereby limiting corrosion. As an example (Mindess, Young and Darwin 2002), concrete containing silica fume have superior corrosion performance compared to concrete without silica fume at the same water to cement ratio. The initial reduction in pH associated with the use of silica fume is more than offset by the reduction in permeability.

The presence of chloride ions can add to the corrosion process by destroying the oxide film on steel and producing ferrous chloride corrosion products. Even at high alkalinity, significantly high concentrations of chloride can initiate the corrosion process. Once the chloride content exceeds a threshold level, chloride ions can break the passive layer to form an anode on the steel surface, starting the corrosion process. Factors that can influence the chloride threshold are the type of cement, water to cement ratio, curing and compaction, moisture content, type of steel and surface condition, and oxygen availability (Nuclear Energy Agency 2002). Chloride ions can also react directly with iron ions to produce corrosion byproducts. Chloride ions and iron ions combine to form iron-chloride complex (EQUATION 2.6), which then reacts with hydroxyl to form ferrous hydroxide and also releases the chloride ions that allow the reaction to continue (EQUATION 2.7) (Mindess, Young and Darwin 2002).





## 2.2 Transport Mechanism of Chloride in Concrete

Build-up of chlorides on concrete surfaces allows for ingress of corrosive solution further into the concrete reaching the embedded steel. The mechanism of penetration depends on whether the surface is fully saturated or cycles between wetting and drying. Chloride ions are transported by hydrostatic pressure when the surface is saturated and by absorption when the surface is subjected to wet-dry cycling (Gergely, et al. 2006). The steady-state flow of liquid under hydrostatic pressure is directly proportional to the hydraulic gradient and can be described by Darcy's law (EQUATION 2.8), where the coefficient of permeability is influenced by the pore structure of concrete (Bioubakhsh 2011). Specifically:

$$v = Q/A = K(\Delta h/L) \quad (2.8)$$

Where:

$v$  = velocity of flow

$Q$  = flow rate

$A$  = cross-sectional area of the sample

$K$  = coefficient of permeability

$\Delta h$  = drop in hydraulic head

$L$  = thickness of sample

The equation suggests that water is driven through the concrete when there is a difference in hydraulic head. However, the contribution of permeability is minimal for concrete that is not under constant water pressure (Bioubakhsh 2011). Another mechanism associated with the transport of chlorides through concrete is diffusion. Diffusion occurs when there is a concentration gradient. Models for prediction of chloride ingress are based on Fick's

laws. Fick's first law describes diffusion under unidirectional and constant mass transfer, where the rate of transfer across a section area is proportional to the concentration gradient and the diffusion coefficient. Fick's second law describes diffusion when the concentration changes with time. The diffusion coefficient can be assumed a function of many variables such as maturity, temperature, humidity, water-cement ratio, cement type, aggregate size, curing regime, and chloride concentration (Bioubakhsh 2011). Liquid can also be transported into the concrete through absorption. Absorption occurs in unsaturated porous concrete by capillary suction or sorptivity. The transport mechanism is driven by surface tension and is a function of the liquid viscosity, density, surface tension, and the pore structure of the porous material (Pitroda 2013). The pore structure of concrete depends on a variety of factors including concrete mix-design, curing regime, and compaction. The sorptivity of concrete can be determined from the linear relationship between the square root of time and the depth of liquid penetration from the surface (EQUATION 2.9).

$$A = b + S\sqrt{t} \quad (2.9)$$

Where:

$A$  = depth of liquid penetration

$b$  = initial absorption

$S$  = sorptivity

$t$  = time

### 2.3 Protective Strategies used in Highway Bridges

Based on the known chemical reaction process of corrosion, strategies to protect against corrosion usually minimize the availability of oxygen and moisture required to supply the cathodic reaction. This can be achieved through four general categorical approaches: reduction of the permeability of the concrete, installation of protective membranes on the concrete, application of protective coatings on the steel, and active suppression of the electrochemical process (Mindess, Young and Darwin 2002).

Corrosion protection measures are based on four keys considerations: environment, materials of construction, design detailing, and cost (Kogler 2012). Environmental considerations take into account the potential for corrosive chemicals and excessive moisture to remain in contact with the steel surface for an extended amount of time. Type of environment can range from the rural area, where there may be limited exposure to chemical or deicing salt to the marine environments, where there is constant exposure to airborne salt and moisture. Regions with high average daily traffic (ADT) and significant winter precipitation may experience more severe exposure due to more frequent use of deicing salt. Typical design options will be site-specific, where more corrosive environments will require a high durability protection system. Other options can include detailing in a way to avoid contact between corrosive agents and steel surfaces. However, such measures are generally not cost effective.

According to Albrecht and Hall (2003) research on atmospheric corrosion of structural steel indicates that the use of weathering steel shows benefits over carbon steel within various environments. A compilation of reported test results is shown in FIGURE 2.4. As shown in the figure, corrosion losses for weathering steel stabilize over time to

provide protection against further corrosion in rural and industrial environments. In marine environments, the corrosive loss is significantly lower for weathering steel, but does continue to progress further over time rather than stabilize.

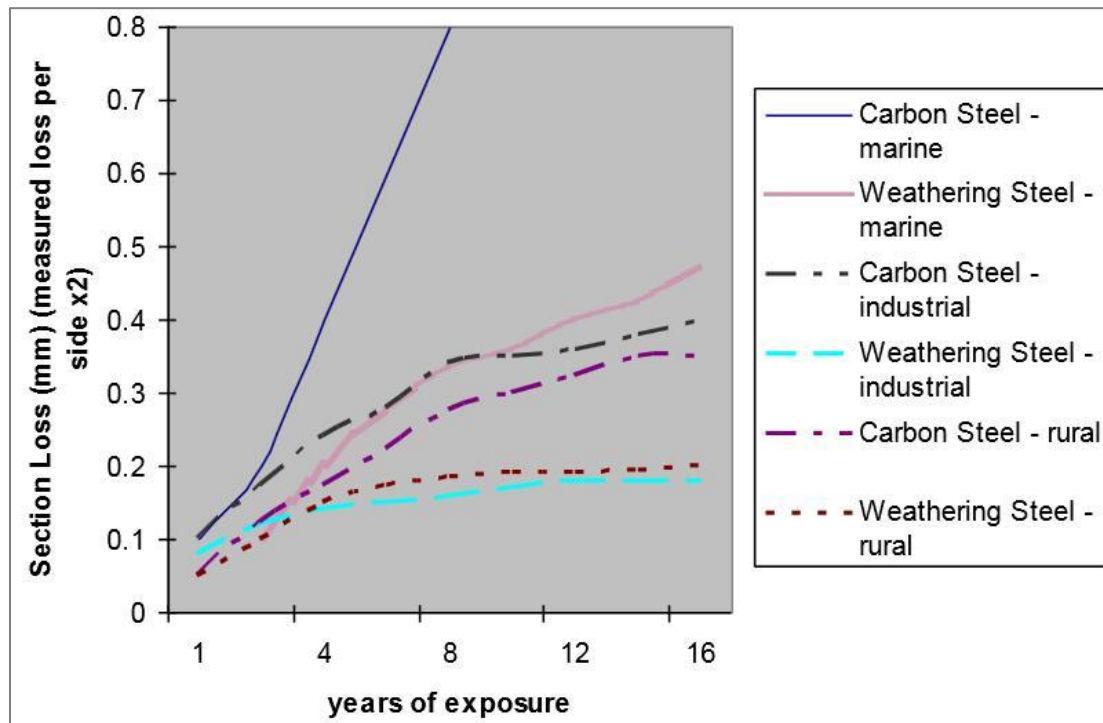


FIGURE 2.4: Graph of corrosive for carbon and weathering steel in various environments (reproduced from (Kogler 2012))

A special characteristic of weathering steel is the ability to form an adhering corrosion product layer that protects the interior steel from further corrosion. Compared to ordinary structural steel, the basic metallurgical difference of weathering steel is the addition of chromium, copper, and nickel alloying elements. However, research indicates that the ability for weathering steel to fully develop an anticorrosive layer depends on the geometry, environmental conditions, and steel composition (Morcillo, et al. 2013). The process requires cycling between wet and dry conditions and requires rain water to flush

the surface of contaminants followed by a fast drying time without ponding. Furthermore, according to Morcillo (2013), bare weathering steel is not recommended in continuous moist exposure or marine atmospheres where the protective layer does not form.

Another protective strategy against steel corrosion is design of systems that can prevent the chlorides from coming into contact with the steel. FHWA Technical Advisory T5140.22 (1989), “Uncoated Weathering Steel in Structures” provides several guidelines for proper application and maintenance of uncoated weathering steel. Design details include: diverting water from vulnerable components, painting superstructure steel girder over a length at least 1.5 times the depth of girder from bridge joints, and eliminating details that may possibly collect or trap chloride-laden water. Maintenance measures also described in the guideline include maintaining roadway drainage through removal of deposits and vegetation.

For coated structural steel, the current practice is to use a multicoat system. Surface preparation includes abrasive-blasting to remove millscale. This process not only removes initial contaminants that promote corrosion, but also enhance coating performance. Similar surface preparation is performed on bare weathering steel. The first coating is usually a zinc-rich primer followed by two additional coating layers over the primer. The zinc-rich primer provides protection to the steel substrate by acting as the sacrificial layer during corrosion. An intermediate epoxy coating provides protection from moisture, oxygen, and electrolytes. The top-most coating adds physical protection against deterioration from ultra-violet radiation and provides long term aesthetic. The three coating system with inorganic or organic zinc-rich primer, epoxy midcoat, and

polyurethane topcoat can have an estimated service life of 30 years (Kline 2008). Two-coat and one-coat systems are also considered in some applications as reducing the number of coats can greatly reduce the initial production cost. Current research has focused on verify the effectiveness of reduced coatings without sacrificing corrosion protection performance. Research through the FHWA by Yao, Kodumuri and Lee (2011) evaluated the possibility of a one-coat system as a performance comparison to the standard two and three coats systems. Performance was evaluated using accelerated laboratory testing and outdoor exposure conditions. Results from the research ranked the traditional three-coat system as having the best overall performance followed by one-coat high-ratio calcium sulfonate alkyd (HRCSA) and high-build waterborne acrylic (HBAC). Conclusions from the research indicated that HRCSA performed well in both accelerated laboratory testing and under outdoor exposure conditions (Yao, Kodumuri and Lee 2011).

An alternative to painted or epoxy coated protection of steel surfaces is metalized coating. The process typically involves melting zinc or aluminum alloy onto the steel surface. Sealer and finish coat can also be added in addition to metalizing for further protection. The process provides excellent corrosion protection even in marine environments (Kogler 2012). Hot-dip galvanization is a popular method of coating an entire steel component with zinc. Bridge guard rails are typically galvanized steel. The process involves dipping a component into molten zinc, which can be repeated for multiple layers. Corrosion protection performance will depend on the thickness of the zinc cover. A limitation of the process is the requirement to fully immerse the component, which restricts the size of the components that can be galvanized.

Preventive measures to protect embedded steel from corrosion in concrete include the use of high-quality impermeable concrete with low water to cement ratio and large concrete cover. Also, the recommended concrete cover for reinforcement is 2 ½ inches (American Concrete Institute 2011). Some of the methods to lower the permeability of concrete include: addition of pozzolans in the mix design, using high density concrete overlays, and using high-strength concrete to prevent cracking. Pozzolans commonly used in concrete mix are coal fly ash (pulverized fuel ash or PFA), ground granulated blast furnace slag, silica fume, and metakaolin (calcined clay). These pozzolans must first be converted into amorphous or glassy form and should be finer than 325 mesh (45 microns) to react readily in the curing process (Vitro Minerals 2006). During the curing process, pozzolans act as supplementary cementation materials and the process can continue over many years. Addition of pozzolans results in a denser, harder, and more durable concretes, with reduced permeability and as well as greater resistance to deterioration. Although these measures can not completely prevent corrosion, the rate of penetration of corrosive agents can be reduced.

Another effective method in the protection of bridge decks is to use protective membranes. The membrane can be placed directly onto the newly constructed or existing bridge deck then overlaid by an asphalt wearing surface to produce a barrier to penetration of moisture and deicing salts. According to the National Cooperative Highway Research Program (NCHRP) Synthesis 425 (2012), 60% of U.S. state agencies use waterproof membranes on bridge decks with greater usage on existing bridge decks than new bridges. The membrane product can be either pre-formed sheet system or liquid system. Both systems involve the application of a primer on the concrete surface

followed by installation of the membrane and then a tack coat for increased bond to the asphalt overlay. A similar membrane system has been used on concrete decks in parking garages (Mailvaganam and Collins 1999). The system consists of first using sealer or primer for adhesion of the membrane, then installing the waterproof membrane, and finally installing a wear coating. The waterproof membrane serves to seal existing cracks and prevent the further ingress of chloride ions and water. The wear coat should contain embedded aggregate to provide abrasion resistance and protect the membrane. A tie coat is added to bond the aggregate to the wear coat. However, using a membrane system has its own limitations. Application of membranes is not possible at joints or curbs where contaminated water can leak underneath. Another common problem is improper bonding with the concrete surface, which allows for chloride-laden water transport underneath the membrane. A limitation of waterproof membrane system on bridge decks is the service life of the wearing surface, as de-bonding can occur for grades greater than 4% (National Cooperative Highway Research Program 2012). According to NCHRP Synthesis 425 (2012), expected service life of waterproof membranes range from 16 to 20 years for installation on new bridge decks and as low as 6 years on existing bridge decks.

A more widely use alternative in protection of bridge deck corrosion is using fusion-bonded epoxy coating on the surface of embedded steel. Adding an epoxy coat allows protection from penetration of water, air, or chemicals that promote corrosion of the rebar. The coating also serves as an electrical insulator to minimize the flow of corrosion current (Smith and Virmani 1996). The outer coating prevents the formation of anodes when the coating is adhered tightly to the steel, also preventing the steel from acting as a cathode. Recent study on the service life of uncoated steel rebar (black rebar)



and epoxy coated rebar (ECR) in bridge deck estimates that the service life for black rebar is 35 years while the service life for ECR is 70 years (Boatman 2010). However, using epoxy coating has an adverse effect when the coating is not tightly bonded to the steel surface. Prolonged exposure of ECR to moist environments can result in debonding and softening of the coating (Smith and Virmani 1996). The result is accelerated corrosion due to crevice corrosion, where high concentrations of chloride ions buildup under the coating (Bioubakhsh 2011). The same phenomenon is true for exposed coated steel. Special considerations such as fabrication, transportation, erection methods, and service environment should be properly addressed in specifications to ensure the integrity of the coating.

Recent developments also take advantage of the electrochemical process of corrosion to prevent corrosion by using conducting polymers. The use of polypyrrole and polyaniline electrodeposited on steel component can act as anodic protection to reduce the rate of corrosion (El-Shazly and Wazzan 2012). The polymerization process used in layering passivizes the iron surface with a layer of iron tartrate to buffer the metal in corrosive environments.

#### 2.4 Test Methods for Evaluation of Corrosive Effects of Deicing Chemical

Several testing methods have previously been developed to evaluate the corrosive effects of coated and uncoated steel surfaces, including both standardized methods and methods developed for individual research projects. Standardized methods included those from the American Society for Testing and Materials (ASTM) and International Standards Organization (ISO). Both organizations provide testing protocols for evaluating atmospheric corrosion and corrosion during immersion in salt solutions.

Standard test methods for evaluation of atmospheric corrosion is outlined in ASTM G50 “Standard Practice for Conducting Atmospheric Corrosion Tests on Metals” (ASTM 2010) and ISO 9226 “Corrosion of Metals and Alloys - Corrosivity of Atmospheres – Determination of Corrosion Rate of Standard Specimens for the Evaluation of Corrosivity” (ISO 2012). These tests are used to evaluate corrosion resistance of metals when exposed to service weather at a particular testing site. Quantitative data are recorded as mass loss that is then converted to a corrosion rate. Accelerated test methods include those that expose test specimens to extreme corrosive environments, such as salt spray and immersion in salt solution. Standards for immersion tests include ISO 11130 “Corrosion of Metals and Alloys – Alternate Immersion Test in Salt Solution” (ISO 2010), and ASTM G31 “Standard Guide for Laboratory Immersion Corrosion Testing of Metals” (ASTM 2004). Test procedures developed by the Strategic Highway Research Program (SHRP) cover evaluation of corrosive effects of deicers or other aqueous solutions through continuous immersion of test specimens in solution (SHRP 1992). The recommended testing period for the SHRP test is up to 8 weeks for data collection. Alternatives to these standards include the addition of cycling the test specimen between wet and dry to better represent field exposure. An example of a cyclic immersion test is the test procedure by the Pacific Northwest Snowfighters (PNS). The test procedure calls for application 30 mL of test solution per square inch of steel coupon surface (Pacific Northwest Snowfighter 2010). The sample coupon is immersed for 10 minutes followed by 50 minutes of air exposure over a testing period of 72 hours for each test. Corrosion rates are calculated based on percent mass loss over the testing period. The Society of Automotive Engineers (SAE) also adapted cyclic corrosion testing in their

standardized test method. Metal test specimens are placed in an enclosed climate controlled chamber and subjected to a humid stage, salt application stage, and dry stage (SAE International 1998). Due to the complex nature of corrosion, detailed procedures are often specific to the application and results are typically used for comparative purposes.

Test procedures used in this study for evaluation of different deicing strategies on reinforced concrete are based on ASTM G109 “Standard Test Method for Determining Effects of Chemical Admixtures on Corrosion of Embedded Steel Reinforcement in Concrete Exposed to Chloride Environments” (ASTM 2007). The testing setup consists of concrete samples with two embedded layers of reinforcing bars, one top rebar and two bottom rebars, that is exposed to cyclic ponding and drying of sodium chloride solution on the top concrete surface (FIGURE 2.5). Typical concrete cover for the top rebar is 0.75 inch. Electrical current flow is monitored between the two layers of reinforcement for signs of corrosion of the top rebar. Researchers using the test method indicate that the time to failure is much longer than the six months noted in the standard (Trejo, Halmen and Reinschmidt 2009). The time required for corrosion of the embedded steel ultimately depends on the rate of chloride ingress through the concrete cover and the amount of chloride required to initiate active corrosion at the reinforcement. Study on the critical chloride content show scattered results that depends on interconnected and time-dependent variables for the quality of steel-concrete interface, the pH of pore solution, and the electrochemical potential of the steel (Angst and Vennesland 2009).

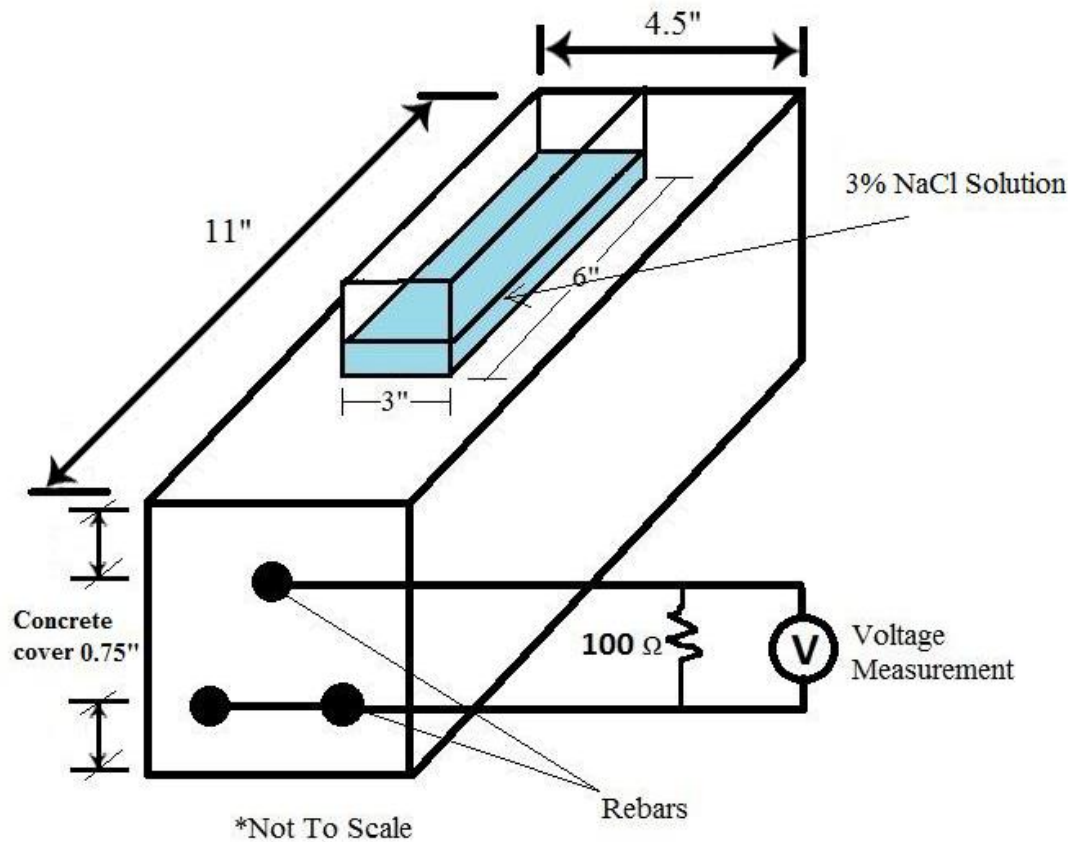


FIGURE 2.5: Specimen setup for ASTM G109 test method

Modifications to the standard test method include adjusting the number of rebars, changing the resistor value between rebar layers, modifying the ponding solution and concentration, or the cycling rate between wet and dry. In the literature, evaluation of the performance of various reinforcing steel and concrete-mix design have been performed using the standard ASTM G109 and a modified ASTM G109 test method. A modified procedure performed by Trejo, Halmen, and Reinschmidt (2009) stored samples at high temperature (100°F) and high humidity environments instead of laboratory room temperature and humidity. The overall results show that 70 out of 216 (32%) standard samples achieved active corrosion and 159 samples out of 335 (47%) modified samples achieved active corrosion after a test period of 49 months. Also, about half of the

activated samples were actively corroding after a testing period of 32 months using standard procedures while only 27 months were needed to achieve corrosion in half of those from modified procedures. The results indicate that high temperature and humidity increase the effective corrosion rate for the modified test method. An active condition indicates that the total corrosion coulombs (C) (calculated from the voltage measurement across the 100  $\Omega$  resistor and test time) had reached 150 C or above. According to ASTM G109, a value of 150 C is consistent with a macrocell current of 10  $\mu$ A over six months, at which point there is sufficient enough corrosion for visual inspection.

Since corrosion of embedded steel largely depends on the rate of chloride ingress in concrete, it is useful to investigate the transport mechanism. Differences in chloride buildup are observed between exposure conditions of wet/dry cycling and continuous immersion. Concrete specimens exposed to the same salt concentration in wet/dry cycles tend to show an increase in surface concentration, while the surface concentration is held constant for immersed specimens. The net effect has been shown to result in similar chloride profile for both exposure conditions after six months of exposure (Bioubakhsh 2011). However, this same study showed that an increase in temperature from the original 20°C to 30°C or 40°C resulted in greater chloride content for specimens exposed to wet/dry cycles after the same test period. This is due to an increase in the initial sorptivity of the concrete surface when the initial moisture content is low and stabilizes as the number of cycle increases causing the moisture content to reach equilibrium (Bioubakhsh 2011). When the moisture content is low, the effective porosity is greater and the higher volume of empty pores encourages the absorption. The study indicates that the depth of free chloride penetration is initially smaller than the depth of salt

solution penetration due to chloride binding. Due to reduction in absorption, the depth of salt solution eventually decreases while chloride penetration continues with each wetting phase through diffusion. The study also indicates that the depth of chloride penetration can be predicted from the equilibrium weight sorptivity, salt solution concentration, concrete mix, time, and number of cycles.

### CHAPTER 3: LABORATORY ASSESSMENT OF CORROSIVE EFFECTS ON BARE AND COATED METAL SPECIMENS

The use of sodium chloride as a deicing strategy for road safety is a major cause for chloride initiated corrosion on exposed structural steel members of highway bridges. The steel components subject to corrosion include above deck guardrail, below deck girders, and reinforcing steel embedded in concrete. Deicing treatments applied to the bridge deck will eventually migrate to different exposed surfaces either as solid or in dissolved liquid form through vehicle traffic and environmental factors, such as wind and gravity. Solution concentrations on steel components can vary from saturated solutions, in the case of direct exposure from the brine application, to a range of lower concentrations developed by dissolution of granular salt into solution that will depend on the amount of dispersion and precipitation. This study is aimed at evaluating the corrosive effects of different levels of salt concentration on coated and bare metal specimens. The study was conducted for typical coating methods and steel alloys used in North Carolina bridges. This chapter presents the methodology and experimental results obtained from three different test methods: The Strategic Highway Research Program (SHRP) test method for evaluation of corrosive effects of deicing chemical on metals (SHRP H-205.7), a modified SHRP cyclic corrosion test, and a scribing test for evaluation of painted or coated specimens subjected to corrosive environments (ASTM D1654 and D7087). Analysis of the results is used to determine the corrosion rate for different metal types at

various sodium chloride concentrations as well as coating performance against undercutting of corrosive solutions around a scribe line for each coating type.

### 3.1 SHRP H-205.7 Test Method

#### 3.1.1 Summary of Test Method

The SHRP test method for evaluating the effect of deicing chemicals on metals involves submerging metal coupons of different composition into prescribed concentrations of deicing solutions for different exposure times to evaluate the corrosion rates (SHRP 1992). The test method is outlined in SHRP-H-205.7 (1992) with reference to ASTM Standards: G31-72 Standard Practice for Laboratory Immersion Corrosion Testing of Metals (ASTM 2004), G1 Standard Practice for Preparing, Cleaning, and Evaluating Corrosion Test Specimens (ASTM 2003), and C876 Standard Test Method for Half-Cell Potentials of Uncoated Reinforcing Steel in Concrete (ASTM 2009). The range of steel types evaluated in the current study was selected by the NCDOT committee overseeing the research project and are the most frequently used alloys in NC bridges. The grades included were ASTM A36: standard specification for carbon structural steel, A572: standard specification for high-strength low-alloy columbium-vanadium structural steel, and A588: standard specification for high-strength low-alloy structural steel with atmospheric corrosion resistance (ASTM International 2014). This testing method is applicable to bare metal coupons only and is used in this study as a preliminary test for corrosive effects on bare metal specimens at 3% and 23% concentrations relative to control samples in deionized water. The study was conducted over an eight week period. The test was intended to be used to evaluate the corrosion rate for each metal type at the two extreme concentrations. However, limitations in application of the methodology to



the proposed research tasks ultimately required modification of the standard SHRP method.

### 3.1.2 Details of Testing Materials and Equipment

The ASTM G31-72 recommendation was followed by using sacrificial steel specimens with large surface-to-mass ratio and small ratio of edge area to total surface area to minimize the area of exposed end grain (ASTM 2004). Also, careful dimensional measurements were made to permit accurate calculation of exposed area. A band saw was used to cut each 3/16 inch thick specimen into 1 inch by 2 inch dimensions. To identify each steel grade, a hole of 1/4 inch diameter was drilled into each specimen using a metal drill press at unique locations. Each coupon was also stamped with a unique serial number using a hammer-stamp tool. FIGURE 3.1 shows the dimensions and layouts for each steel grade.

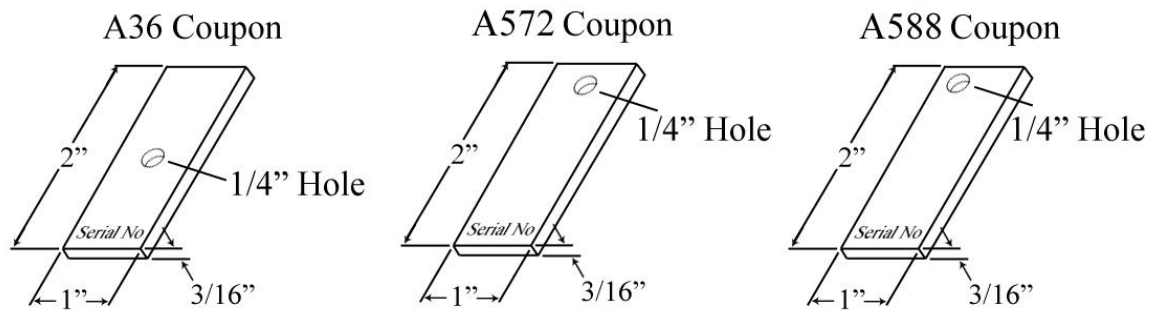


FIGURE 3.1: Test coupon layouts for each steel grade

The primary equipment for the SHRP test included an air pump, flow meter, pH meter, saturated calomel electrode, and voltmeter. The air pump and flow meter were used as part of the aeration system to deliver and regulate air flow to all the test cells. The pH meter and voltmeter along with the calomel electrode were used to monitor the

acidity of the solutions and the corrosion potential. FIGURE 3.2 shows the primary equipment used for the test setup.

Cleaning of corroded test specimens was performed according to ASTM G1 to ensure an ideal cleaning procedure that would only remove corrosion products and not the base metal. An ultrasonic cleaner was used according to SHRP recommendations. The acid solution used for ultrasonic cleaning contained 50 grams of stannous chloride and 20 grams of antimony trioxide in 1,000 mL concentrated hydrochloric acid. Other cleaning materials included a metal wire brush, acetone, and ethanol. Cleaned specimens were weighted using an analytical balance with 0.1 mg resolution.

Other setup materials included:

- 1) Fishing line: for hanging metal specimen in each test cell.
- 2) Insulated electrical wire: for connecting the test electrode to the voltmeter.
- 3) Brass screws and nuts: for attaching electrical wire to the test electrode.
- 4) Silicon sealer: for sealing the electrical wire to the test electrode.
- 5) Test cell container: 2.5 quart plastic container to hold the deicing solution.
- 6) Test cell lid: for covering of test solution and hanging of the metal specimens.
- 7) Air Tubing: for directing air to each test cell.
- 8) Sodium chloride and deionized water: for preparing test solutions.
- 9) Magnetic stirrer: for dissolving salt into solution



FIGURE 3.2: SHRP test equipment: cleaner, air pump, flow meter, electrode, and meters

### 3.1.3 Details of Test Procedure

Test cells were prepared using 2.5 quart plastic containers. Each cell was cleaned using ethanol and air dried prior to filling of test solutions. Testing solutions were prepared using deionized water to ensure that water-treatment ions, such as chloride, were absent from the control solution. Selected concentrations were measured as a percent weight of sodium chloride dissolved in deionized water. A magnetic stirrer was used to fully dissolve the salt into solution. Initial pH of each test solution was recorded. Each test cell contained a total of nine specimens of a particular steel type: eight test specimens and one “electrode” specimen. Specimens were cleaned, rinsed twice with

acetone, air dried, and weighed to the nearest 0.1 mg as the initial weight. A nylon string was tied to each test specimen at the  $\frac{1}{4}$ " hole to allow the specimens to be suspended inside the test cell. "Electrode" specimens were prepared by attaching an insulated electrical wire to a single metal specimen using screw and nut. The electrical connection at the screw was sealed using silicon to prevent development of a cathodic surface at this connection. Test cell lids were punched with nine hanging locations around the circumference for hanging of the specimens and a center hole to attach the air tubing. FIGURE 3.3 shows the setup for the immersion test.



FIGURE 3.3: SHRP H-205.7 test setup with specimens submerged in solution

Start-up procedures included filling the test cell with prepared solution and placing the lid in position with specimens hanging in solution. An air tube was attached through the lid at the center to facilitate aeration of the solution. The air bubble rate was maintained at around 100 cc air/min. Test cells were filled with solution so that test specimens were fully submerged. Throughout the test duration, any evaporation of the solution was compensated for by adding additional deionized water. Each test was conducted within a test cell for one steel type at a particular sodium chloride concentration. Selected exposure times were one, two, three, four, six, and eight weeks as recommended by SHRP. At the end of each exposure time, test specimens were removed for cleaning and reweighing along with measuring the pH and corrosion potential within each test cell. One specimen was removed from each test cell at one, two, three, and four weeks exposure time and two specimens were removed at six, and eight weeks. The corrosion potential was measured by placing the calomel electrode inside the solution and connecting the wire to the negative terminal of a volt meter along with the wire from the electrode specimen to the positive terminal.

After each specimen was exposed for the prescribed durations, it was removed for cleaning and reweighing. The removed specimen was first placed in water followed by wire brushing of the surface to remove loose corrosion products. Acetone was used to wipe away any remaining rust particles. The specimen was then placed into acid solution to be cleaned using an ultrasonic cleaner. After removal from the acid solution, the specimen was rinsed and wiped dry with acetone. The same cleaning procedure was used on uncorroded coupons to determine the mass lost due to cleaning only.

TABLE 3.1 shows the mass loss from the cleaning procedure for uncorroded coupons. FIGURE 3.4 shows corroded specimens before and after the cleaning process. Interestingly, control specimens exposed in deionized water were visually more corroded than those exposed to 23% NaCl.

TABLE 3.1: Mass loss of test specimen due to cleaning only

Steel Type	Original weight (g)	After cleaning (g)	Mass loss (g)
A36	48.4433	48.4323	0.011
A572	46.6577	46.5963	0.0614
A588	42.4916	42.3465	0.1451

Corrosion rates were determined based on corrected mass lost, specimen area, time, and specimen density. Specimen densities used were 7.85, 7.85, and 7.87 (g/cm<sup>3</sup>) for A36, A572, and A588, respectively (MatWeb 2011).

$$CR = \frac{(KW)}{(ATD)} \quad (3.1)$$

Where:

$CR$  (mpy) = corrosion rate (mils per year)

$K$  = constant =  $3.45 \times 10^3$  (unit conversion factor)

$W$  = corrected mass loss (mg)

$A$  = specimen area (cm<sup>2</sup>)

$T$  = time (hr)

$D$  = specimen density (g/cm<sup>3</sup>)

In addition, a repeated study with the same procedures was conducted for A36 steel at 23% concentration to determine whether including the electrode specimen inside



the testing solution and changing the testing solution at each exposure time would have an effect on the corrosion rate.

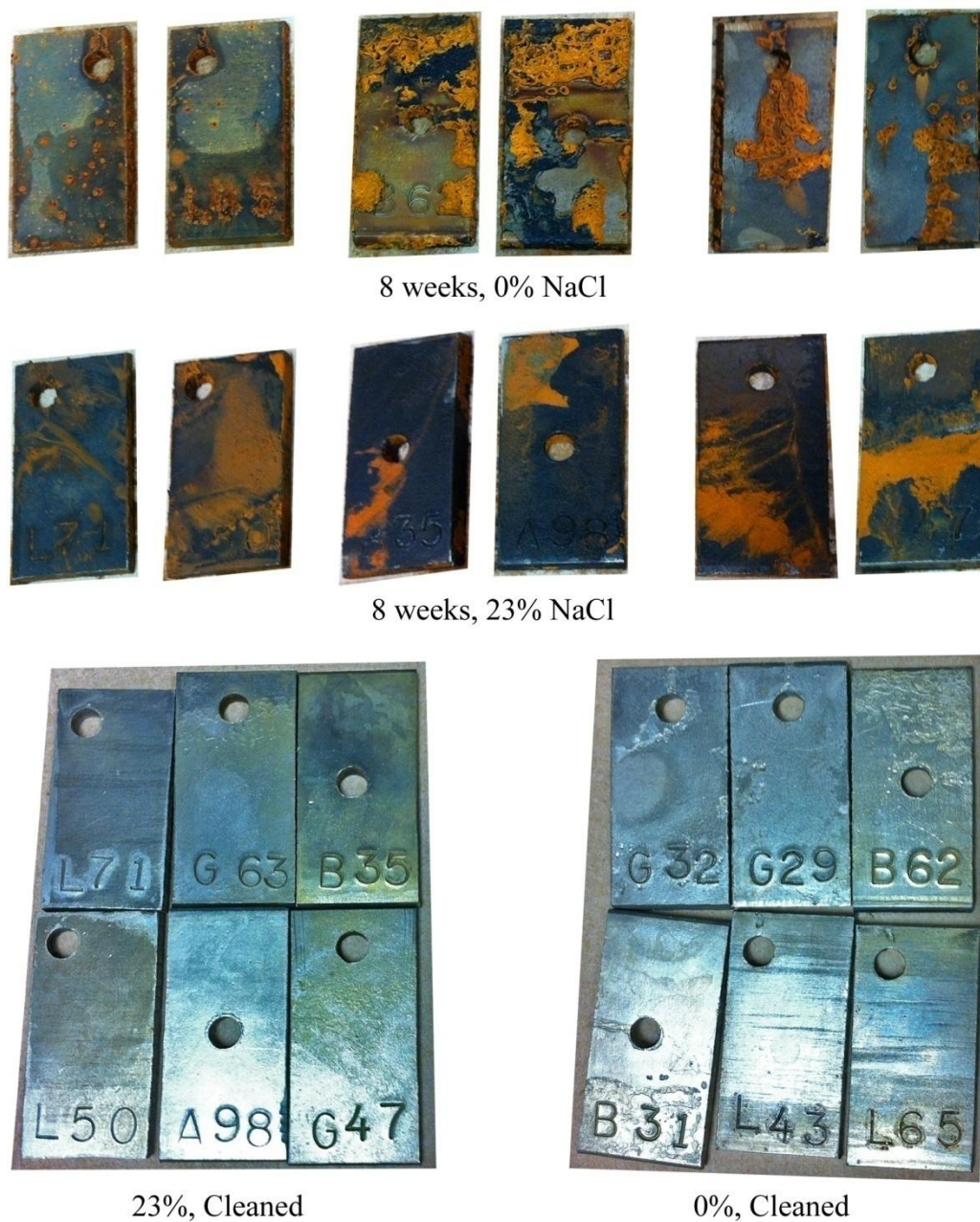


FIGURE 3.4: Corroded specimens after 8 weeks of exposure before and after cleaning

#### 3.1.4 Results from SHRP H-205.7 Test

Results for A36 steel with exposure to solution of 0%, 3%, and 23% sodium chloride concentrations are shown in TABLE 3.2 and plotted in FIGURE 3.5. Results for A572 and A588 steel are shown in TABLES 3.3 and 3.4 and FIGURES 3.6 and 3.7, respectively. Mass losses presented on the plot for the 6<sup>th</sup> and 8<sup>th</sup> week exposure times were averaged. While the results exhibit expected corrosive losses for specimens exposed to 3% sodium chloride solutions, the results obtained for the specimens exposed to 23% brine solutions appear unexpectedly low. In particular, results for all three steel types would indicate that the mass loss for exposure to 23% salt concentration is almost similar to those exposed to only deionize water.

TABLE 3.5 shows the result for A36 steel tested at 23% concentration with three different conditions: with (1) or without (2) electrode specimen in the solution and using the same test solution for the duration of the test or with (3) electrode specimen and replacing the solution at each exposure time. The results indicate that including the electrode specimen in the test solution and periodically replacing the test solution have little impact on the mass loss for 23% salt concentration.



TABLE 3.2: Results for A36 steel at 0%, 3%, 23% NaCl using SHRP

<b>A36 Steel</b>					
<b>Weeks</b>	<b>Mass Loss (mg)</b>	<b>Corrected Mass Loss (mg)</b>	<b>Corrosion Rate (mpy)</b>	<b>pH</b>	<b>Potential (-mV)</b>
0% Deionized Water					
1	-169.5	-180.5	-36.688	6.7	320.5
2	30.3	19.3	1.961	6.45	261.5
3	37.3	26.3	1.782	6.8	330
4	81.1	70.1	3.562	7.76	341.6
6	219.4	208.4	7.060	8.17	423
6	226.3	215.3	7.294	8.17	423
8	384.5	373.5	9.490	7.93	602
8	427	416	10.569	7.93	602
3% NaCl Solution					
1	242.8	231.8	47.116	7.4	725
2	269.1	258.1	26.231	6.41	740
3	498.1	487.1	33.003	6.24	753
4	749.8	738.8	37.542	6.04	741
6	941.3	930.3	31.515	5.93	760
6	577.3	566.3	19.184	5.93	760
8	1301.3	1290.3	32.783	6.96	742
8	835.9	824.9	20.959	6.96	742
23% NaCl Same Solution with Electrode					
1	14.1	3.1	0.630	4.85	719
2	37.2	26.2	2.663	5.15	720
3	45.4	34.4	2.331	5.47	737
4	71.5	60.5	3.074	5.9	748
6	183.3	172.3	5.837	6.22	725
6	175.1	164.1	5.559	6.22	725
8	261.9	250.9	6.375	7.15	714
8	252.6	241.6	6.138	7.15	714

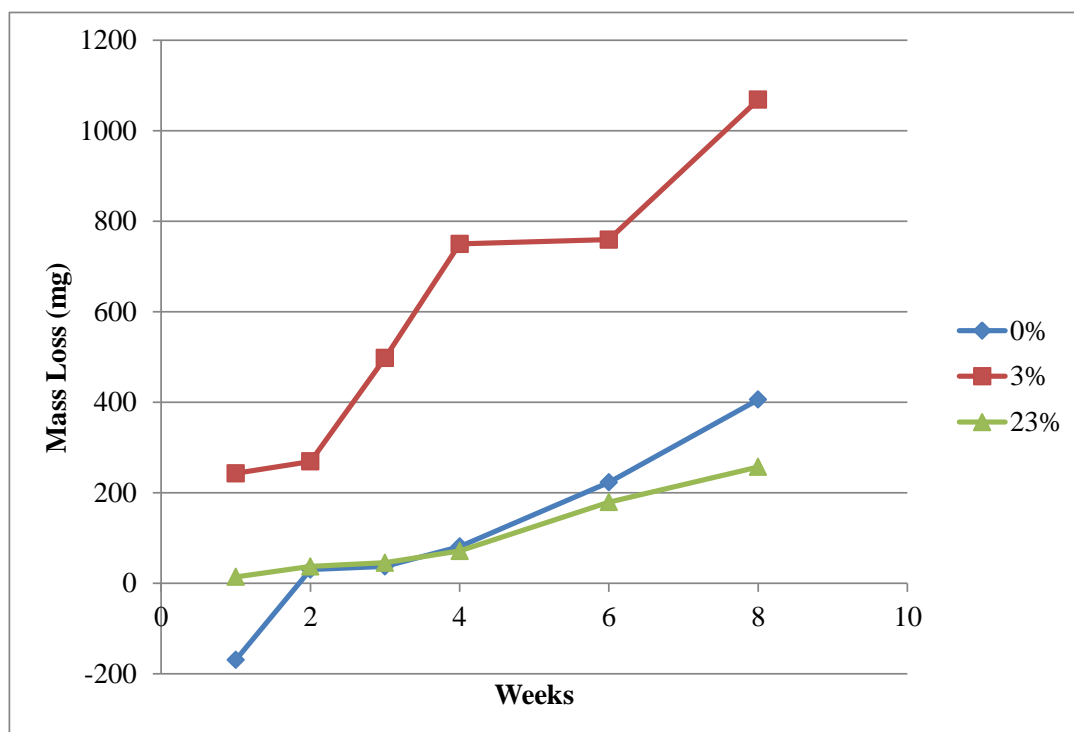


FIGURE 3.5: Results for A36 Steel using SHRP test method

TABLE 3.3: Results for A572 steel at 0% and 23% NaCl using SHRP

<b>A572 Steel</b>					
<b>Week</b>	<b>Mass Loss (mg)</b>	<b>Corrected Mass Loss (mg)</b>	<b>Corrosion Rate (mpy)</b>	<b>pH</b>	<b>Potential (-mV)</b>
0% Deionized Water					
1	71.7	10.3	2.086	6.25	225.2
2	77.5	16.1	1.630	6.74	319.6
3	113.1	51.7	3.489	7.05	265.3
4	108.6	47.2	2.389	7.43	300.1
6	193.3	131.9	4.451	8.14	231
6	195.3	133.9	4.519	8.14	231
8	228.5	167.1	4.229	7.88	268
8	226.3	164.9	4.174	7.88	268
23% NaCl Solution					
1	-71.2	-132.6	-26.849	5.1	701
2	125.1	63.7	6.449	5.19	734
3	-15.9	-77.3	-5.217	5.49	747
4	-1.6	-63	-3.189	5.83	735
6	200.6	139.2	4.698	6.21	698
6	251.1	189.7	6.402	6.21	698
8	312.2	250.8	6.348	6.98	712
8	174.3	112.9	2.858	6.98	712

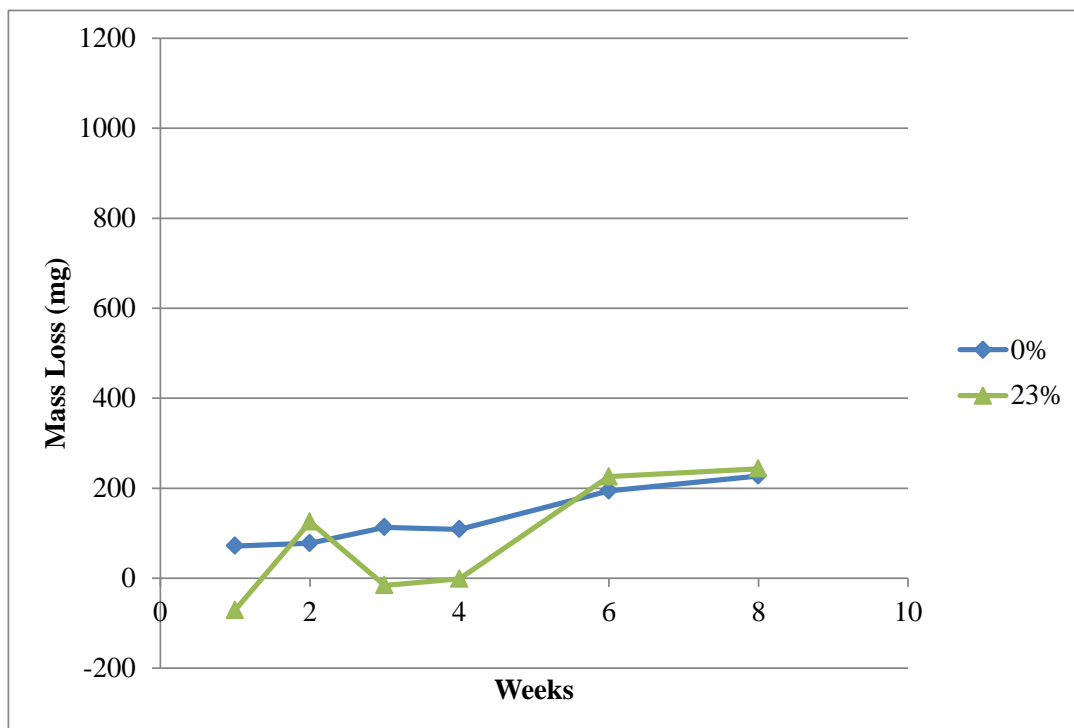


FIGURE 3.6: Results for A572 Steel using SHRP test method

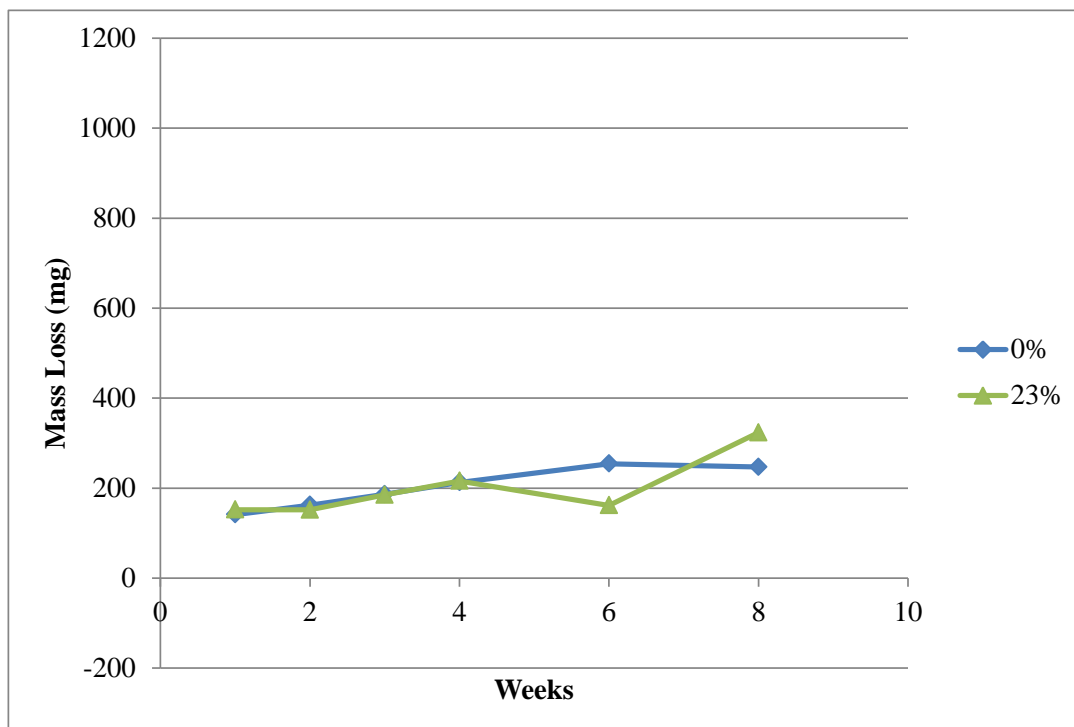


FIGURE 3.7: Results for A588 Steel using SHRP test method

TABLE 3.4: Results for A588 steel at 0% and 23% NaCl using SHRP

<b>A588 Steel</b>					
<b>Week</b>	<b>Mass Loss (mg)</b>	<b>Corrected Mass Loss (mg)</b>	<b>Corrosion Rate (mpy)</b>	<b>pH</b>	<b>Potential (-mV)</b>
0% Deionized Water					
1	141.3	-3.8	-0.768	6.8	267.1
2	162.3	17.2	1.739	6.37	285.6
3	186.3	41.2	2.777	7.28	237.3
4	212.7	67.6	3.418	7.13	230.1
6	251.1	106	3.573	8.14	231
6	257.1	112	3.775	8.14	231
8	253.1	108	2.730	7.9	221
8	240.7	95.6	2.417	7.9	221
23% NaCl Solution					
1	152.1	7	1.416	5.65	700
2	151.8	6.7	0.677	4.95	714
3	185	39.9	2.690	5.44	724
4	216	70.9	3.584	5.74	710
6	192.8	47.7	1.608	6.34	711
6	130.2	-14.9	-0.502	6.34	711
8	303.1	158	3.994	7.18	705
8	343.9	198.8	5.025	7.18	705

TABLE 3.5: Results for A36 steel at 23% NaCl

<b>A36 Steel</b>					
<b>Week</b>	<b>Mass Loss (mg)</b>	<b>Corrected Mass Loss (mg)</b>	<b>Corrosion Rate (mpy)</b>	<b>pH</b>	<b>Potential (-mV)</b>
23% NaCl Same Solution With Electrode					
1	14.1	3.1	0.630	4.85	719
2	37.2	26.2	2.663	5.15	720
3	45.4	34.4	2.331	5.47	737
4	71.5	60.5	3.074	5.9	748
6	183.3	172.3	5.837	6.22	725
6	175.1	164.1	5.559	6.22	725
8	261.9	250.9	6.375	7.15	714
8	252.6	241.6	6.138	7.15	714
23% NaCl Same Solution Without Electrode					
1	26.3	15.3	3.110	7.35	420
2	51.5	40.5	4.116	7.4	441
3	96	85	5.759	7.53	443
4	103.6	92.6	4.705	7.29	461
6	167.3	156.3	5.295	7.29	446
6	136.7	125.7	4.258	7.29	446
8	192.8	181.8	4.619	6.02	443
8	255.3	244.3	6.207	6.02	443
23% NaCl Change Solution With Electrode					
1	27.3	16.3	3.313	7.34	729
2	54.5	43.5	4.421	6.98	750
3	103.5	92.5	6.267	7.1	749
4	109.8	98.8	5.021	6.85	723
6	171.1	160.1	5.424	6.82	716
6	173.6	162.6	5.508	6.82	716
8	218.1	207.1	5.262	6.02	725
8	233.7	222.7	5.658	6.02	725

### 3.1.5 Conclusion for SHRP H-205.7 Test

At higher concentrations of sodium chloride dissolved in the solution and the corresponding lower pH, it is expected that corrosion is more severe. On the contrary, the results obtained indicated decreased corrosion activity for fully saturated 23% brine solution. In some cases, the mass loss observed is less than the control deionize water solution. However, since corrosion of iron requires oxygen and the solubility of oxygen in solutions with high salt concentrations is significantly low, the corrosion process is consequently inhibited. Due to this phenomenon within higher concentration solutions as well as the non-representative exposure of the steel specimens under continuous submersion, the research team developed a modified test program to subject the coupons to cyclic exposure to sodium chloride solutions followed by air exposure and drying.

### 3.2 Modified SHRP H-205.7 Test Method: Cyclic Corrosion Test

Results from the standard SHRP method indicate there is a limitation in testing corrosive effects on bare metal surfaces at high sodium chloride concentrations. Since the SHRP procedure requires each specimen to be fully submerged for the duration of the test, there may be insufficient dissolved oxygen to supply the corrosion reaction. To allow for sufficient levels of dissolved oxygen and better simulation of natural atmospheric exposure, a modified testing procedure was developed. The modified procedure involved cycling of the test specimen between submersions in the test solution and natural atmospheric drying. The timing for each cycle was selected for sufficient exposure of the specimen surface to testing solution and a drying time that would result in complete drying of the specimen during atmospheric exposure. The process aims to produce more realistic replication of the natural corrosion process, since constant submersion is not typical for steel components in highway bridges. This test method was modeled from Q-Lab Technical Bulletin on cyclic corrosion testing (Q-Lab Corporation 2009). Additional cleaning procedures were also used for more sufficient removal of corrosive byproduct.

#### 3.2.1 Test Procedures

Similar preparations of test specimens and data collection procedures were adopted from the SHRP method. Likewise, the test duration was selected to be eight weeks and removal of corroded specimens was performed at 1, 2, 3, 4, 6, and 8 week exposure time with duplicate specimens for 6 and 8 weeks. Each test cell contained solution at a particular concentration with eight test specimens of a metal type or coating type (one for each exposure time). In addition, the study was conducted for 0%, 3%, 5%,



and 23% sodium chloride concentration for all three metal types: A36, A572, and A588. Coated specimens were also included in the test matrix. Coating types included were: galvanized A36 steel, painted A572, epoxy coated A572, and epoxy coated A588. The coating process was performed by the NCDOT. In general to ensure consistency with field applications, the test setup was similar to the SHRP procedure except the metal specimens were hung using fishing line from a lever arm above the test cell or container. Each test cell contained eight test specimens of a single metal type at a particular salt concentration. The complete setup of the test contained 28 test cells, representing the matrix formed by four different concentrations for three metal types and four coating types. During the test procedure, specimens were cycled in solution for two minutes followed by atmospheric drying for two hours. Similar to prior tests, evaporation of the test solution over the duration of the test was compensated for by adding deionized water to return the test solution to the original level.

Equipment and material used for the cyclic corrosion test included: wooden stands, AC powered linear solenoid actuators, a wall-plug timer to control the dunking cycle, 5 gallon pails with sand to serve as a counter-weight, and 2.5 quart plastic buckets to contain the test solutions. A schematic of the developed apparatus is shown in FIGURE 3.8. Each lever arm was attached with testing specimens at one end and the other with counter-weights. The arm was connected to a wood stand with a metal hinge to allow for a seesaw motion. The dunking of the specimens was controlled by two linear solenoids with 1" retraction stroke for each lever arm. A wall timer provided power to the solenoids at each dunking interval for two minutes at every two hours. When power was switched on, each solenoid retracted, pulling the counter-weight end up and lowering

the specimen end into placed containers with testing solution. After two minutes, power was switched off releasing the solenoid and bringing the specimens out of solution due to the slightly heavier counter-weight end. The test set up used two lever arms, each supporting 112 specimens. FIGURE 3.9 shows a photograph of the test setup used for the cyclic corrosion test.

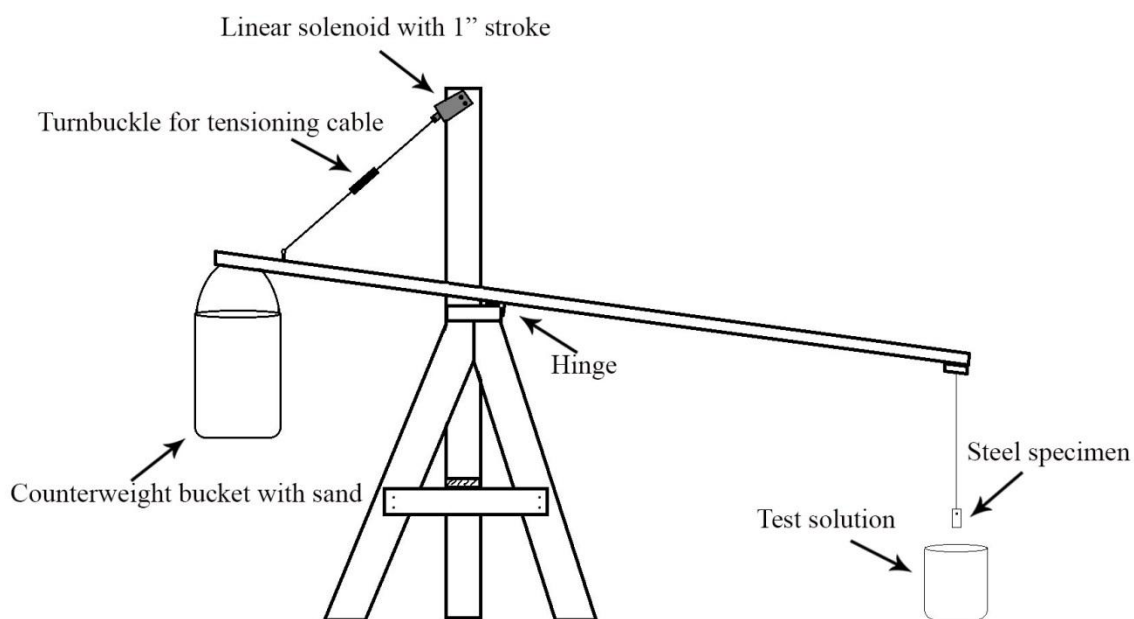


FIGURE 3.8: Schematic of dunking apparatus



FIGURE 3.9: Fixtures used for dunking motion in cyclic corrosion test

The cleaning process for corroded specimens consisted of mechanically cleaning with a metal wire brush, follow by ultrasonic acid bath, then sand blasting. Acetone soaked paper towels were used to remove corrosion byproducts between each cleaning process. Masses of cleaned, corroded specimens were adjusted based on cleaning of an uncorroded specimen for each metal type, shown in TABLE 3.6, to account for nominal sacrificial losses due to the cleaning process.

TABLE 3.6: Mass losses from cleaning of un-corroded specimens

Steel Type	Acid cleaning (mg)	Sand blasting (mg)	Total (mg)
A36	11.0	12.0	23.0
A572	61.4	8.7	70.1
A588	145.1	11.1	156.2
Galvanized A36	N/A	53.7	53.7

### 3.3 Results for Modified SHRP Test Method: Cyclic Corrosion Test

One test specimen was removed for each of the exposure time of 1, 2, 3, and 4 week from the test cell and two specimens were removed for the 6 week and 8 week exposure time to be cleaned and reweighed. FIGURE 3.10 shows the visual condition of test specimens after four weeks exposure to the cyclic testing routine. APPENDIX 3.1 presents the full mass loss data after cleaning for all test specimens over the test program.

Visual inspection of epoxy coated and painted specimens showed no sign of distress during the eight week test period. After rinsing with water, the mass difference found for epoxy coated and painted specimens ranged from 120 mg in mass gain to 21 mg in mass loss. Due to no sign of visual deterioration and a mass difference that is within the uncertainty bounds of the test and cleaning method, it is concluded that both epoxy coated and painted specimens performed well over the duration of the test procedure with no significant degree of corrosion recorded. Further evaluation of coated specimens was performed through an additional test using scribed specimens that is presented later in the chapter.

Cleaning of galvanized specimens included only sand blasting since acid cleaning of galvanized specimens was not possible due to chemical reaction of the zinc layer and acid solution. Visual observation of galvanized specimens indicated that corrosion occurred only on the zinc protective layer. This is evidence from the buildup of only white corrosive byproduct, typical of galvanization and not brown ferric rust of the base metal. The percent mass loss of the galvanized layer is plotted in FIGURE 3.11. The plot indicates a steady increase in loss of the protective layer up to the fourth week. Once the loss reaches about 70% of the original mass, little additional loss occurred for the

remainder of the test program. Galvanized specimens exposed to 5% NaCl concentration exhibit the highest mass loss follow by 3% while those exposed to 23% exhibit the lowest.

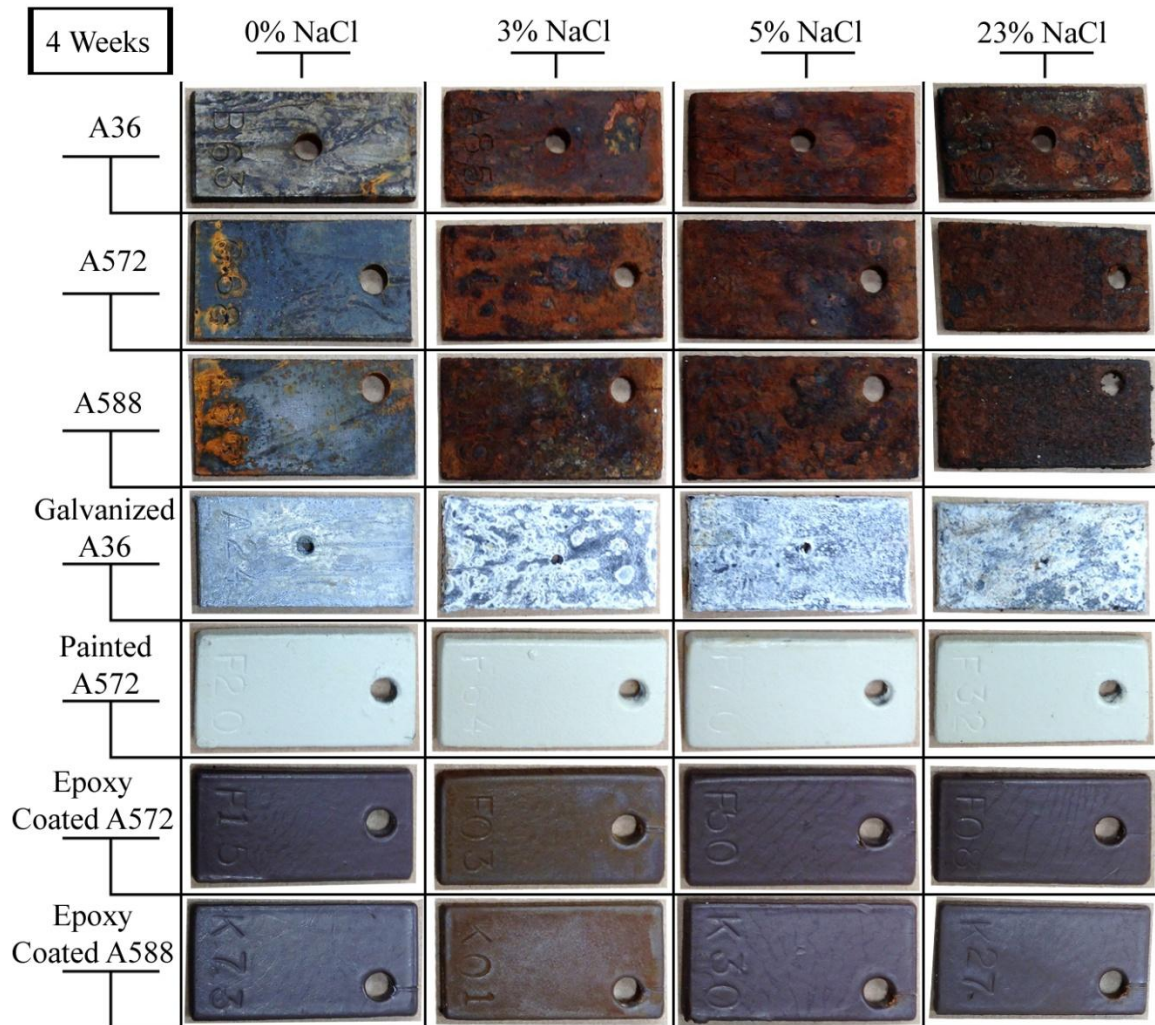


FIGURE 3.10: Test specimens with 4 weeks exposure before cleaning

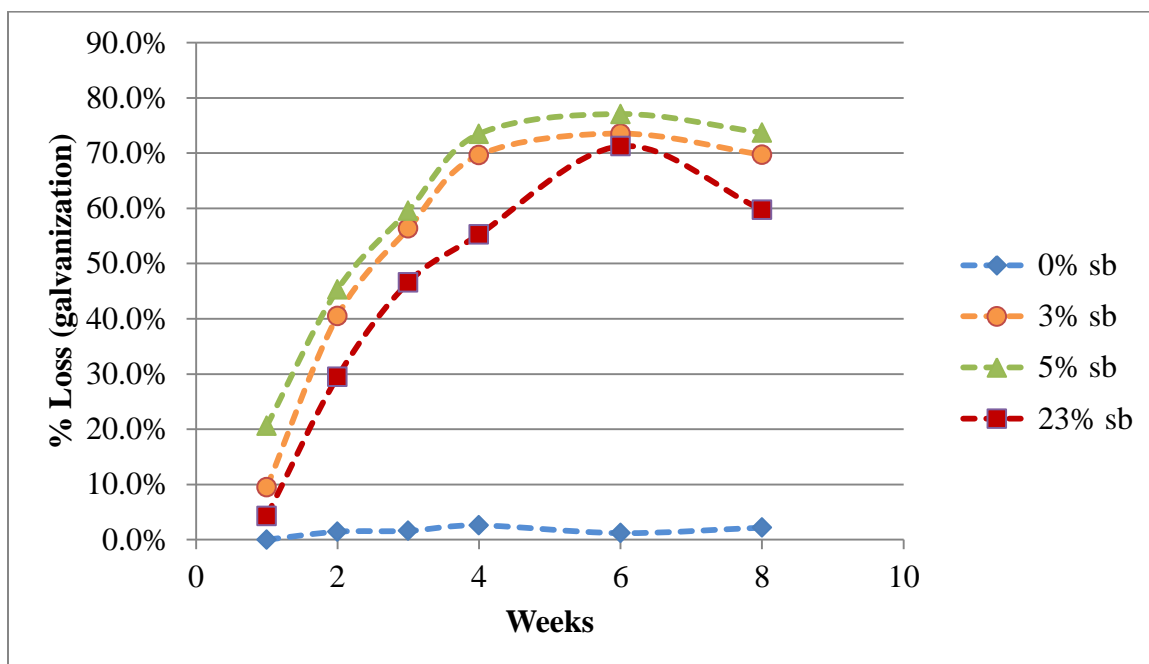


FIGURE 3.11: Percent loss of galvanized layer in NaCl solutions

FIGURES 3.12 and 3.13 show the 8 week bare steel test specimens exposed to 0%, 3%, and 23% NaCl concentrations after acid cleaning and sand blasting, respectively. Specimens exposed at 5% sodium chloride concentration were visually similar to those exposed at 3%. As seen in FIGURE 3.12, acid cleaning alone was not effective in removing all corrosion byproducts in heavily corroded specimens. Plots showing mass loss results for acid cleaning alone and after sand blasting can be seen in FIGURES 3.14, 3.15, 3.16, and 3.17. In the higher corrosion cases, as seen for 3% and 5% concentrations, sand blasting results show a more reasonable trend, where higher corrosion is observed with longer exposure. Also potential unwanted sandblasting effects were minimized, as seen in the 0 and 23% concentration results. Final corrosive losses of test specimens after acid cleaning, sandblasting and adjusting for loss due to cleaning are shown in TABLE 3.7.



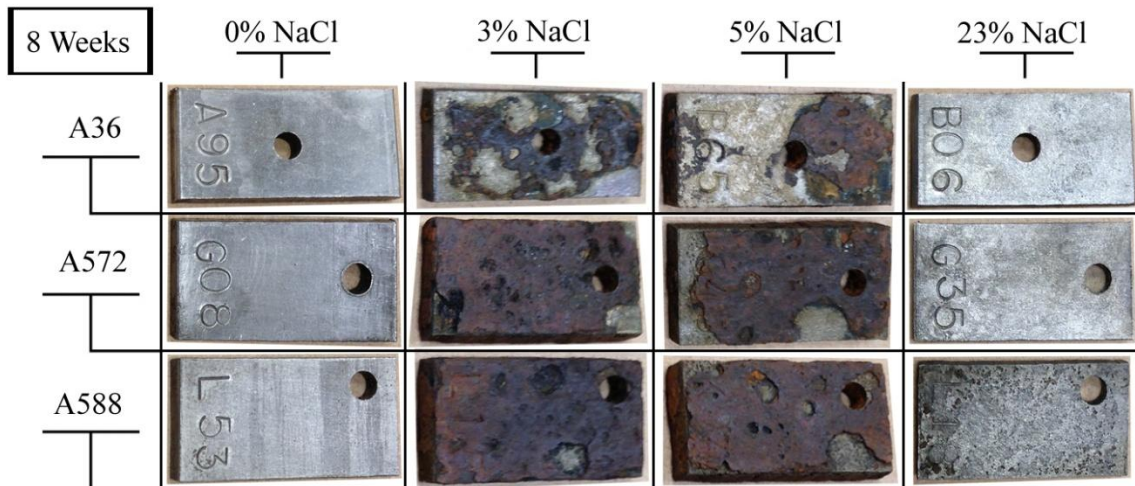


FIGURE 3.12: Test specimens after acid cleaning

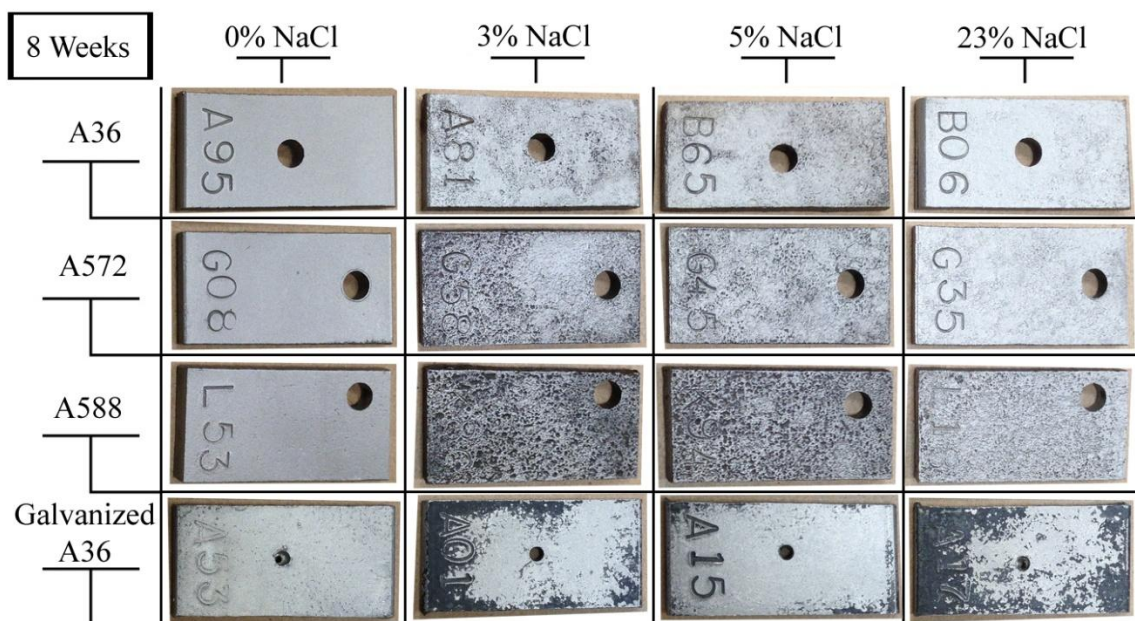


FIGURE 3.13: Test specimens with 8 weeks exposure after sand-blasting

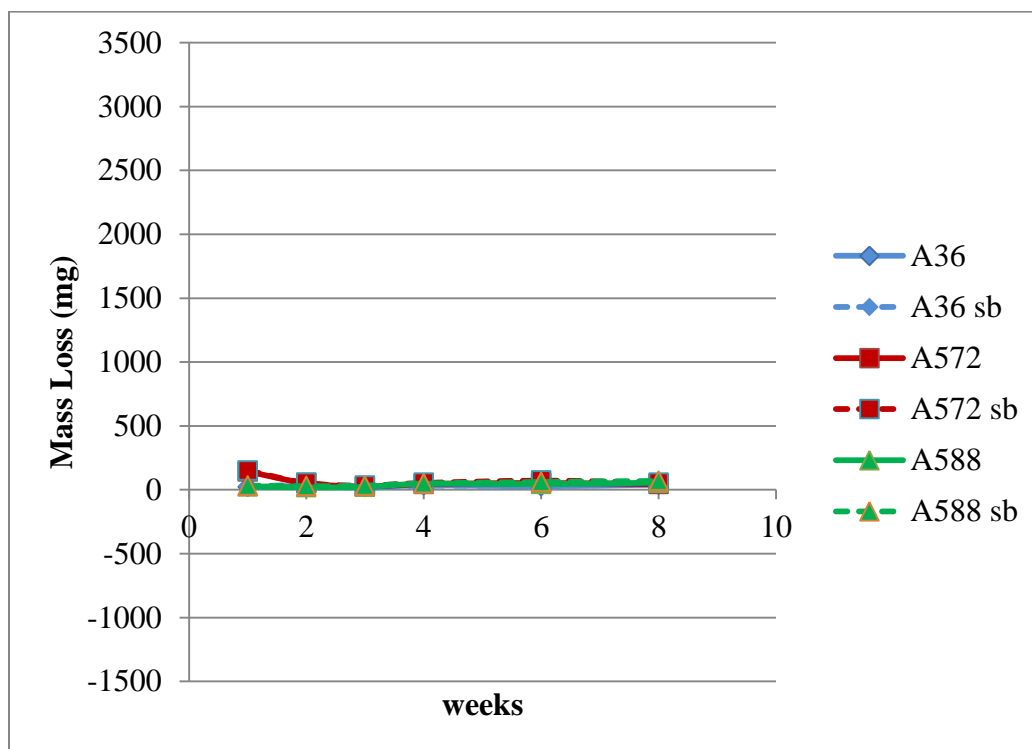


FIGURE 3.14: Mass loss result for specimens after acid clean and sandblasting (sb), at 0% NaCl



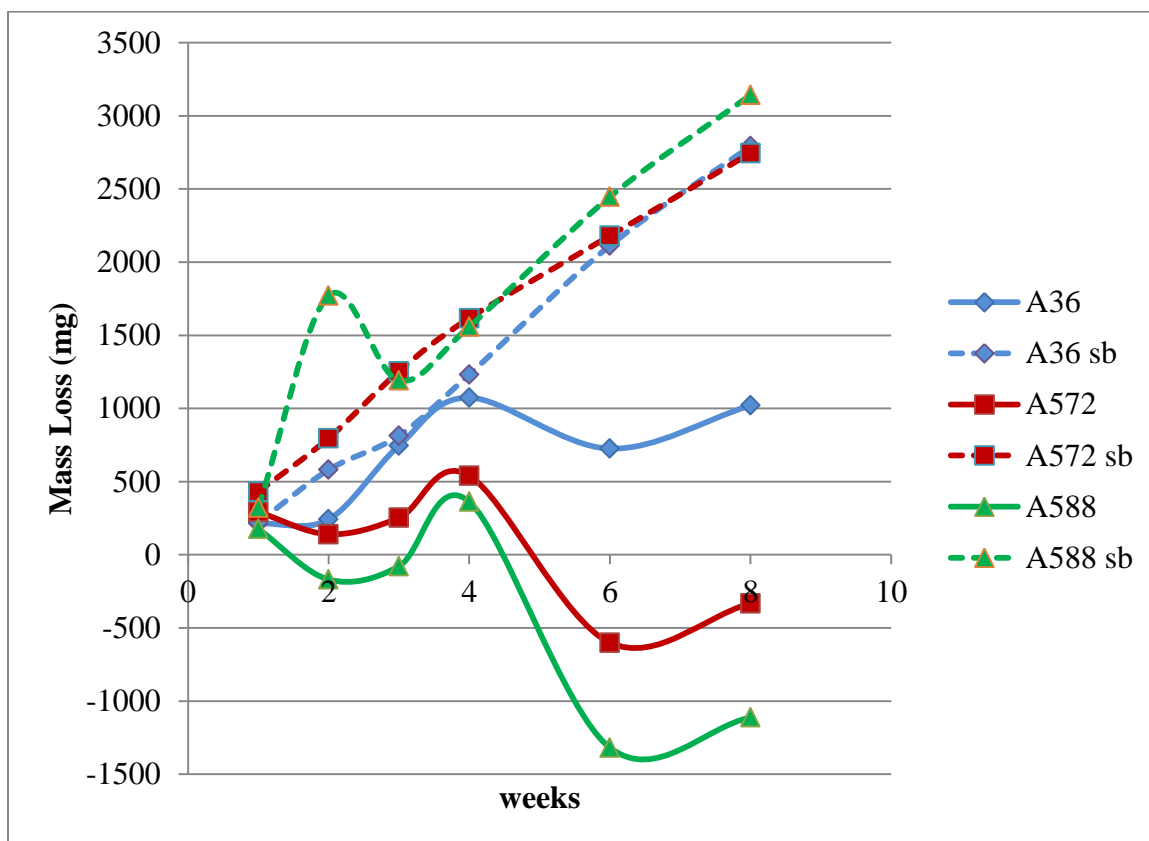


FIGURE 3.15: Mass loss result for specimens after acid clean and sandblasting (sb), at 3% NaCl

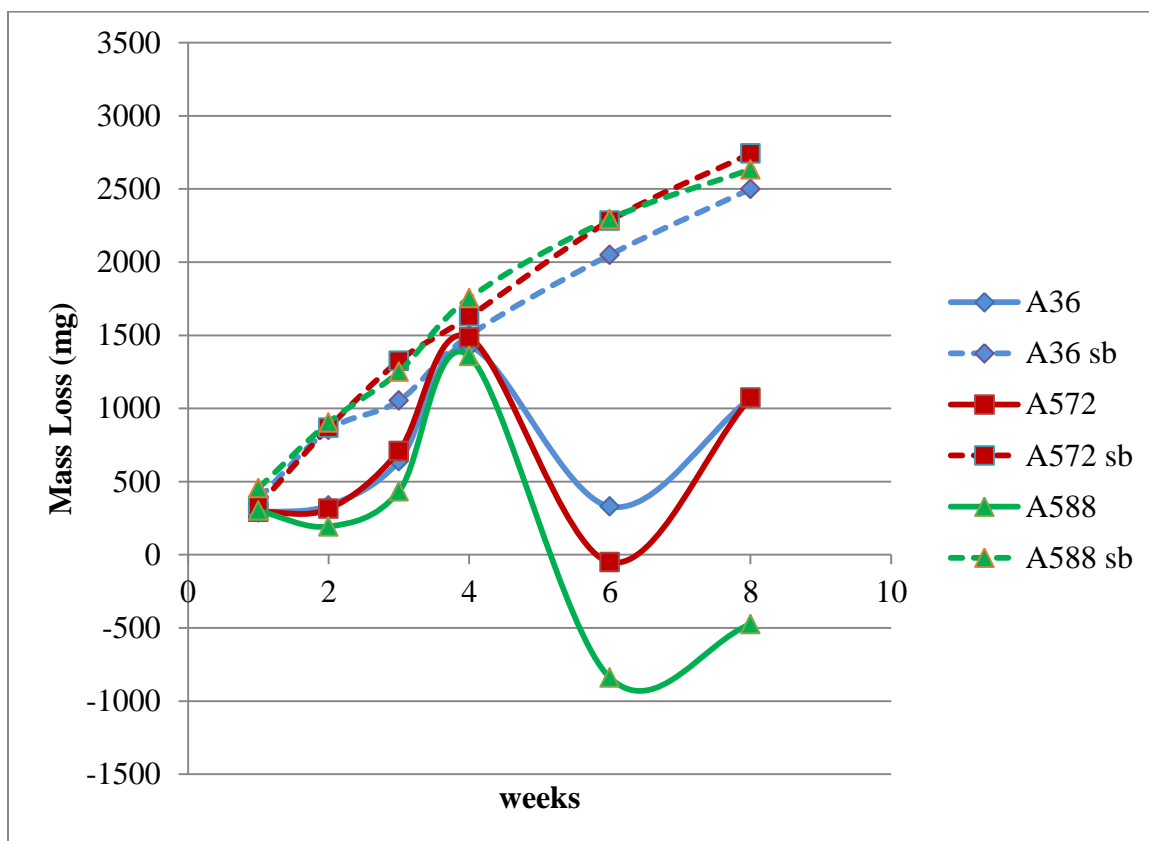


FIGURE 3.16: Mass loss result for specimens after acid clean and sandblasting (sb), at 5% NaCl

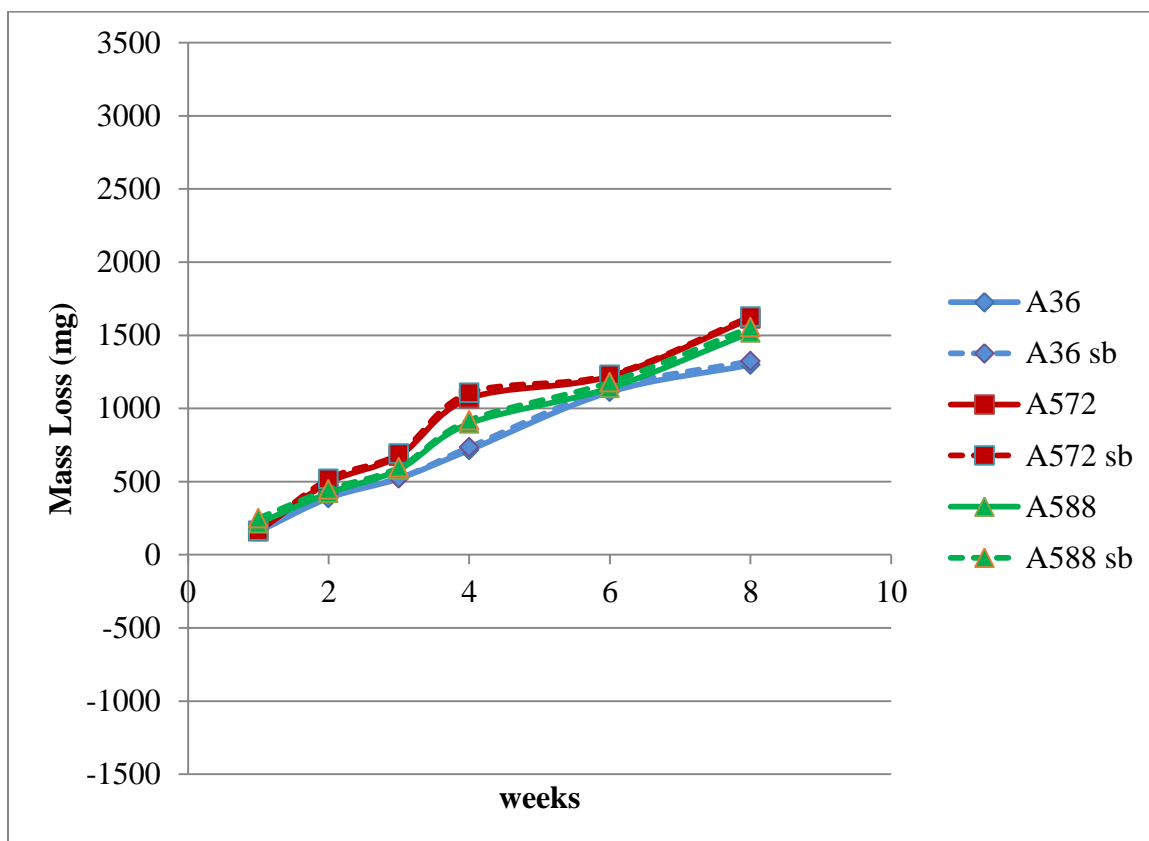


FIGURE 3.17: Mass loss result for specimens after acid clean and sandblasting (sb), at 23% NaCl

TABLE 3.7: Corrosive mass loss after acid cleaning and sand-blasting

<b>Corrosive loss (mg)</b>				
<b>NaCl%</b>	<b>0%</b>	<b>3%</b>	<b>5%</b>	<b>23%</b>
<b>1 Week</b>				
<b>A36</b>	26	221.8	383	162.8
<b>A572</b>	151.1	430.7	335.3	164.8
<b>A588</b>	33.4	321.4	454.5	249.1
<b>2 Week</b>				
<b>A36</b>	37.4	580.7	852.7	416.5
<b>A572</b>	54	796.8	867.9	517.2
<b>A588</b>	28.7	1771	903.7	445.8
<b>3 Week</b>				
<b>A36</b>	18.7	814.1	1053	523.2
<b>A572</b>	33.2	1253.7	1324.5	691.3
<b>A588</b>	33.2	1191.6	1251.2	596.1
<b>4 Week</b>				
<b>A36</b>	32.2	1231.8	1499.7	734.8
<b>A572</b>	53.8	1616.7	1628.4	1105.6
<b>A588</b>	49.3	1559.4	1754.3	918.5
<b>6 Week</b>				
<b>A36</b>	32.7	2112.7	2049.75	1137.6
<b>A572</b>	71.75	2179.65	2283.35	1228.9
<b>A588</b>	61.5	2446.1	2294.55	1178.8
<b>8 Week</b>				
<b>A36</b>	42.4	2792.1	2499.75	1323.75
<b>A572</b>	55.9	2745.45	2741.8	1627.1
<b>A588</b>	69.6	3141.45	2633.75	1553.9

TABLE 3.8: Mean corrosion rate (mpy) and standard deviation

<b>Alloy</b>	<b>0%NaCl</b>		<b>3%NaCl</b>		<b>5%NaCl</b>		<b>23%NaCl</b>	
	Mean CR	S Dev	Mean CR	S Dev	Mean CR	S Dev	Mean CR	S Dev
<b>A36</b>	2.36	1.76	60.73	10.04	74.16	7.97	36.73	3.45
<b>A572</b>	7.48	11.4	79.56	6.75	79.01	9.14	45.17	8.24
<b>A588</b>	3.04	1.86	77.2	6.96	83.37	9.85	36.54	3.43

The average corrosion rate was calculated for each concentration and metal type based on the formula in EQUATION 3.1. TABLE 3.8 shows the average corrosion rate in mils per year for each metal type at each concentration. An average mass loss for steel type A588 at 2 weeks with 3% exposure was not included in the average corrosion rate calculation due to an unexpected high value within the plotted trend, as indicated in FIGURE 3.14. Results after sand blasting exhibit expected increases in corrosive losses with time for all steel types. A36 steel shows slightly less corrosive loss compared to A572 and A588 steel. A572 and A588 steel exhibited comparable corrosive loss across all tested salt concentrations. Similar corrosive loss is seen for 3% and 5%, while specimens subject to 23% solution exhibited less corrosion across all three steel types. Plot of mass loss against solution concentration for each steel type helps to identify this trend, as seen in FIGURE 3.18.

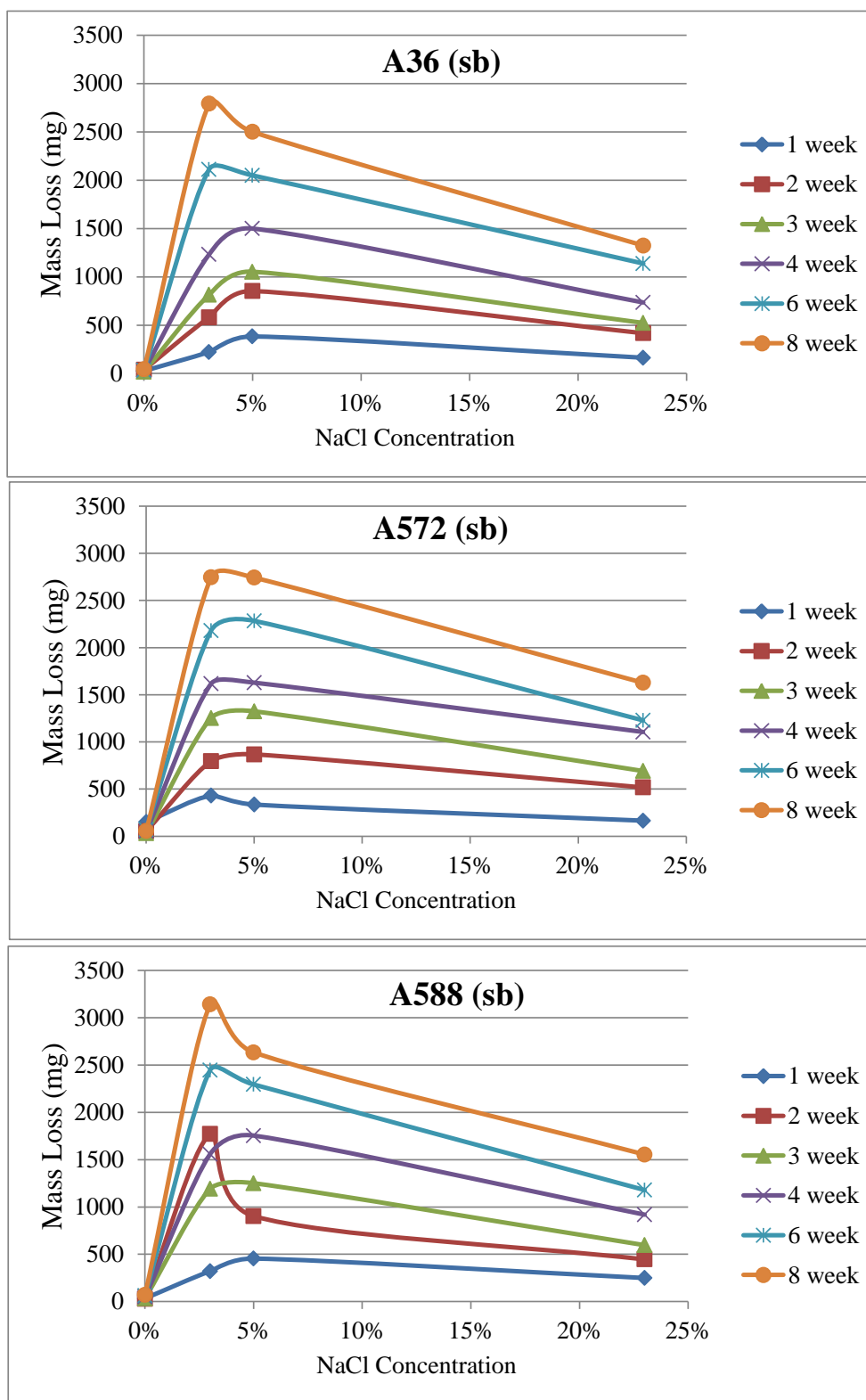


FIGURE 3.18: Comparison of corrosive losses measured as a function of solution concentration

### 3.4 Modified SHRP: Scribe Test for Evaluation of Painted or Coated Specimens

For evaluation of coating methods and their effectiveness after exposure to corrosive environment, a test program was conducted based on two ASTM methods: D7087: An Imaging Technique to Measure Rust Creepage at Scribe on Coated Test Panels Subjected to Corrosive Environments (ASTM 2005) and D1654: Evaluation of Painted or Coated Specimens Subjected to Corrosive Environments (ASTM 2008). The study was performed on painted A572, epoxy coated A572 and A588, and galvanized A36 steel over eight weeks exposure with 3% sodium chloride solution and 0% (deionized water) as a control solution. This test method provides a means to compare the development of corrosion on the substrate between different coatings and metal types. The results are based on rust creepage area measurements around the scribe line after eight weeks of corrosive exposure. Each coating system is rated for corrosion performance through representative mean creepage calculated using imaging software.

#### 3.4.1 Test Procedure

Coated specimens were scribed using a motorized circular blade. A Dremel tool with 1 mm thick circular blade was used to scribe each specimen along its length. Each scribe line was cut by positioning the blade at 90 degree angle penetrating the coating and scratching the bare metal surface. Scribe lines were approximately 3 cm in length positioned clear from the specimen edge or hole. FIGURE 3.19 shows scribed specimens for each coating type.

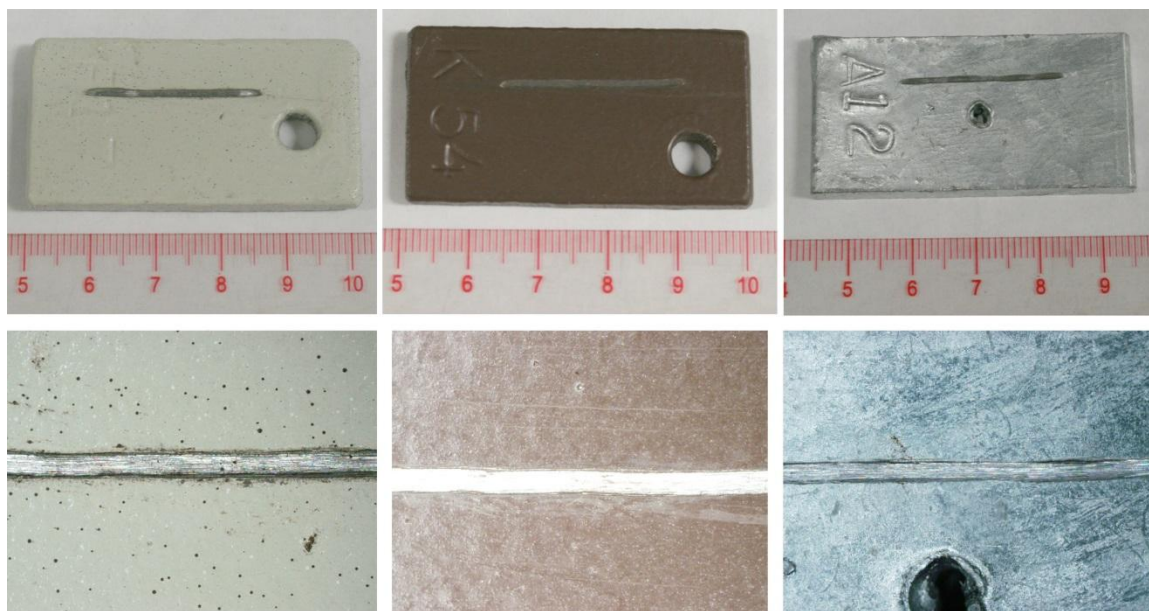


FIGURE 3.19: Scribed painted, epoxied, and galvanized specimens, from left to right

Throughout the duration of the test, specimens were exposed to 3% concentration of sodium chloride solution and deionized water as the control. Test specimens were cycle between wetting and drying for eight weeks. The test matrix used the modified SHRP method to dunk the specimen in test solution for two minutes follow by atmospheric drying for two hours. The same dunking apparatus from the previous cyclic corrosion test was used for the test set-up. Coating systems were galvanized A36, painted A572, epoxy coated A572, and epoxy coated A588 steel. There were three replicates of each coating type. A total of 24 specimens were setup over eight test cells to accommodate the four different coating systems at 0% and 3% salt concentration. Each test cell contained three replicates of a particular coating and solution concentration. FIGURE 3.20 shows the test set-up with specimens hung from a lever arm that can lower and raise specimens in and out of the test container. The specimens were allowed to cycle for a period of eight weeks. Evaporation of test solutions was compensated for by



refilling test containers with deionized water to the original solution level. Photographs of each specimen were taken at the end of each week.



FIGURE 3.20: Scribe test set-up for cyclic wetting and drying corrosive exposure

At the end of the eight week test period, specimen coating was removed to examine the corrosion of the substrate. Painted and epoxied coatings were removed by soaking the specimens in acetone followed by mechanical removal using a metal wire brush until the coating was cleared from around the scribed area. The specimen surface was rinsed and wiped clean using paper towel soaked in acetone. Galvanized specimens were cleaned by dissolving the galvanized layer in acid solution and then cleaned with acetone. The acid solution used contained 50 gram stannous chloride and 20gram antimony trioxide in 1,000 mL concentrated hydrochloric acid. Cleaned specimens were

examined and photographed using a microscope. The scribed area observed under microscope was 17.5 mm along the length of the scribed line. Imaging analysis was performed using the Olympus Stream Essentials software package.

Rating of undercutting at the scribe line for each coating system was determined based on areas of the substrate that were discolored due to corrosion. The software package used features the capability to capture and examine an area of 17.5 mm by 13 mm, which was the area used to examine the test specimen. Before capturing images of corroded specimens, the software was calibrated using a known length at a particular zoom of the microscope. Images of corroded specimens were captured at the calibrated zoom from a mounted camera on the microscope. The captured image was then imported to the software for analysis. Rust creepage areas were determined for each specimen by tracing the discolored corroded area around the scribe line and using the software to calculate the total area. The area calculated included the original area of the scribe line. FIGURE 3.21 shows the microscope and a screen shot of the tracing method used.

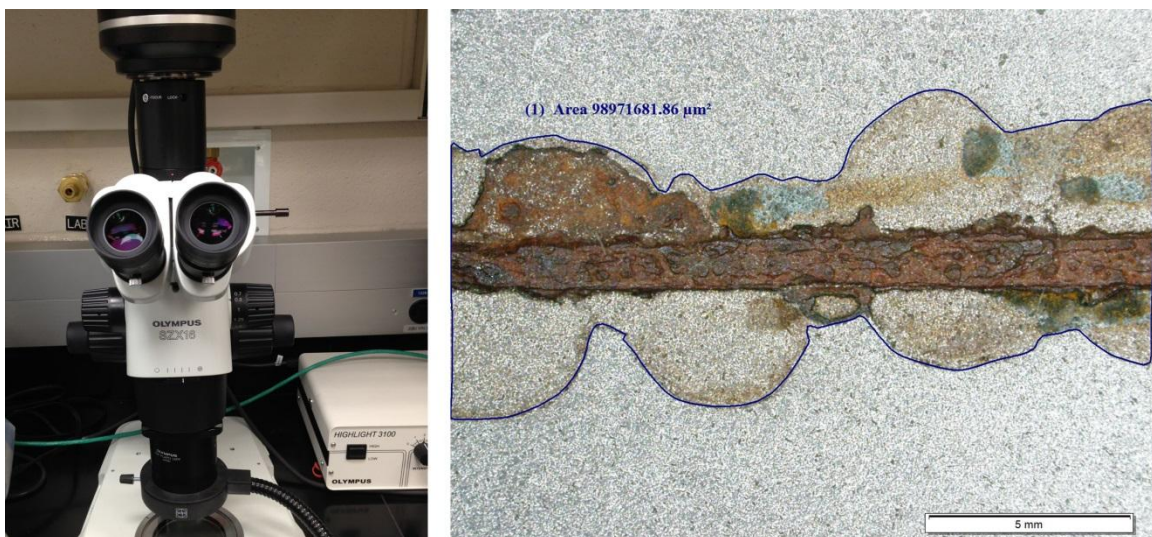


FIGURE 3.21: Corroded area determination using microscope captured image

The mean creepage was calculated based on ASTM D7087 from the obtained discolored areas and the analyzed scribe length using EQUATION 3.2. A rating number was determined for each coating system using the table provided in ASTM D1654. A replicate of the table is shown in TABLE 3.9. The rating number is used as a mean for comparison and is test-method specific.

The mean creepage was calculated as:

$$C = \frac{A}{2L} \quad (3.2)$$

Where:

$C$  = mean creepage (mm)

$A$  = area of creepage obtained by tracing (mm<sup>2</sup>)

$L$  = length of scribe line from which corroded area was integrated (mm)

(17.5 mm for this study)

TABLE 3.9: Rating table used based on ASTM D1654

Rating of Undercutting at Scribe Using Mean Creepage	
Millimeters	Rating Number
Zero	10
Over 0-0.5	9
Over 0.5-1.0	8
Over 1.0-2.0	7
Over 2.0-3.0	6
Over 3.0-5.0	5
Over 5.0-7.0	4
Over 7.0-10.0	3
Over 10.0-13.0	2
Over 13.0-16.0	1
Over 16.0 to more	0

### 3.4.2 Results

Weekly images of the specimen after exposure to the test solutions are presented in FIGURES 3.21 and 3.22 for 0% and 3% sodium chloride concentrations. Images selected for the figure were of the visibly worst specimen condition out of the three replicates. Similar corrosion progression was observed for the remaining two replicates.

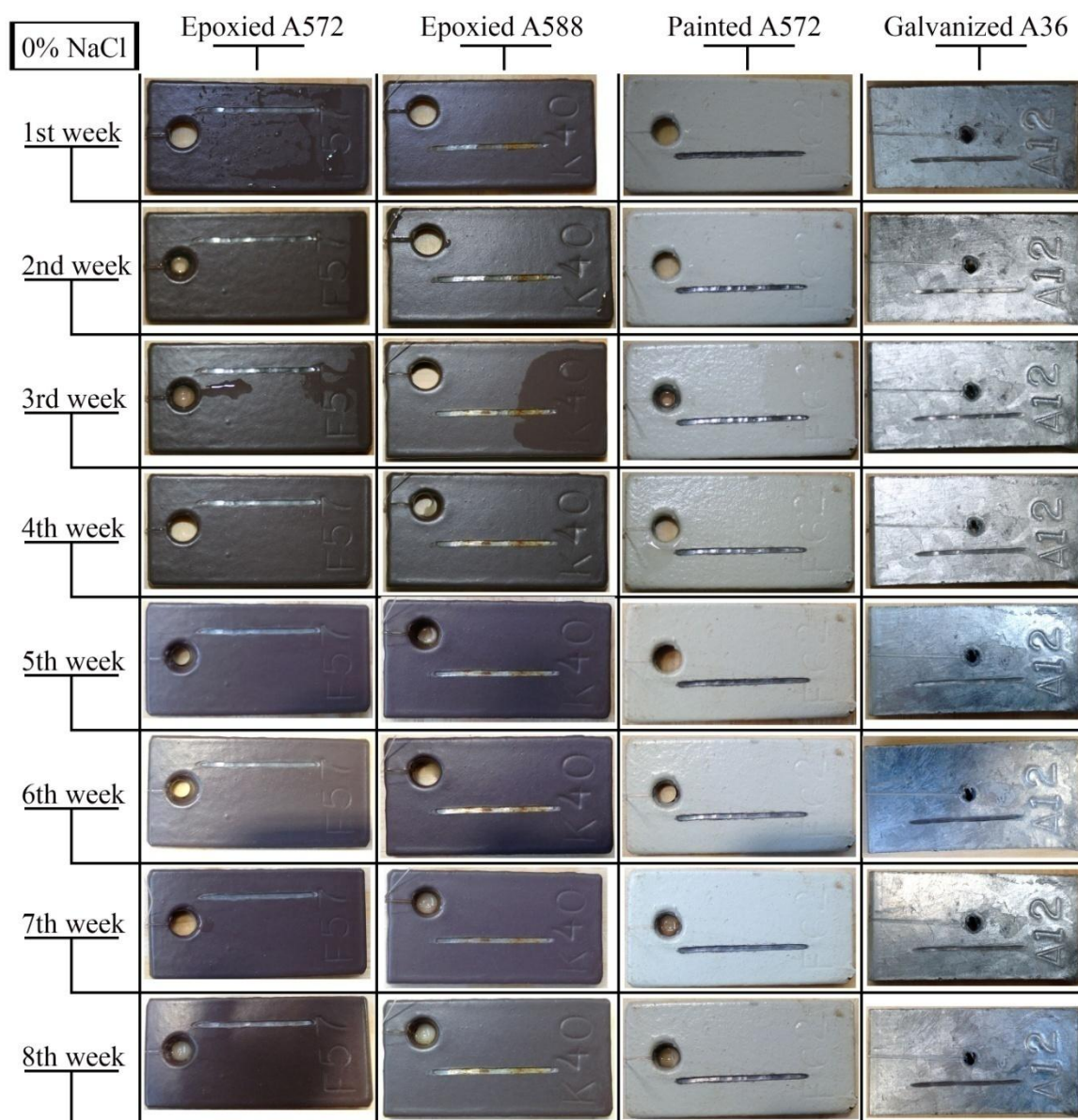


FIGURE 3.22: Weekly images of coated specimens in deionized water



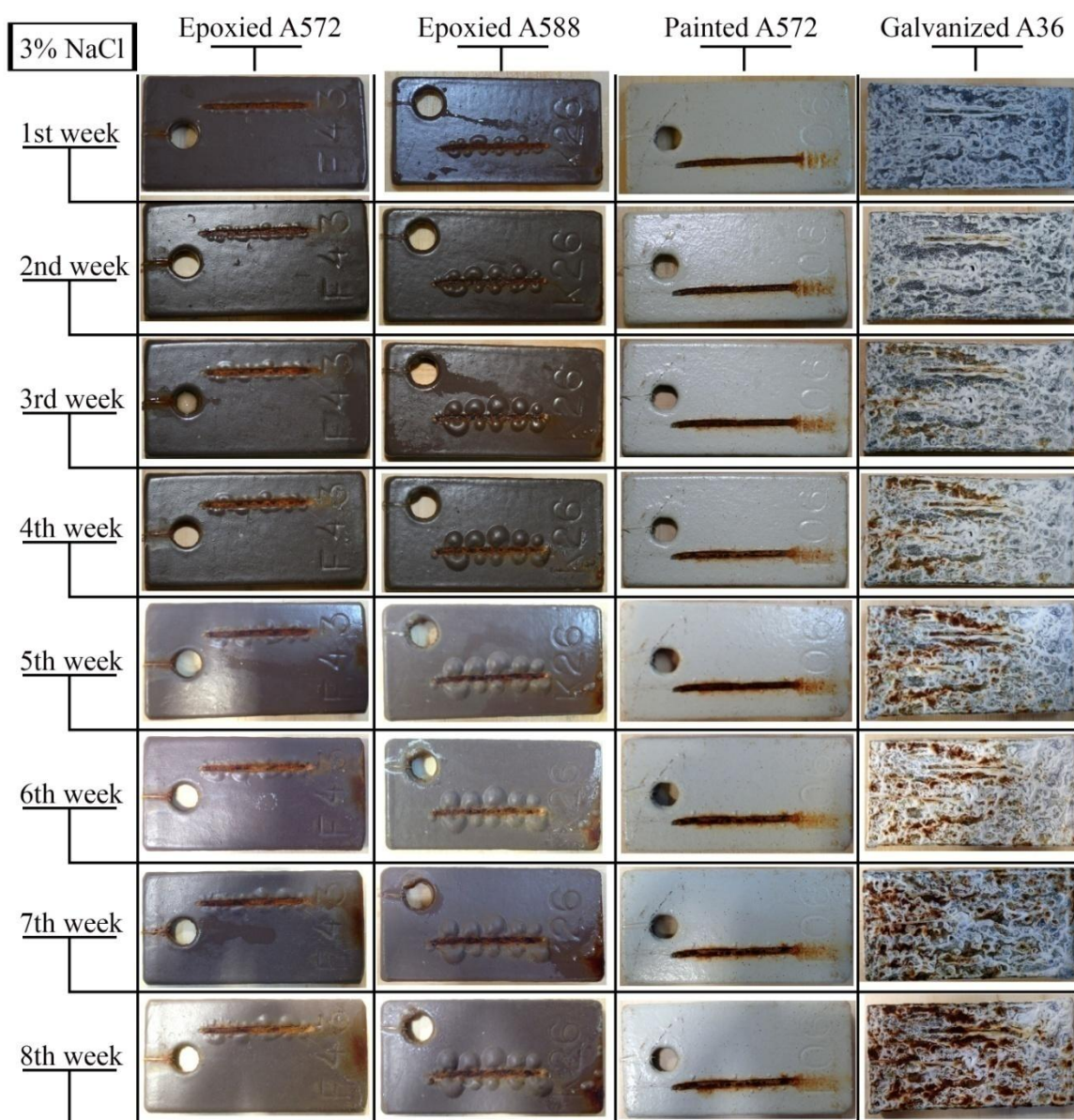


FIGURE 3.23: Weekly images of coated specimens under 3% NaCl

No coating damage was observed for the 0% deionized water control solution in all four coating systems over the entire eight weeks test period of this study. Slight rust discoloration was observed at the scribe line for epoxied A588; however, no progression of corrosion was observed with increased exposure time in deionized water. Coated specimens in 3% NaCl test solution showed corrosion damage for all four coating

systems. In particular, coating blistering was observed for both epoxied and painted specimens. Evaluation of blisters was based on the ASTM D714 standard for evaluating degree of blistering of paints (ASTM 2009). The blister sizes were assigned a numerical value on a scale from 10 to 0, where 10 indicates no blistering and 8 represents the smallest size that can be seen by unaided eye. A four step scale was used for blister size; with 8, 6, 4, and 2 assigned as the blister size get larger. Frequency was rated also on a four step scale consisting of few, medium, medium dense, and dense.

TABLE 3.10 below shows the size and frequency rating for epoxied and painted specimens exposed to 3% NaCl. Blistering was seen only along the scribe line and no blistering was observed at other coating surfaces. For reference, a number 2 rating corresponds to a blistering size of 2.5 mm or above in diameter. Observation of blisters in various coatings indicates that epoxy on A588 steel is the most susceptible out of the three coating systems followed by epoxy on A572. The best coating system was observed to be paint on A572 with respect to blistering damage.

TABLE 3.10: Size and frequency rating for blistering of epoxied and painted specimens

3% NaCl	A572 P		A572 E		A588 E	
	Size	Frequency	Size	Frequency	Size	Frequency
Week 1	10	n/a	8	Medium Dense	6	Medium Dense
Week 2	10	n/a	6	Dense	4	Medium Dense
Week 3	10	n/a	6	Dense	2	Dense
Week 4	8	Few	6	Dense	2	Dense
Week 5	8	Medium	6	Dense	2	Dense
Week 6	8	Medium	6	Dense	2	Dense
Week 7	8	Medium	6	Dense	2	Dense
Week 8	8	Medium Dense	6	Dense	2	Dense

Unlike the epoxied and paint specimens that show corrosion only occurring around the scribe line, galvanized A36 specimens experience a wider area of corrosion across the galvanized surface. Since the galvanized coating is a zinc metal layer, it is designed to naturally corrode as a sacrificial coating. Image results of galvanized specimens show a clear progression of corrosion on the galvanized layer with time. The image also indicates that more corrosion occurred toward the upper end of the specimen where more brownish discoloration can be seen. Unlike the upper end, the bottom end experienced more exposure to the test solution with longer wetting period due to gravitational flow from the upper end. Build-up of white byproducts can also be seen concentrated toward the bottom end of the specimen. The build-up of insoluble products that form are a potential combination of crystalized salt and zinc patina or corroded zinc byproducts. The build-up of byproducts creates an impervious layer that slows the corrosion of the zinc, which could explain why the bottom end is less corroded. FIGURE 3.24 shows microscope images at the scribe line of three galvanized specimens at the end of eight weeks exposure. With the galvanized layer removed, little corrosion is seen on the scribe line; instead most of the corrosion occurred on the zinc layer with remnants of corrosion products throughout the specimen surface. Due to the protective galvanized layer, little to no corrosion is seen on the base metal surface outside of the scribe line.

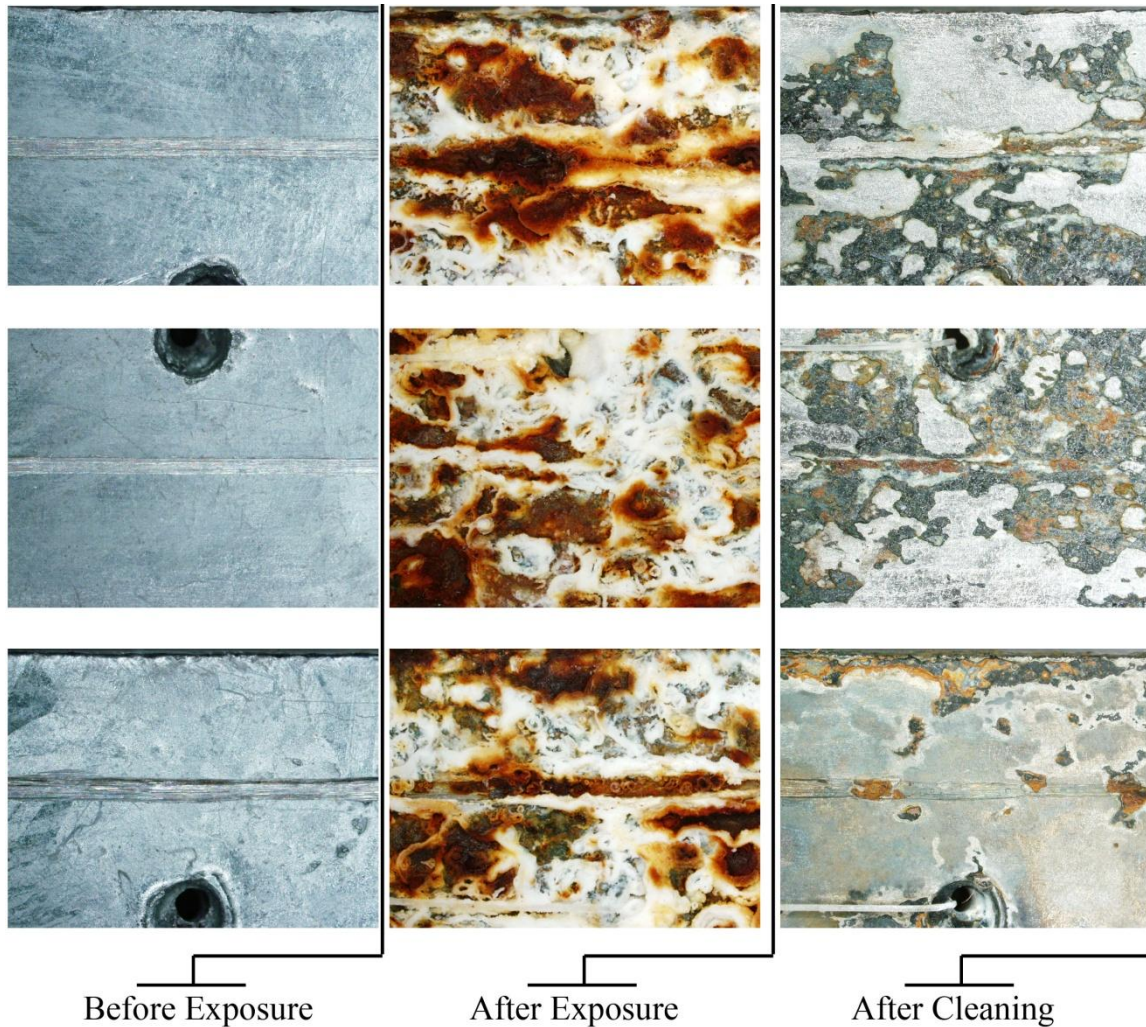


FIGURE 3.24: Microscope images of galvanized specimens

Calculations of mean creepage for scribed epoxy coated and painted specimens were calculated based on the rust areas under the coating and the scribe length of 17.5 mm using EQUATION 3.2. Captured images of rust areas after removal of epoxy and paint coatings are shown in FIGURE 3.25 to 3.26. Results of rust area, mean creepage, and rating of failure at scribe are shown in TABLE 3.11 for three specimens of each coating system. Rating numbers were determined based on TABLE 3.9. The rating ranges from 0 to 10, with 10 being the highest rating indicating zero rust creepage under



the coating. Rating numbers were consistent for all three specimens with painted A572 having the highest coating performance with a value of 8 follow by epoxied A572 at 6 then epoxied A588 at 5.

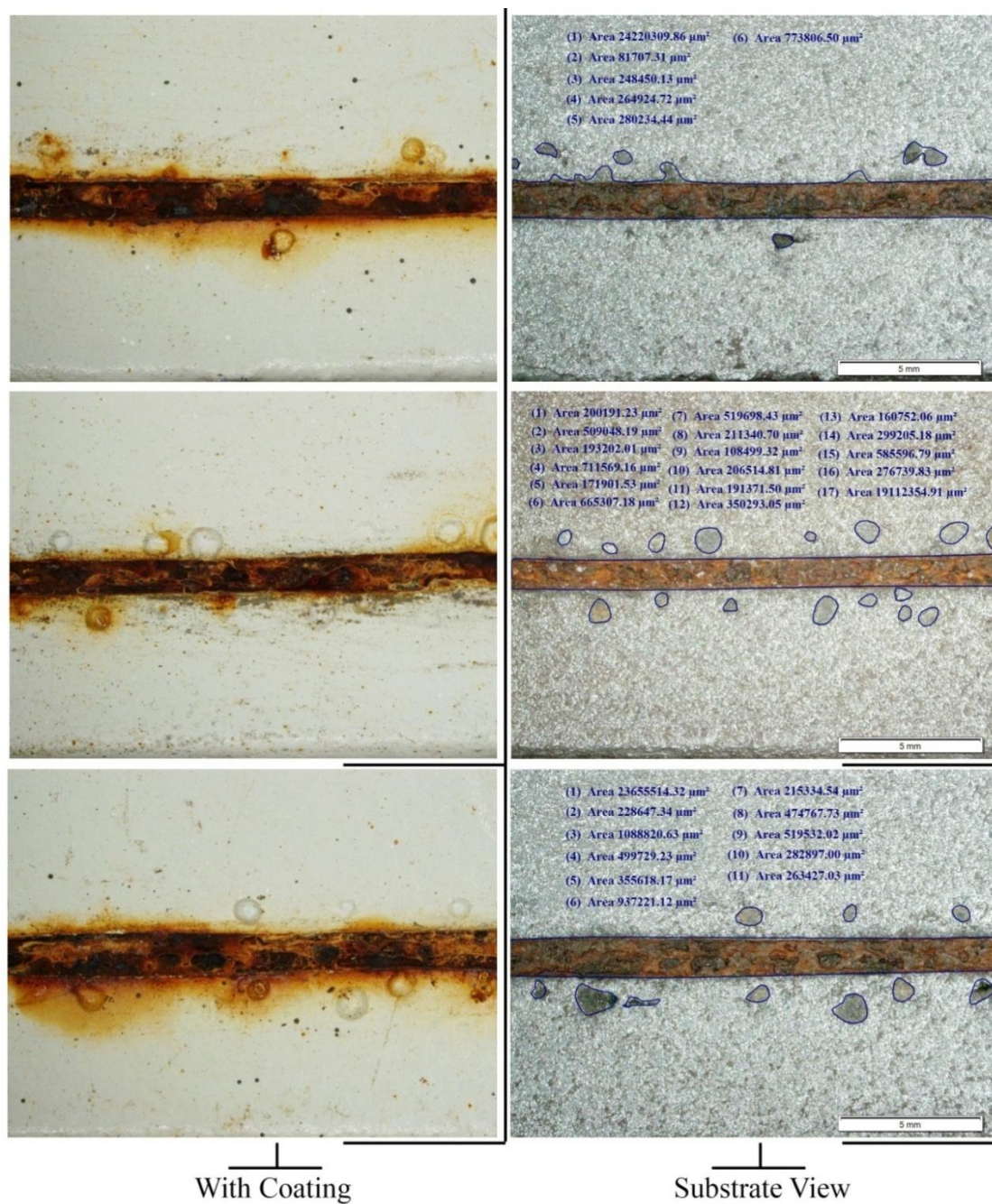


FIGURE 3.25: Microscope images of painted A572 specimens



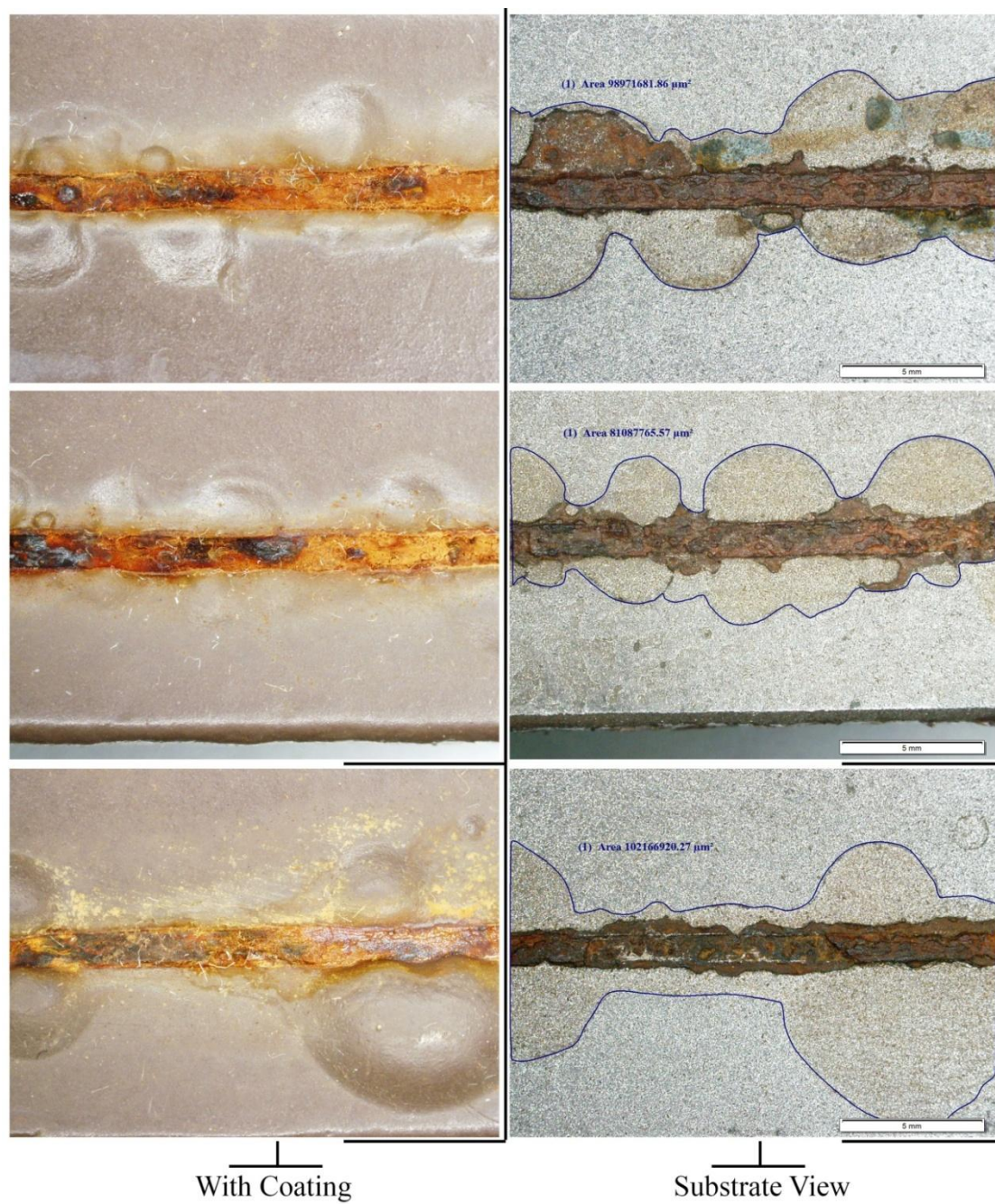


FIGURE 3.26: Microscope images of epoxied A572 specimens



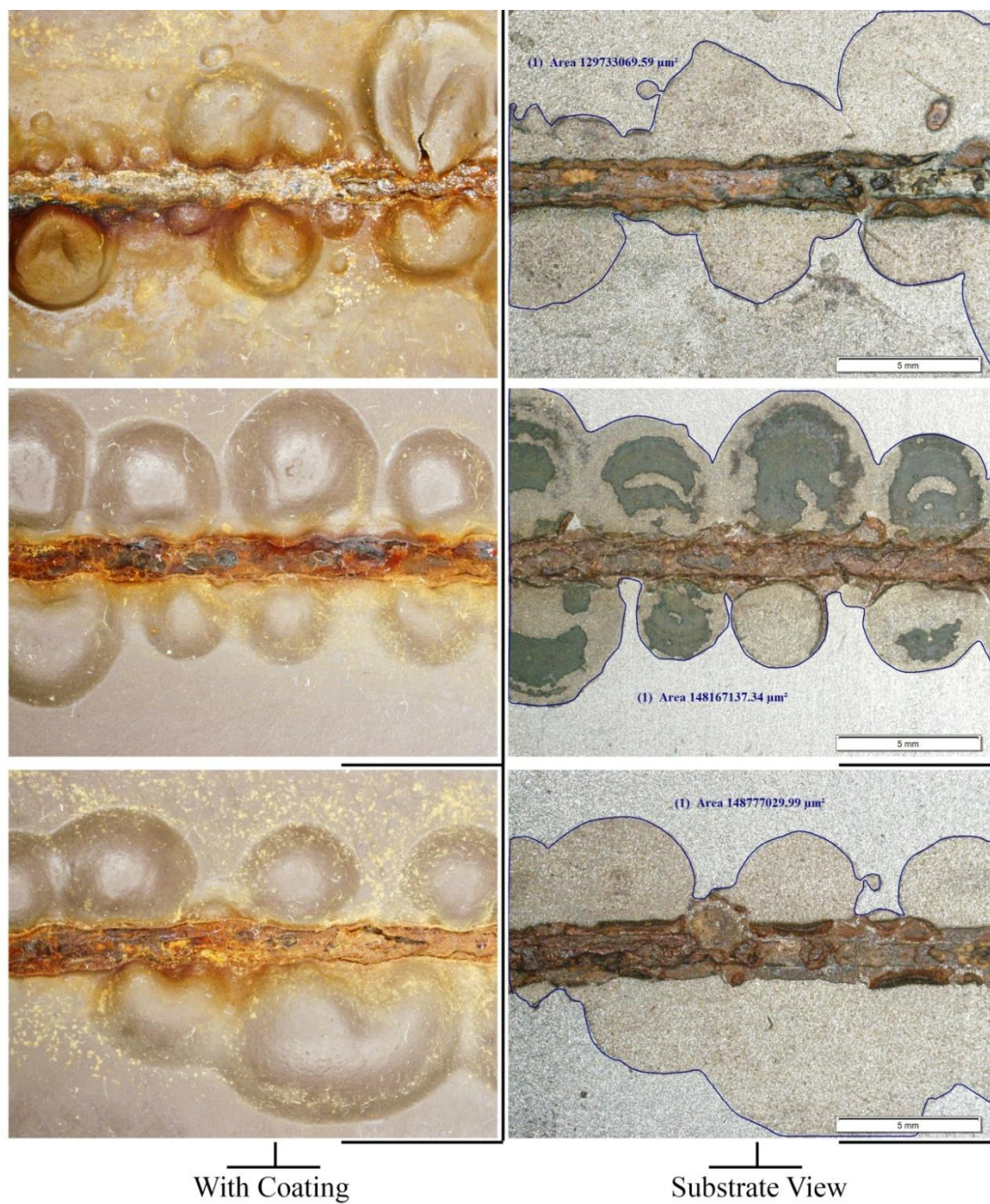


FIGURE 3.27: Microscope images of epoxied A588 specimens

TABLE 3.11: Result of scribe test for painted and epoxied specimens

Specimen Number	Rust Area (mm <sup>2</sup> )	Mean Creepage (mm)	Rating
Epoxied A572			
F11	81.09	2.31	6
F13	102.17	2.92	6
F43	98.97	2.83	6
Painted A572			
F74	24.47	0.70	8
F12	28.52	0.81	8
F06	25.87	0.74	8
Epoxied A588			
K54	129.73	3.70	5
K39	148.78	4.25	5
K26	148.17	4.23	5

The result of the laboratory program indicated that painting of exposed bridge steel should be preferred over epoxy coating. The performance has been shown to be better for both blistering and mean creepage. However, the study is limited to laboratory conditions where actual environmental factors were not considered. Further research and field performance monitoring is advised prior to making changes in maintenance policy.

## CHAPTER 4: FIELD SAMPLING OF CORROSIVE LOSS ON BRIDGE GIRDERS

To generate quantitative data for evaluating the impact of sodium chloride deicing and anti-icing application strategies on the transport of chlorides and associated corrosive losses observed on bridge girders, a field test program was conducted on a sample of nine bridges in North Carolina. The study was conducted over one winter season for selected bridges in the Greensboro and Asheville regions. This chapter presents the methodology and experimental results obtained from installation of sacrificial steel coupons on girder components under typical field exposure conditions at specific locations across the bridges in the study. The field installation of samples replicates natural factors that cannot be readily simulated under laboratory conditions and produces spatial data on the superstructure elements most susceptible to corrosive damage under each of the sodium chloride treatment strategies. Statistical analysis of material losses in the field samples is presented to evaluate predominant factors associated with corrosive loss in superstructure elements exposed to deicing and anti-icing solutions in normal service conditions.

### 4.1 Details of Experimental Test Program

Steel specimens used were 3/16 inch thick, uncoated A36 steel bar stock with dimensions of 23.5 inches in length and 2 inches in width (FIGURE 4.1). Prior to cleaning, each specimen was stamped with an identification number for reference. Surface preparation of the specimens included sand blasting to achieve a uniform gray metal surface followed by cleaning with acetone to remove corrosive ions and surface

contaminants. The samples were weighed to the nearest 0.01 gram prior to installation in the field.

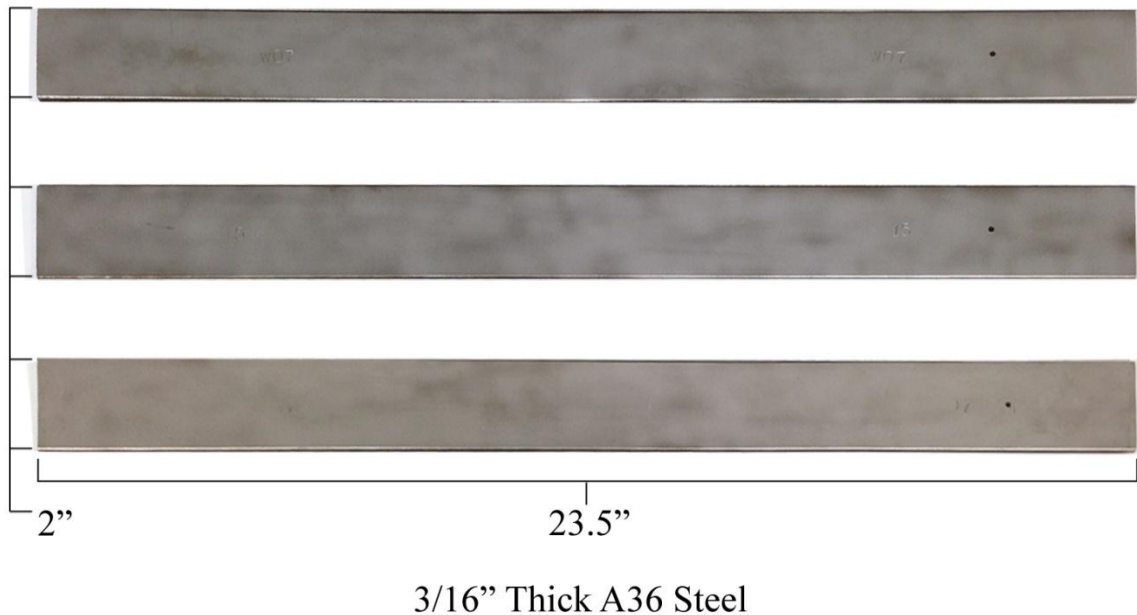


FIGURE 4.1: Steel specimens prepared prior to installation on bridge girders

Field installation sites were selected at both exterior and interior girders (FIGURE 4.2). At each exterior and interior girder location, sample specimens were mounted on both the web and bottom flange of the girders, designated as exterior for exposure toward the outside and interior for exposure on the inside under the bridge deck (FIGURE 4.3).



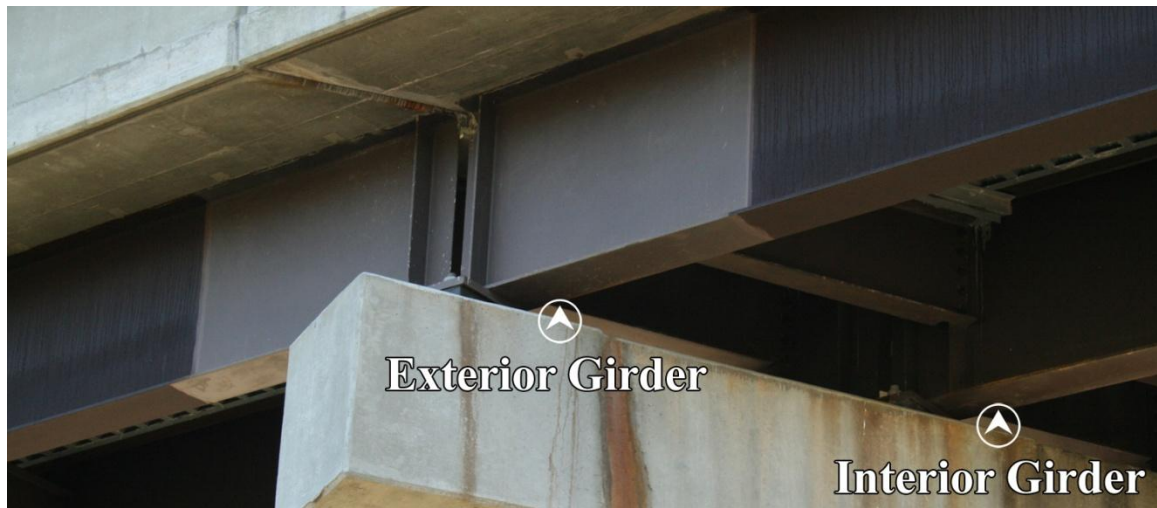


FIGURE 4.2: Testing sites for atmospheric exposure of metal coupons



FIGURE 4.3: Coupons placement and location for atmospheric exposure

Circular ceramic magnets were used to attach the specimens to the bridge girders. Prior to attachment, each steel sample was wiped with de-natured alcohol to remove any residual chloride introduced during handling in the field. The sacrificial coupons were installed at the end of November 2012 and collected at the beginning of March 2013 to capture corrosive effects over one representative winter season. The selected set of

bridges included six bridges in Greensboro and three bridges in Asheville. The deicing applications applied to each bridge were obtained from NCDOT reports that designated the treatment type and number of treatments applied. A summary of the report is presented in TABLE 4.1. This sampled set of bridges included: three bridges receiving four applications of granular deicing treatment in Greensboro, three bridges receiving two applications of anti-icing brine and two applications of granular deicing treatment in Greensboro, and three bridges receiving eight applications of salt-sand mix deicing treatment in Asheville.

TABLE 4.1: Deicing application data for all bridges

Bridge Locations		Brine	Granular	Total
Greensboro	NC 62 over I-85	2	2	4
	Vickery Rd over I-85 Business	0	4	4
	Mt Hope Church Rd over I-40	0	4	4
	US 220 NB over NC 62	2	2	4
	McConnell Rd over I-40	0	4	4
	NC 62 over 421	2	2	4
Asheville	SR 1684 over US 19,23,70	0	0	8
	SR 2207 over US 19,23	0	0	8
	SR 2531 over I-40	0	0	8



## 4.2 Corrosive Losses Measured by Location

The sacrificial steel coupons were collected after exposure from one winter season. Visual images of corroded steel specimens are shown in FIGURE 4.4 for Greensboro bridges and FIGURE 4.5 for Asheville bridges. Overall, steel specimens retrieved from Asheville were more heavily corroded than those from Greensboro. This is expected since the number of salt-sand deicing treatments was twice as much. The amount of observed corrosion also indicates that for Asheville bridges, specimens mounted on webs of exterior girders were visibly more corroded than those mounted on interior girders. Most specimens mounted on the web of interior girders showed partial corrosion with one end more heavily corroded than the other, where for exterior girders full surface corrosion was observed. This difference in the spatial severity of corrosion may be linked to special transport phenomena. A plausible conclusion from these differences in corrosion severity along the height of the specimens is that the transport of chlorides through the expansion joint down to surfaces of the interior webs is different than the transport of chlorides across the surface of exterior girders. Specimens mounted on the flange for Asheville bridges showed a significant amount of corrosion for both exterior and interior girders. Specimens mounted on flange locations for Greensboro bridges also showed higher corrosion compared to those mounted on web locations. Minimum surface corrosion was seen on specimens installed on the webs of exterior girders for granular salt application and the web of interior girders for brine pretreatment with granular salt.
















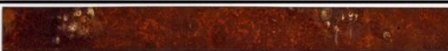
































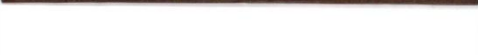

Greensboro Bridges:		Granular salt	Brine + Granular salt
Location	Exterior Girder		
Web-exterior			
			
			
			
			
Web-interior			
			
Flange-exterior			
			
			
Flange-interior			
			
			
Interior Girder			
Web-interior			
			
			
			
			
			
Flange-interior			
			
			
			
			
			

FIGURE 4.4: Corroded steel specimens for Greensboro bridges prior to cleaning


















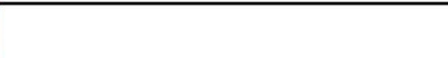














Asheville Bridges:		Salt-sand mix	
Location	Exterior Girder		
Web-exterior			
			
			
			
Web-interior			
			
			
			
Flange-interior			
			
Interior Girder			
Web-interior			
			
			
			
			
Flange-interior			

FIGURE 4.5: Corroded steel specimens for Asheville bridges prior to cleaning

Exposed test specimens were cleaned and reweighed according to ASTM G1 standard practice for preparing, cleaning, and evaluating corrosion test specimens (ASTM 2003). The cleaning process included wetting and mechanical removal of corrosion byproducts using a wire brush followed by ultrasonic cleaning in acid solution, then sand blasting. The acid solution used consisted of stannous chloride, antimony trioxide, and concentrated hydrochloric acid. The mass loss of each specimen after cleaning was

measured and the corrosive loss was determined by comparing the original mass to the mass of the cleaned corroded steel. To compensate for the mass loss of base metal due to the cleaning process alone, an unexposed and un-corroded specimen was cleaned using the same cleaning procedure. Control mass loss during acid cleaning and sand blasting were determined as 0.40 gram and 0.22 gram, respectively. These mass losses due to cleaning were then used as an adjustment factor when determining the mass loss in field specimens due to corrosion only. Mass losses recorded for 71 sacrificial coupons that were retrieved from the field are shown in TABLE 4.2 in grams. The average recorded mass loss by location with respect to the treatment type in Greensboro and Asheville bridges are shown in TABLE 4.3 and FIGURE 4.6. The calculated percentages are based on the mass loss with respect to the original coupon mass. It is important to note that Asheville bridges received twice the number of applications as Greensboro bridges which likely explains an overall higher average mass loss observed at all locations, with the exception of the web of interior girders.

TABLE 4.2: Mass losses for field samples after adjusting for cleaning controls

Location	Greensboro Bridges						Asheville Bridges		
	G1	G2	G3	G4	G5	G6	A1	A2	A3
<b>Exterior Girder</b>									
Web-exterior	1.50g	0.42g	0.48g	5.60g	1.00g	1.38g	3.18g	7.30g	11.40g
Web-exterior				5.24g		1.34g	2.22g	8.18g	7.40g
Web-exterior									5.34g
Web-exterior									11.20g
Web-interior		0.28g	0.54g			0.02g	4.54g	4.84g	9.66g
Web-interior						2.94g	4.92g	4.02g	
Web-interior									6.84g
Web-interior									8.68g
Flange-exterior	4.10g	2.84g	2.88g		2.68g				
Flange-interior	1.90g	2.42g	4.04g	1.12g	2.84g		5.86g	5.02g	
<b>Interior-Girder</b>									
Web-interior	0.42g	-0.04g	4.00g	0.36g	0.92g	0.84g	1.52g	5.78g	0.50g
Web-interior	0.54g		0.68g	2.54g	8.32g	0.50g	1.12g	3.30g	2.00g
Web-interior							1.28g	4.66g	
Web-interior							2.14g	3.28g	
Flange-interior	2.42g	1.34g	0.32g	1.10g	2.42g	1.82g		12.70g	
Flange-interior	1.46g		0.64g	7.74g	2.84g	3.72g			

\*Empty cells imply no coupon was mounted

TABLE 4.3: Average mass loss and loss as a percentage of original mass for all treatment types

Location	Exterior Girder, Exterior Web	Exterior Girder, Interior Web	Exterior Girder, Exterior Flange	Exterior Girder, Interior Flange	Interior Girder, Interior Web	Interior Girder, Interior Flange
Greensboro Granular Salt (4 Applications)	0.63g (0.053%)	0.41g (0.034%)	2.80g (0.236%)	3.10g (0.261%)	2.78g (0.234%)	1.51g (0.127%)
Greensboro Granular & Brine (4 Applications)	3.01g (0.253%)	1.48g (0.125%)	4.10g (0.345%)	1.51g (0.127%)	0.87g (0.073%)	3.04g (0.256%)
Asheville (8 Applications)	7.04g (0.593%)	6.21g (0.523%)	n/a	5.44g (0.459%)	2.56g (0.216%)	12.68g (1.07%)



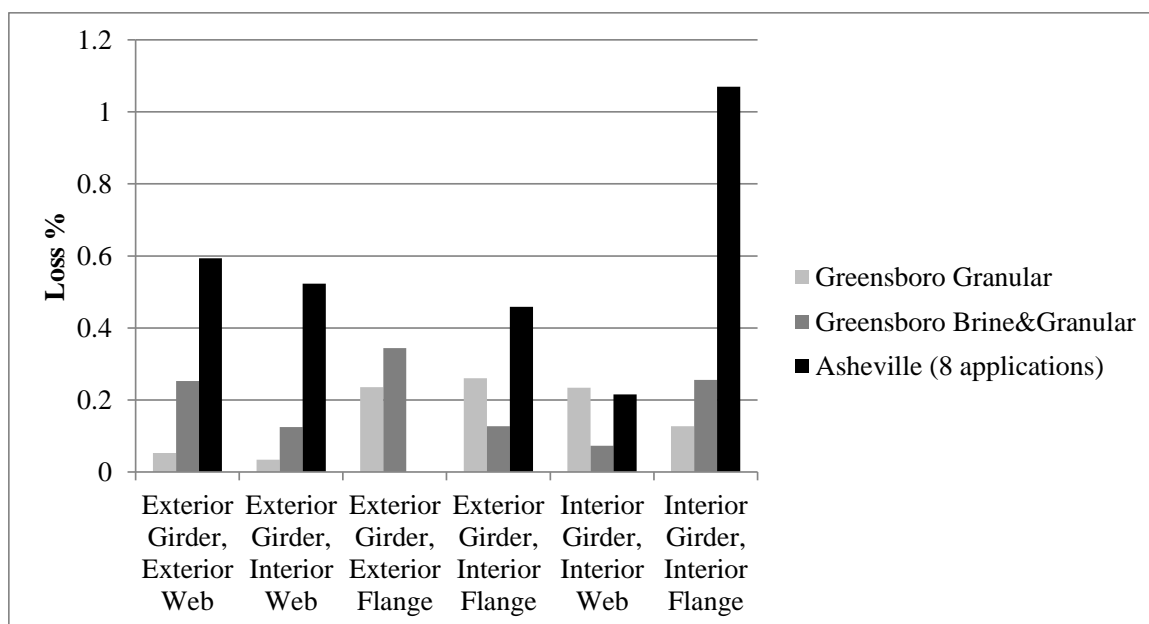


FIGURE 4.6: Average percent losses for girder locations and treatment types

The test results show that for the three different deicing treatments the average corrosive losses across all testing locations are 0.158% for four granular salt applications, 0.197% for two granular applications and two brine applications, and 0.572% for eight salt-sand deicing applications. When normalized to per application, the corresponding results are 0.0395% for granular salt, 0.0493% for brine anti-icing followed by granular deicing, and 0.0715% for salt-sand deicing mix. In term of spatial susceptibility of superstructure components, specimens installed on flanges were found to experience about 1.5 times more corrosive loss compared to those on webs after comparing the average corrosive losses across all flange and web locations. Additionally, the highest overall corrosive mass loss was found at the interior flange of the interior girder. This measurement was taken on a bridge with an expansion joint in poor condition, so it is

expected that the interior girder experienced higher chloride concentrations from gravity directed flow of deicing treatment from the treated lane on the deck above. Bridges receiving only granular treatment in Greensboro exhibited the highest corrosive loss at interior flanges of the exterior girders with an average of 0.0653% loss per application. Likewise, bridges receiving both granular treatment and brine anti-icing in Greensboro exhibited the highest corrosive losses at the exterior flanges of exterior girders with an average of 0.0863% per application. Lastly, bridges receiving salt-sand deicing in Asheville exhibited the highest corrosive losses at the interior flanges of interior girders with an average of 0.134% per application. In the case of Asheville bridges, no sample was retrieved for exterior flanges of exterior girders. However, from field observations the appearance of corrosion on the exterior and interior flange surface of exterior girders is similar. In all three treatment scenarios, the higher corrosive losses measured at the flange locations relative to the web locations reinforce expected concerns related to corrosion across the bottom flange of girders. This is a rational finding since the bottom flange of a girder is a horizontal surface that can easily collect corrosive run off from the bridge deck and splash-up of chloride-laden mist from below deck traffic. It is also correlated with field observations during bridge inspections. However, even though the results show that the flange yields the highest corrosive loss, these findings are based on a limited sample size for the flange location and corrosive losses were recorded across the webs of the girders.

In the case of Greensboro bridges, which were reported as receiving either four applications of granular salt or four applications of granular salt with brine, there is an overall higher corrosive loss on bridges receiving granular salt with brine pre-treatment.

Computing the average total mass losses at all the test locations, the overall mass loss for bridges receiving both brine and granular treatment is 1.25 times that of those receiving granular treatment alone. Supporting this trend, higher corrosive loss from the combination of brine and granular salt applications can be seen at four out of six test locations. The exceptions are interior flange locations at exterior girders and interior web locations at interior girders where granular treatment alone exhibited higher loss.

#### 4.3 Statistical Analysis of Probable Significant Factors

Further study of the experimental data with the functional properties of the bridges and locations of the specimens were performed using the MiniTab statistical regression and modeling software package. The software was used to examine factors that may significantly affect the corrosive losses of steel bridge components in addition to the significance of the deicing or anti-icing treatment strategy employed. Factors that were considered included bridge age, under clearance height, traffic count, railing type (open or solid), deck joint condition rating, and traffic direction (whether the test location was facing oncoming traffic below the bridge). This functional information was obtained from NCDOT bridge inspection reports along with observations recorded during field work. The corrosive mass losses were normalized to losses per application for the analysis by dividing by four for Greensboro samples and eight for Asheville samples.

FIGURE 4.7 presents the independent effects or main effects for each of the factors on the mean corrosive mass loss in grams, with the overall mean represented by the horizontal line. The collection of plots show the average corrosive loss associated with each factor independently, which can be used to evaluate whether there is a likely significant effect on the average amount of corrosive mass loss linked to that factor. For



instance, the main effects plot for railing type indicates that regardless of whether the railing on the bridge was open or solid there was no significant effect on the amount of corrosion since there is no statistically significant difference in the average corrosive loss measured in either case. Similarly, whether the sample is facing oncoming traffic or not did not produced a significant effect on average mass loss, since this plot also exhibits a flat slope. In both cases, the small variation can readily be attributed to error and uncertainty in the sampling, interaction effects from other factors, and the limited sampling size. In contrast, the main effects plot for sampling location is useful in identifying which locations experience the most corrosive loss. The highest mean corrosive loss is associated with the exterior flange follow by exterior web, interior flange, then interior web surfaces.

The plot for application types reveals that salt-sand mix treatments in Asheville produced the highest average corrosive losses follow by bridges receiving brine with granular treatment then granular treatment alone. Plots of other factors including bridge age, traffic count, and clearance indicate that there are significant effects associated with each factor. The traffic count in particular indicates that with low traffic count there is an overall higher corrosive loss; however, a clear trend cannot be implied over the entire range for traffic count. Similarly for the others factors, only a particular condition within the range seemed to promote higher corrosive mass loss.

The main effects plots can provide useful indications of general trends associated with each condition within each factor; however, it lacks consideration of the interaction amongst factors on the corrosive loss observed. Also, bias from the data set could arise from grouping of conditions that may isolate only a particular bridge or set of bridges. A

good example of this effect can be seen in the plot for deck and joint condition that implies that there is a slightly higher average mass loss on bridges with “good” rating compared to “fair” and “poor”. While statistically this may be the case, since the main effects plot takes into consideration all the average effects from all other factors, such a conclusion can be misleading. In other words, the data may show that there is a higher overall loss for “good” deck rating, but this may not be true for each individual factor. Interaction effects between other factors that may be more significant can skew the overall average and mask the actual relationship between joint conditions and expected corrosion losses.

The interaction effects model was developed to take into consideration the effect of multiple factors and how those factors act together to influence the corrosive mass loss. The matrix of resulting interaction effect plots is presented in FIGURE 4.8. An interaction plot is also useful in separating out the more influential variables in instances where several significant effects interact producing a main effects plot that can be misleading, especially when the differences in individual effects is large. There are no interaction effects between two factors when the plot shows relatively horizontal lines from one condition to another within a factor plotted against another factor. The horizontal lines indicate that the main effect is neither increasing nor decreasing for each condition. Due to limited collected data, certain interaction plots are incomplete for particular conditions where the data is too sparse and thereby determination of a comprehensive analysis of interaction was not possible.

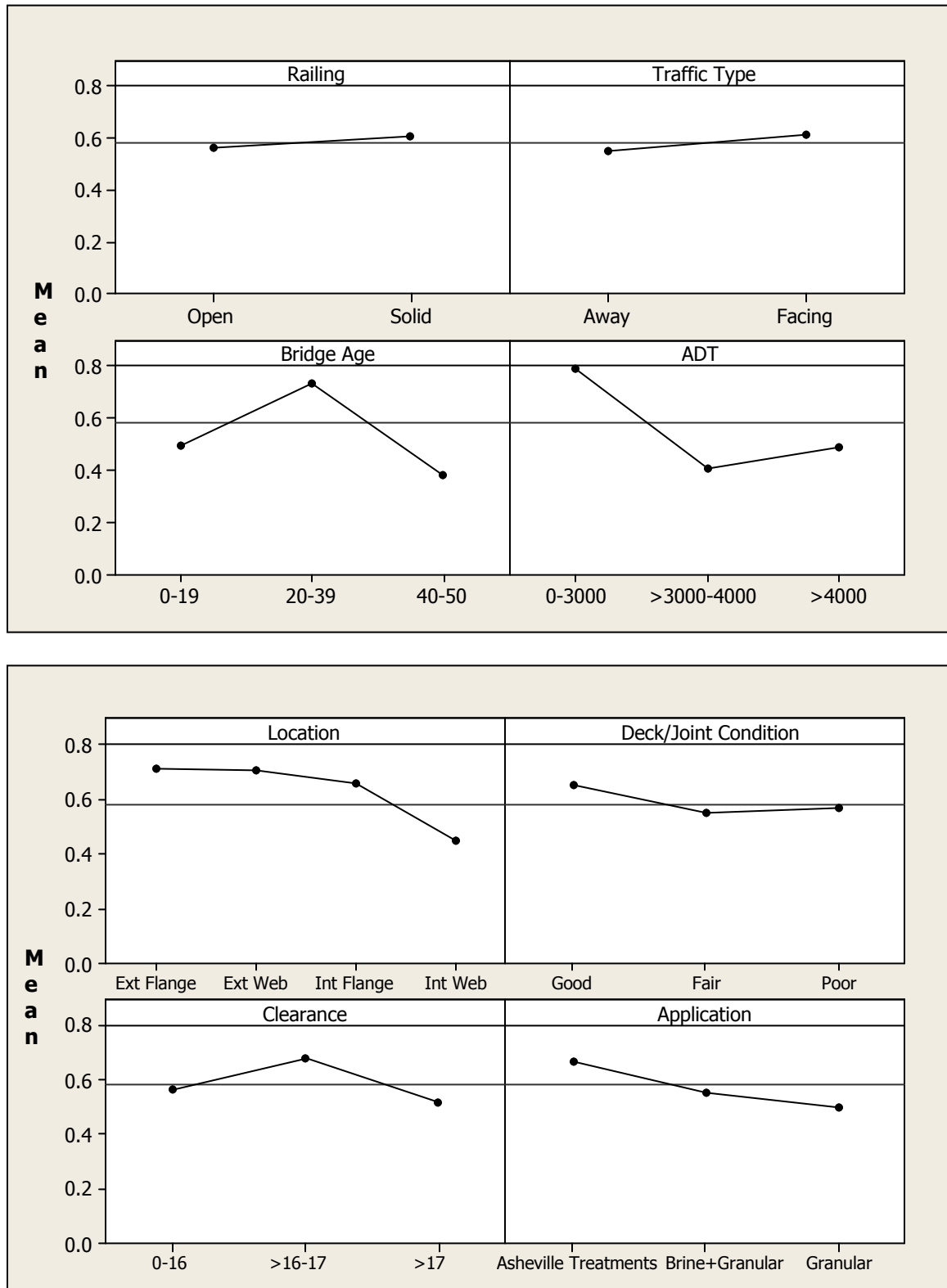


FIGURE 4.7: Main effects plots for explanatory factors on mean corrosive loss in grams

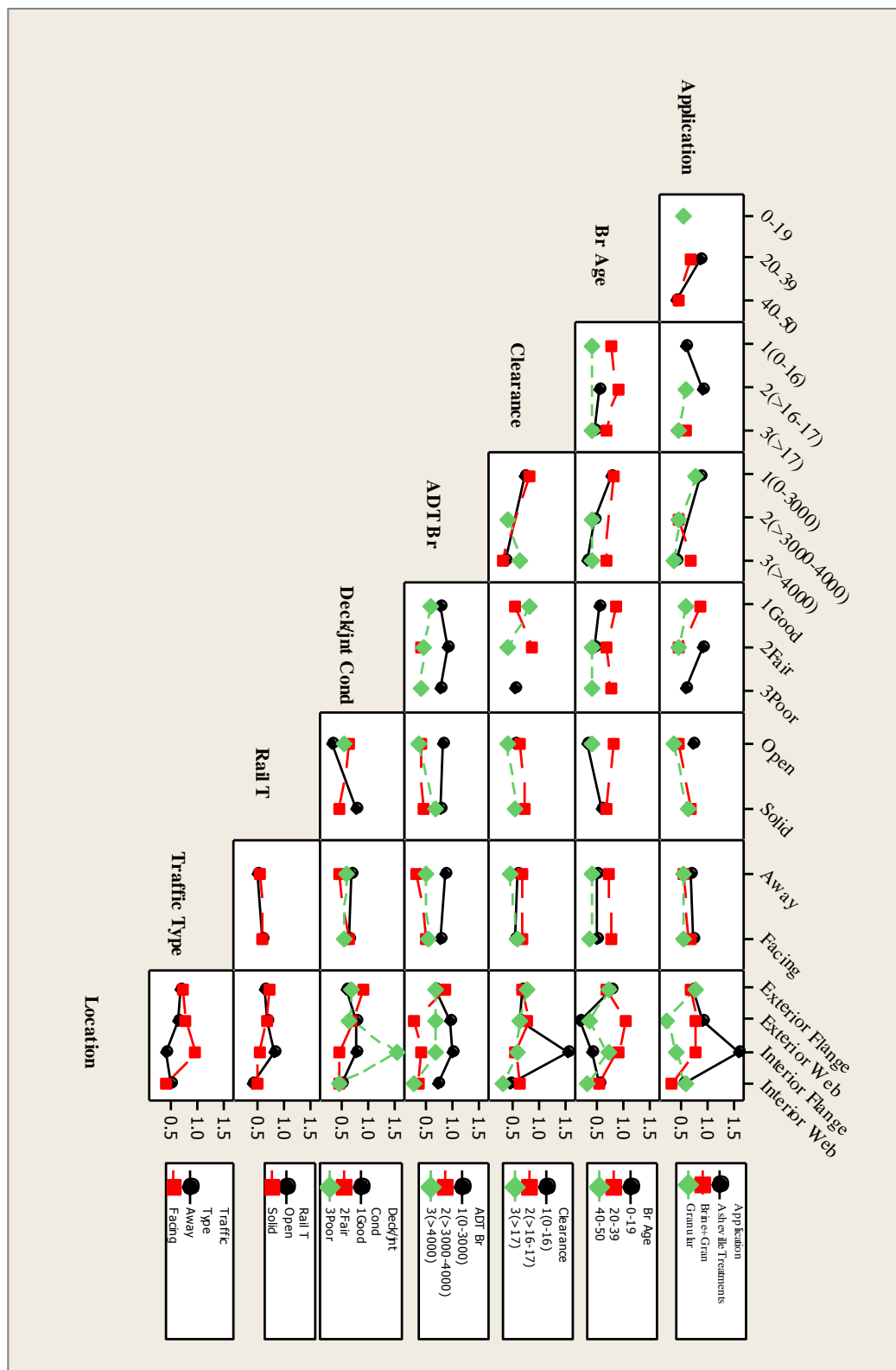


FIGURE 4.8: Interaction effects of explanatory factors on mean corrosive loss in grams

The following list of factors identifies significant effects and interactions observed by the research team when interpreting the main effects and interaction effect plots from the statistical model:

Plausible effects supported by expected responses:

- Traffic type by location interaction: there is little to no interaction effect for traffic type with the other factors except location. Traffic type by location shows that the components facing traffic have greater corrosive loss when the location is at an interior flange. This might be expected as vehicular traffic moving under the bridge may aid in the transport of chloride laden moisture to the superstructure components facing the traffic direction.
- Deck/joint condition rating by location interaction: although the main effects plot indicates a higher corrosive loss with joints in good condition, the interaction effects plot clearly shows that one of the most significant factors is joint condition and that bridges with poor joint condition exhibited markedly higher corrosive losses on the interior flange of girders, which is where the chloride build-up would be expected to occur if transported through the expansion joint. Note, however that the only bridges featuring poor condition ratings for the expansion joint were in Asheville, so this influence of condition rating can only be concluded for granular/salt-sand deicing mixes and should not be generalized yet to brine anti-icing applications without further experimental evidence.
- Application type: Salt-sand mix treatments in Asheville showed the highest corrosive loss, however the main effect is greatly skewed by a very large

average corrosive loss measured at the interior flange in the Asheville set of bridges. As noted, the bridges in Asheville also have more compromised expansion joints than those in Greensboro. Therefore, the larger measured rates of corrosion are not unexpected since the expansion joint is the primary route by which chlorides can transport to steel components below the deck. In the absence of this outlier, the salt-sand treatments in Asheville are comparable to bridges receiving application of brine pre-treatment and granular deicing. The lowest corrosive losses were measured on components of Greensboro bridges receiving only granular deicing applications.

- Average Daily Traffic: the main effects model indicates that lower traffic count is associated with greater corrosive loss for all deck conditions. This is expected as traffic can transport chlorides from the surface of the bridge. Residual concentrations and long-term corrosion may be higher for low ADT bridges. At high ADT, the effect is less for brine with granular application. The interaction effects model shows that when the joint condition is good, there is little difference in corrosive losses observed below the deck. However, for bridges with fair or poorly rated joints, the low ADT bridges are associated with significantly higher corrosive losses. Again, it is important to note that the set of bridges sampled only produced bridges with poor joint condition in Asheville, which received salt-sand mix. Therefore, too many conclusions should not be drawn from this statistical model without further study.

Unexpected effects:

- Age by rail type interaction: greater corrosive losses are observed in mid-range age bridges (20-39 years) for open rail type versus closed rail.
- Age by location interaction: mid-range age bridges (20-39 years) consistently exhibited the highest corrosive losses, with a particularly high difference in corrosive losses at web of exterior girders.

The interaction effects plot can help to identify the interaction of factors or predictors; however, when interpreting the interaction effect one must also consider the statistical significance of each predictor variable. A stepwise regression analysis is appropriate to identify a useful subset of predictors and to model the relationship between the response and predictors. In Minitab, a forward stepwise regression procedure starts with an empty model and progressively adds the most significant variable for each step until all variables not in the model have p-values that are greater than the specified alpha value. For each predictor, the statistical test computes a p-value that indicates the probability that the coefficient for the predictor is zero. A low p-value, typically less than 0.05 indicates that the associated explanatory variable is statistically significant to the model at the 95% confident level or better. The selected alpha value is 0.2, which will allow explanatory variables with p-value less than or equal to 0.2 to enter the model. It is important to note that a p-value can change when additional variables are added during the stepwise process. The method aims to create a general linear model that considers all feasible explanatory variables but then selects only those variables that have the most significant predictive power.

The regression analysis included 21 candidate predictors and mass loss in gram for each coupon as the response. The three deicing treatment types included salt-sand for Asheville bridges and applications of brine and granular for Greensboro bridges. All three variables were entered as continuous variables with the number of treatment applied for each type as indicated in TABLE 4.1. Other predictors were input as categorical variables with assignment of either 1 or 0. For rail type, 1 indicates a solid rail and 0 indicates an open rail. Likewise, for traffic type 1 indicates the mounted coupons were facing traffic. Remaining categorical predictors were coded with 1 if the condition is true under that category and 0 if it is false. TABLE 4.4 shows a summary of all predictor variables used for the regression analysis. The output produced by MiniTab for this reduced order model is shown in APPENDIX 4.1.

The initial regression run considered all predictor variables, which ended after six steps with six remaining variables. As noted during step 4 the p-value for rail type increased from 0 to 0.724 when the term for clearance above 17 feet was added to the model. At the last step, the p-value for rail type was reduced to 0.5, also the highest for all remaining variables followed by 0.022 for good joint condition. With such a high p-value, rail type can be concluded as not statistically significant for the model. Rail type also showed a variance inflation factor (VIF) of 3.98, the highest from the remaining variables. The VIF value measures the level of variable redundancy, ranging from 1 to 10, with 1 as not correlated and 10 for highly correlated to other predictors. Rail type indicated a moderate level of redundancy and statistical insignificance to the model and therefore can be removed without jeopardizing explanatory power of the model. The second regression was run with rail type removed from the set of predictors.



TABLE 4.4: Predictor variables used in stepwise regression analysis

<b>Candidate Term</b>	<b>Category (continuous)</b>			
Application Type (3 terms)	Salt-sand	Brine	Granular	
	<b>Category (0, 1 condition)</b>			
Location (4 terms)	Exterior Flange	Exterior Web	Interior Flange	Interior Web
Age(yrs) (3 terms)	0-19	20-39	40-50	
Clearance (ft) (3 terms)	0-16	>16-17	>17	
ADT(Average daily traffic) (3 terms)	0-3000	>3000- 4000	>4000	
Joint Condition (3 terms)	Good	Fair	Poor	
Rail Type (1 term)	Solid	Open		
Traffic Type (1 term)	Facing	Away		

The MiniTab output for the second regression analysis is shown in APPENDIX 4.2. The analysis ended in five steps, with salt-sand, granular, age (20-39), ADT above 4,000 and interior web as remaining predictors. P-values for all five predictors show statistical significance at 93.9% confidence level with the highest p-value of 0.061 for ADT above 4,000. VIF's for all predictors range from 1.59 to 2.29 indicating low redundancy in explanatory variables. The result for both forward selection methods did not include brine application as a remaining predictor, due to the selected alpha value at 20%. However, brine application is an important predictor to include in the final regression model along with granular and salt-sand. Including brine application in the model will

enable general comparison of the corrosive impact between the three different application types. Consequently, the MiniTab output with brine manually included in the analysis is shown below:

**Predictors included: Salt-sand, Brine, Granular, Age (20-39), ADT(>4k), Interior Web**

Method

Categorical predictor coding (1, 0)

Analysis of Variance

Source	DF	Adj SS	AdjMS	F-Value	P-Value
Regression	6	1112.01	185.336	37.32	0.000
Salt-sand	1	245.80	245.797	49.49	0.000
Brine	1	6.89	6.889	1.39	0.243
Granular	1	140.81	140.809	28.35	0.000
Age(20-39)	1	43.06	43.064	8.67	0.004
ADT(>4k)	1	24.63	24.628	4.96	0.029
Interior Web	1	45.61	45.607	9.18	0.004
Error	65	322.83	4.967		
Lack-of-Fit	43	225.54	5.245	1.19	0.340
Pure Error	22	97.29	4.422		
Total	71	1434.85			

Model Summary

S	R-sq	R-sq(adj)	R-sq(pred)
2.22859	77.50%	75.42%	73.68%

Coefficients

Term	Coef	SECoef	T-Value	P-Value	VIF
Salt-sand	0.6752	0.0960	7.03	0.000	3.32
Brine	0.453	0.385	1.18	0.243	2.63
Granular	0.729	0.137	5.32	0.000	1.60
Age(20-39)					
1	1.982	0.673	2.94	0.004	3.01
ADT(>4k)					
1	-1.266	0.569	-2.23	0.029	1.89
Interior Web					
1	-1.680	0.554	-3.03	0.004	1.98

Regression Equation

Mass Loss (g) = 0.6752 Salt-sand + 0.453 Brine + 0.729 Granular  
+ 1.982 Age(20-39)\_1 - 1.266 ADT(>4k)\_1 - 1.680 Interior Web\_1

Fits and Diagnostics for Unusual Observations

Obs	Mass Loss (g)	Fit	Resid	StdResid	
28	7.740	3.080	4.660	2.17	R
31	8.320	1.235	7.085	3.31	R
62	12.680	7.384	5.296	2.47	R
70	0.500	5.704	-5.204	-2.41	R

R Large residual

The result shows that by including brine, its p-value is 0.243 which put it just above the default alpha value at 0.2. The final regression model is:

$$\begin{aligned} \text{Mass Loss (g)} = & 0.6752 \text{ Salt-sand} + 0.453 \text{ Brine} + 0.729 \text{ Granular} \\ & + 1.982 \text{ Age}(20 - 39) - 1.266 \text{ ADT}( > 4k) - 1.680 \text{ Interior Web} \end{aligned} \quad (4.1)$$

Where:

*Salt-sand, brine, and Granular = application number*

*Age (20-39), ADT(>4k), and Interior Web = 1 if the condition is true*

The final regression model shows positive relationship for salt-sand, brine, granular, and bridge's age between 20 to 30 years and negative relationship for ADT above 4,000 and interior web to mass loss. These relationships are as expected and reinforce the main effects plots for these predictors. According to the model coefficients, granular has the largest impact followed by salt-sand then brine. The final model has an R-squared value of 77.5% and an adjusted R-squared value of 75.42%. These are indications of what percentage of variation in the response is explained by the predictor variables. The adjusted R-squared values only increase with each regression step when the new term improves the model more than would be expected by chance.

The main assumptions for the multiple regression models are: the errors are normally distributed, the variance of the error is equal for all observations, and there is a linear relationship between response and explanatory variables. The model over and under predictions or residuals was plotted to check for normal distribution or bias in the model. FIGURE 4.9 includes the histogram of residuals plot and residuals versus fits plot to check for normal distribution and variance of error for all observation, which should show random distribution of residuals on each side of 0. The plot indicates that the

assumptions for the most part are valid. Linear relationships were established through converting of explanatory variables into binary categories using 0 and 1. It is important to note that the regression model presented was based on the collected data for this study. Potential error could be due to factors that were not considered that could also influence the corrosive loss in the actual field environment. Furthermore, the data set could contain points that have high variability or nonlinearity that are not fitted well in the model. Due to limited data in the data set, there is no statistical basis for eliminating those points and furthermore doing so would create a gap for certain conditions within a factor.

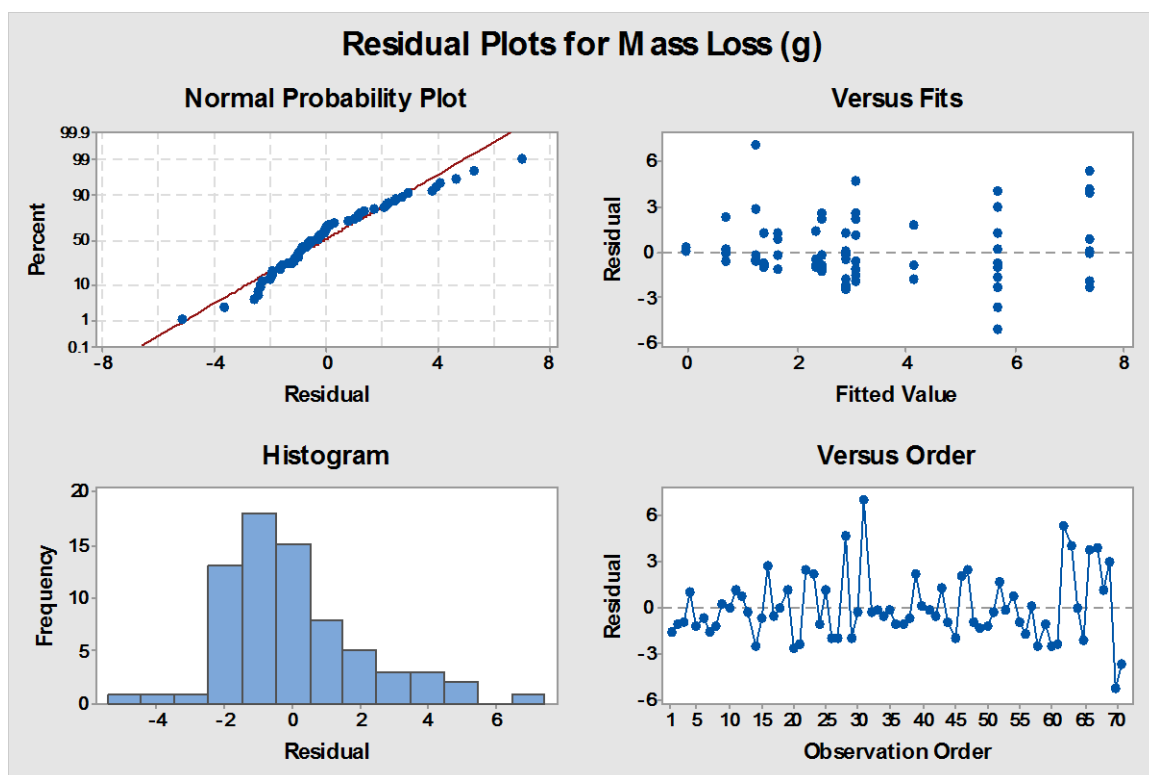


FIGURE 4.9: Plots for checking model assumptions

#### 4.4 Conclusion

A field test program was conducted to generate quantitative data for evaluating the impact of sodium chloride deicing and anti-icing applications on the transport of chloride and the associated corrosive losses on bridge girders. Sacrificial steel coupons were installed at different girder locations under normal service conditions and were retrieved after one winter season to determine the corrosive mass loss. Statistical analysis of the collected mass loss per application indicates that granular treatment is 1.08 times worse than salt-sand mix and 1.6 times worse than brine. This is largely due to granular salt ability to transport to below deck components. Accumulation of granular salt at the joint and increase in chloride measurements at the girders from granular application was observed for field study by Prah-Ennin (2013). Results also indicate that the bottom flange on girders experience about 1.5 times higher in corrosive mass loss compared to web components.

Further statistical analysis of the experimental data with the functional properties of the bridges and locations of the specimens was performed using MiniTab statistical regression and modeling software package. Based on the main effect plots within a particular factor, there is an indication of higher average corrosive loss for: bridges that are between 20-39 years old, bridges with low traffic count, and at exterior flanges. Significant effects and interaction of factors were identified for plausible effects including:

- 1) Lower traffic count is associated with greater corrosive losses, but at high traffic count the effect is less pronounced for granular with brine application.

- 2) Interior flanges facing traffic exhibit greater corrosive loss compared to other locations on interior flanges not facing traffic.
- 3) Bridges with poor joint condition exhibited higher corrosive loss on the interior flange of girders.
- 4) Asheville bridges exhibited large average corrosive loss at the interior flange, which has been attributed to poor condition of expansion joints.

A reduced order model that contained significant variables was constructed to explain the variation in observed corrosive mass loss. The reduced final regression model included six terms: salt-sand, brine, granular, bridge age between 20 to 30 years, ADT above 4,000, and interior web, which were determined to be statistically significant at or above the 75.7% confidence level. The final model has an adjusted R-squared value of 75.42%. The presented model was based only on data collected for this study. With additional observations or inclusion of other important explanatory factors a more complete model can be established.

## CHAPTER 5: LABORATORY EVALUATION OF THE EFFECT OF DEICING AND ANTI-ICING TREATMENTS ON CORROSION OF REINFORCED CONCRETE COMPONENTS

The use of deicing and anti-icing treatments on concrete bridge decks is known to accelerate corrosion of reinforcing steel through the introduction of chlorides. This chapter presents an investigation undertaken to determine whether there are significant differences between the corrosive impacts of brine, granular salt, and salt-sand mix. Controlled applications of sodium chloride deicing and anti-icing strategies on samples that mimic concrete bridge deck were used to generate data on the transport of chloride ions from the concrete surface down to the reinforcing steel. The study was conducted on concrete specimens prepared from a typical bridge deck mix with embedded reinforcing steel. Included in this chapter are the methodology and experimental results obtained from cycles of simulated winter exposure including: freeze-thaw temperatures, wetting and drying, and simulated snow followed by deicing applications. Concrete specimens were monitored for indications of steel reinforcement corrosion by voltage potential measurements throughout the cyclic exposure. Analysis of the specimens was performed after 490 freezing cycles for measurements of accumulated chloride within the first inch of concrete depth. Results were based on the evaluation of the concentration of chloride ions for each deicing and anti-icing application strategy.

## 5.1 Method for Assessing Chloride Ingress and Corrosion in Reinforced Concrete

### Specimens

The standard method for studying the effects of chemical admixtures on embedded steel reinforcement is outlined in ASTM G109, “Determining Effects of Chemical Admixtures on Corrosion of Embedded Steel Reinforcement in Concrete Exposed to Chloride Environments” (ASTM 2007). The test is used to evaluate the corrosivity of embedded metals in concrete exposed to different corrosive environments. The test is set up for a chosen concrete mixture proportion and protective cover that allows chloride ingress from the top of the sample surface down to the steel rebar. The source of the chloride is 3% NaCl solution ponded in a dam on top of the test specimen. Each test specimen includes one top rebar as an anode for corrosion current and two bottom rebars as the cathode. Evaluation of steel corrosion is performed by measuring the voltage across the rebars and calculating the current across a 100  $\Omega$  resistor connected between the top and bottom rebars. A schematic of the test setup is shown in FIGURE 5.1. The current is monitored over the testing period or until a sufficient amount of corrosion is present from visual evaluation.

The test method used in this study utilized similar specimen setups and preparations described above. However, specimens were exposed to chloride through the simulation of typical winter deicing treatments. Instead of ponding chloride solution inside a dam, each testing surface was exposed to cycles of above freezing and below freezing temperatures, snow application, deicing treatments, and water flushing. Each cycle was designed to simulate typical highway bridge exposure during a snow event. In addition to monitoring the voltage across the attached resistor, Rapid Chloride Test



(RCT) of the concrete over various depths was performed to analyze chloride content at the end of the protocol.

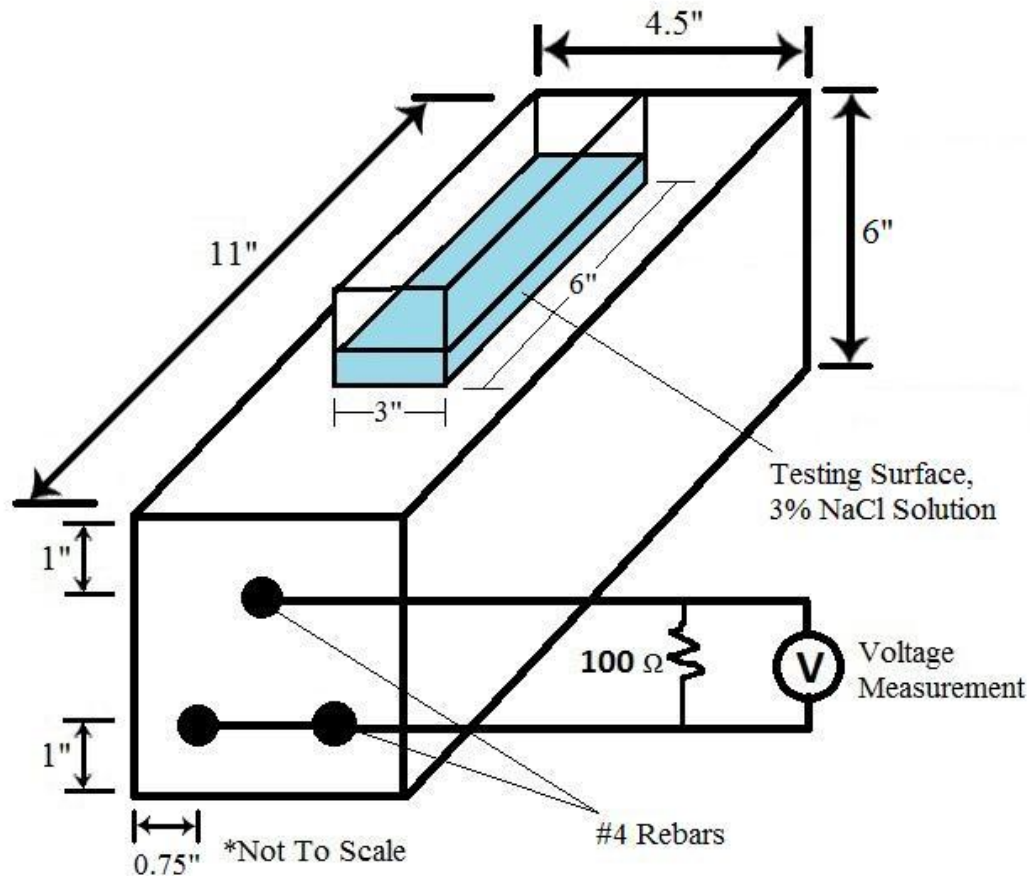


FIGURE 5.1: Schematic of testing setup for reinforced concrete block

## 5.2 Preparation of Test Specimens

Preparation of test specimens was similar to procedures outlined in ASTM G109. Specimens size were 11" x 6" x 4.5" with one reinforcement bar placed centered at 1" from the top and two bars placed 1" from the bottom and  $\frac{3}{4}$ " from the side. The steel reinforcements used were deformed #4 rebar (0.5" diameter). Each bar was wire brushed to bare metal to remove contaminants, previous rust, and mill scale. Bars were trimmed to 14". Each bar was drilled and tapped on one end and fitted with a stainless steel screw

and nut for the electrical connection. Electroplater tape was used to cover the end of each bar leaving a middle portion of 8 inches in bare steel. In addition, 3.5 inches of neoprene tubing was used to cover the ends of each bar over the taped portion. The process exposed about 8 inches of steel within the concrete to be tested and electrically isolated the steel surface at the end of each bar. The protruded tubing at each end was sealed with silicone. Wood molds were prepared for each specimen with holes positioned to support the rebars in place during casting. FIGURE 5.2 shows preparation of the bar and mold. A special specimen was prepared to measure the internal temperature fluctuations within the concrete specimens. A mold that did not contain reinforcing bars was also prepared to be cast with temperature sensors placed along the height of the specimen, as shown in FIGURE 5.3.

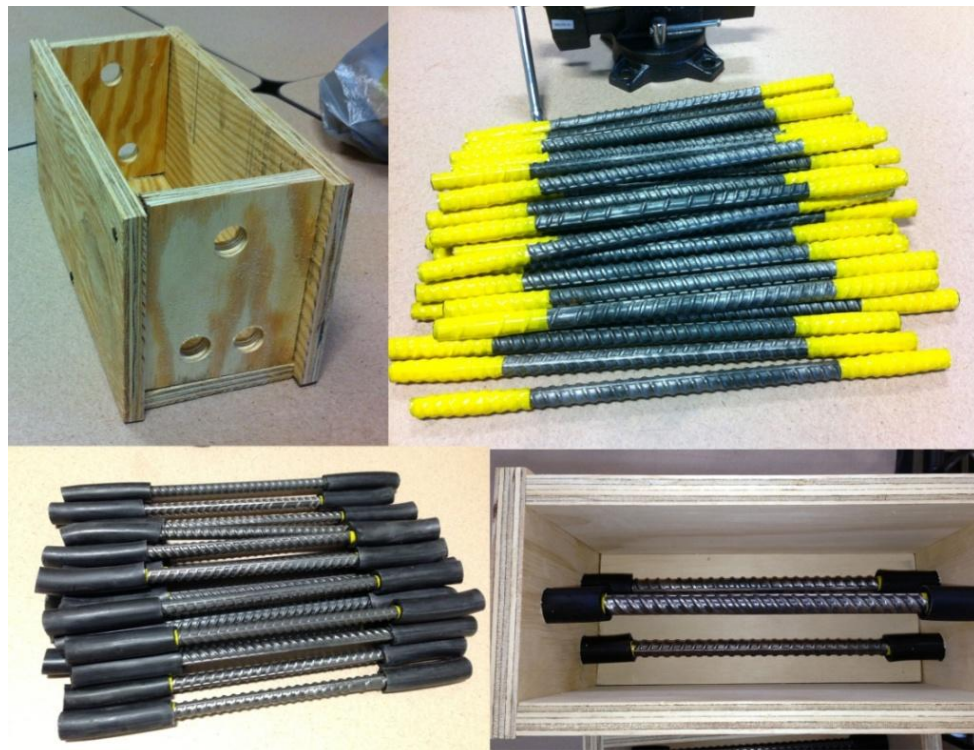


FIGURE 5.2: Preparation of reinforced bars and wood molding



TABLE 5.1: Resistance values of thermistors

Temp (°C)	Rt(Ohm)
-15	15950
-10	12110
-5	9275
0	7162
5	5574
10	4372
15	3454
20	2747

A total of 13 concrete test specimens were prepared, three for controls, three for each of the three deicing application type, and one for use as temperature sensor. The concrete mix used is presented in TABLE 5.2 that was replicated from a concrete deck mix approved by NCDOT for Piedmont area bridges.

TABLE 5.2: Concrete mixture proportions used for cyclic test specimens

Materials	Quantity (lb/yd <sup>3</sup> )
Coarse Aggregate: #78	1,736
Fine Aggregate	1,152
Water	325
Cement	677
Admixture: BASF MB-AE 90	

The air-entraining admixture (MB-AE 90) from BASF was used to obtain 6% air content. The total volume of the batch prepared was 3.7 cubic feet with 65 mL of the air entraining admixture used. In addition to casting the thirteen specimens required for testing, 4" x 8" cylinders were also prepared for compressive strength test. An electric concrete mixer was used to mix the concrete. The final slump and air content measured

were 0.5” and 6 %, respectively. To help consolidate the concrete, a vibration table was also used when filling the wood mold (FIGURE 5.4).



FIGURE 5.4: Pouring of concrete specimens

The specimens were allowed to cure for 28 days submerged in lime water, followed by two weeks of drying aging at 50% relative humidity and 22.8°C (73°F). A 100 Ohm resistor was electrically connected to each test specimen between the top rebar and the two bottom rebars. Plexiglass was used to create a dam on top of each of the 12 specimens. The dams were 3 inches wide and 6 inches long with a height of 3 inches. Epoxy was used to seal the dam to the top of the specimen. Sika Top Seal 107 was used to seal the surface outside of the dam. FIGURE 5.5 shows the completed specimens



loaded in the environmental chamber. Each specimen was placed on wooden support to prevent electrical interference between the sample and the supporting shelf.

A compressive strength test of the concrete was performed on 4" x 8" cylinders to ensure a high enough compressive strength for typical deck-mix. Two cylinders were tested after the 28 days curing period and were found to have achieved 6,278 and 6,975 psi compressive strength.



FIGURE 5.5: Finished specimens with attached wires and resistors

### 5.3 Experimental Test Program

Prepared specimens were labeled for three controls, three samples for brine application, three samples for granular salt application, and three samples for salt-sand mix. The control samples included two blocks that were exposed to the freeze thaw cycle

conditions but had only snow applied without deicing materials. The other control sample was maintained at room temperature with 400 mL of 3% salt solution for two week ponding and drying cycles, as described in ASTM G109.

The test program attempted to simulate field exposure on concrete bridge decks during a typical winter season in North Carolina. Weather features considered when preparing the program included: temperature cycling, above and below freezing temperature (freeze-thaw action), precipitations (rain and snow with wet-dry action), and deicing treatments (brine, granular salt, and salt-sand mix). To create an exposure regimen representative of North Carolina winters, weather information and winter deicing practices were considered. Weather information was obtained from 1991 to 2011 for the city of Asheville, NC through Weather Underground, a weather data service (Weather Underground 2013). The study examined winter seasons over the months of November through March over the 20 year period. The average amount of snow precipitation for one snow event was found to be 0.31 inches (FIGURE 5.6). Average temperatures were found to be  $-0.13^{\circ}\text{C}$  ( $31.76^{\circ}\text{F}$ ) for the daily minimum and  $11.31^{\circ}\text{C}$  ( $52.36^{\circ}\text{F}$ ) for the daily maximum over the entire selected winter season. Out of the 3,019 days in the study, 1,557 days have a minimum temperature that is below freezing and a high that is above freezing temperature. Temperatures on days that indicated a snow event have an average minimum of  $-4.44^{\circ}\text{C}$  ( $24^{\circ}\text{F}$ ) and a maximum of  $3.33^{\circ}\text{C}$  ( $38^{\circ}\text{F}$ ). Further studies of weather information were performed for the first 10 winter seasons (1991-2001) from the 20 years of weather data. The average number of snow or ice and rain events per season is shown in TABLE 5.3.

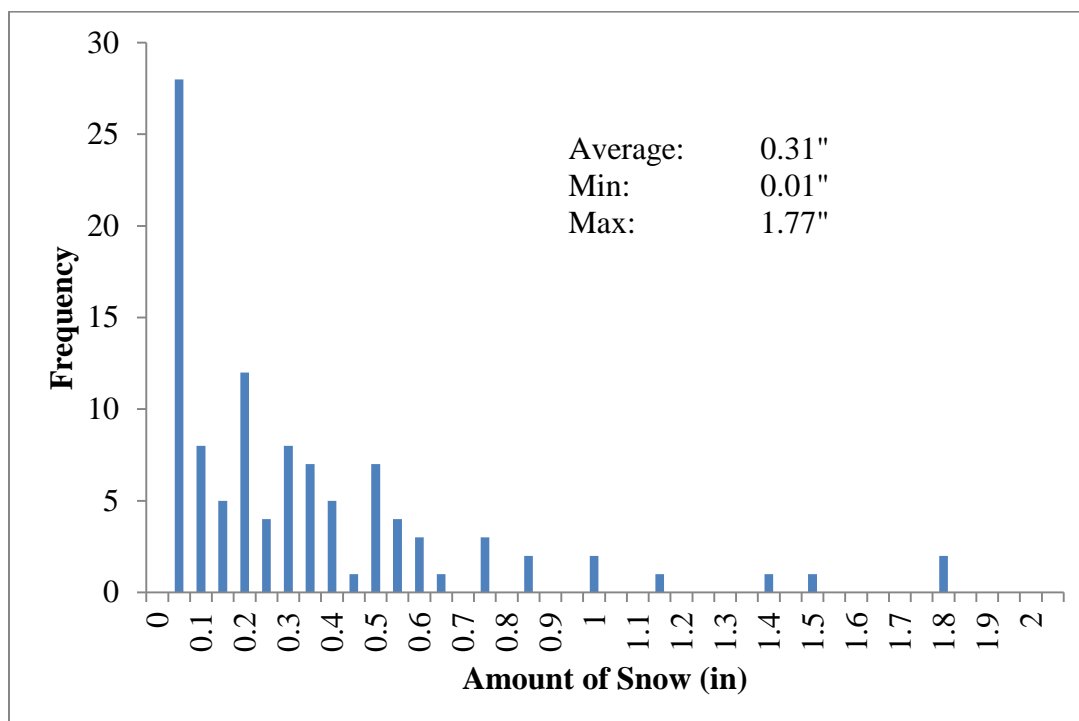


FIGURE 5.6: Amount of snow precipitation per event for 1991-2011 in Asheville, NC

TABLE 5.3: Details of typical winter conditions for Asheville, NC (1991-2001)

Winter Season #	1	2	3	4	5	6	7	8	9	10	
											AVG
Average Snow (in)	0.07	0.25	0.43	0.26	0.45	0.19	0.29	0.21	0.28	0.26	0.27
Average days between snow	32.75	23.25	9.89	4.69	4.55	15.83	11.44	13.14	24.80	13.44	15.38
Total snow events	5	5	10	14	30	7	10	8	6	10	10.50
Total snow (in)	0.37	1.25	4.33	3.67	13.36	1.31	2.92	1.64	1.66	2.55	3.31
Average Rain (in)	0.46	0.44	0.50	0.41	0.36	0.41	0.43	0.31	0.34	0.38	0.40
Average days between rain	4.17	2.94	3.87	2.92	2.57	2.88	2.92	3.04	4.14	4.06	3.35
Total rain events	37	52	39	51	59	53	50	50	37	36	46.40
Total rain (in)	16.9	22.91	19.37	20.76	21.4	21.54	21.59	15.72	12.71	13.78	18.67



Deicing material applications included 23% brine solution applied at a rate of 35 gallons per lane-mile, granular salt at a rate of 150 pound per lane-mile, and 50%/50% salt-sand mix applied at 150 pound per lane-mile. For the exposed surface area of 3"x6" inside the dam, the application rate used were 0.78 mL of 23% brine, 0.402 gram of granular salt, and 0.201 gram of salt plus 0.201 grams of sand for salt-sand mix. These values were scaled up by three times from the actual rates for practical measurement and distribution on the test surface as well as a way to accelerate corrosive effects. APPENDIX 5.2 shows the calculation for determining the application rate for deicing treatments.

The cycle was set up to repeat during a 24 hours period for Monday through Friday, which included flushing with water (as by rain), deicing applications, and snow precipitation. FIGURE 5.7 shows the full one 24 hours cycle for the test program. The temperature was set to cycle between -6°C and 3°C (21.2°F - 37.4°F) in a sinusoidal wave pattern. The temperatures selected were lower than the average daily low for days that indicated a snow event to account for temperature lag on the concrete surface and ensuring adequate freeze-thaw actions. Each daily cycle consisted of seven freeze-thaw actions. The test program ran over 70 days. According to Asheville weather data, for a typical 20 years there are 1,557 freeze-thaw cycles; with a total of 490 simulated freeze-thaw cycles the approximate amount of years is 6.29. The total number of simulated snow events is 70, which can be approximated as 6.67 years based on the historical analysis of the average number of snow fall annually. The whole test program can be summarized as having an average simulated time of 6.5 winter seasons with three times the normal deicing application rate.

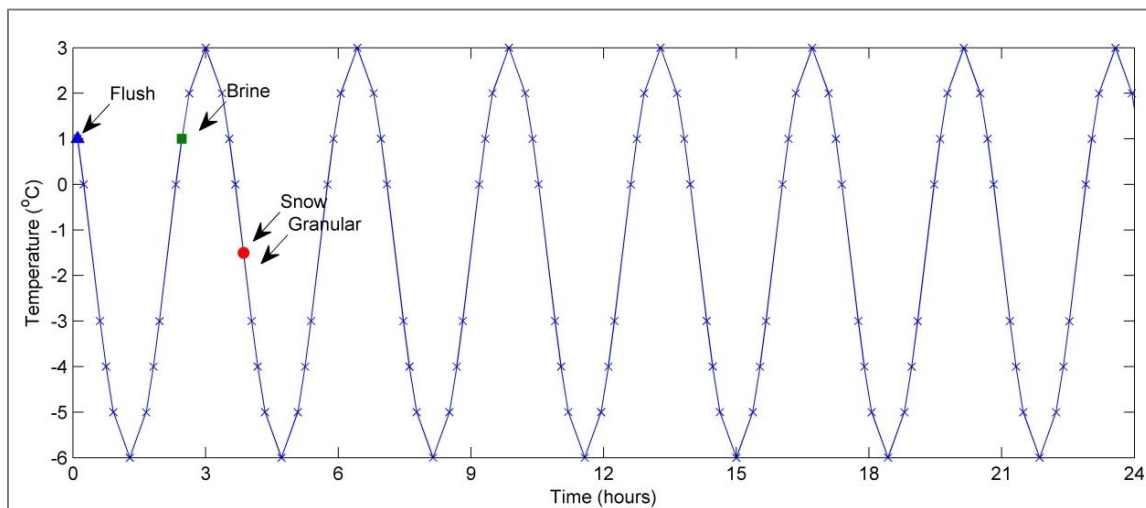


FIGURE 5.7: Environmental chamber setup for one cycle

The start of the cycle consisted of flushing (as by rain) while the temperature was set to 1°C (33.8°F). Flushing was performed by flooding the test surface with water, syringing the solution out of the Plexiglas dam, and then removing excess water with paper towels. Brine was applied two hours and 30 minutes after flushing, when the chamber temperature is at 1°C (33.8°F). The concrete surface was dry at the time the brine was applied, as would be observed in typical field practices. Brine was applied by spraying the measured quantity of solution on the concrete surface using a syringe. This application technique provided for a generally uniform application of the brine across the dammed surface of the specimens. Snow was applied one hour and 30 minutes after brine application when the temperature again declined below freezing. The chamber temperature at this time is -1.5°C (29.3°F) with concrete surface temperature at 0.6°C (33.08°F). Snow was applied using 100 mL cup from finely crushed ice. Specimens receiving granular or salt-sand mix applications received measured quantities of the

deicing chemicals applied manually on top of the snow. The cycle continued to alternate between high and low temperatures until another flush.

During the experiment, data acquisition was achieved by using Campbell Scientific data logger to monitor and record voltage differentials between the rebars and thermistor circuits at one minute intervals (FIGURE 5.8). In addition, current chamber temperature and humidity were recorded using the chamber's built-in sensors.

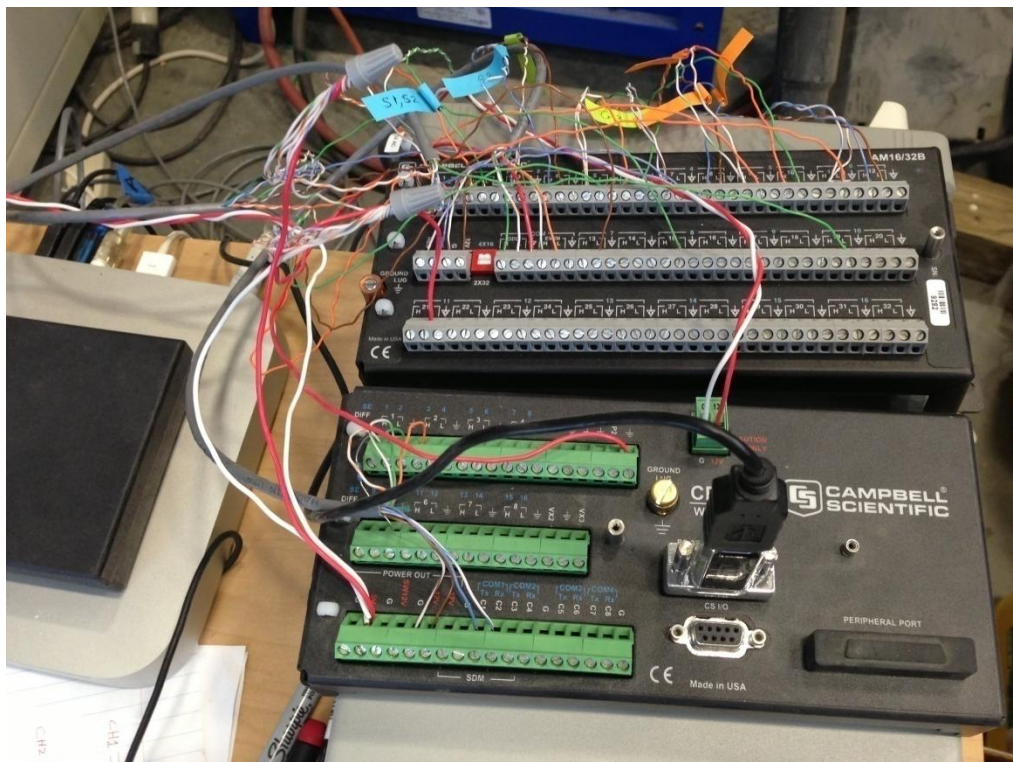


FIGURE 5.8: Data logger used to record voltage readings

Thermistor circuits were set up with a  $7.5 \text{ k}\Omega$  resistor connected in series with the thermistor and 5 V running through the circuit. Voltage measurements were measured across the  $7.5 \text{ k}\Omega$  resistor by the data logger (FIGURE 5.9). The thermistor resistances were calculated according to:

$$R_t = \frac{(V)R_r}{V_r} - R_r \quad (5.1)$$

Where:

$V = 5$  volts

$R_t$  = resistance of thermistor

$R_r$  = resistance of parallel resistor (7.5 kilo-Ohm)

$V_r$  = voltage reading across  $R_r$

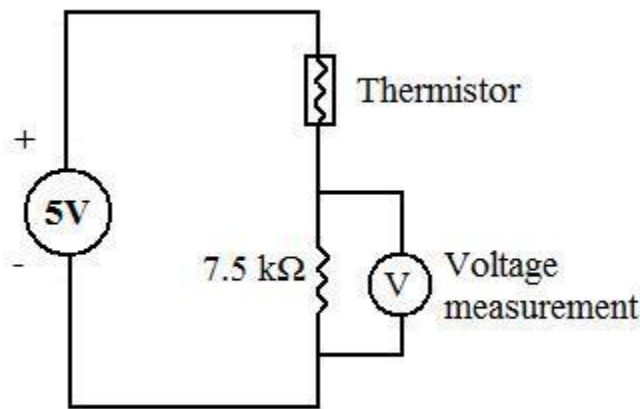


FIGURE 5.9: Schematic of thermistor circuit

Thermistor resistance values were compared to the manufacturer temperature to resistance curve to determine temperature.

FIGURE 5.10 shows the typical recorded temperature with overlay of chamber ambient temperatures and temperatures of concrete block at 0.5" depth. FIGURE 5.11 shows a closer view of temperature readings when brine and snow with deicing treatments was applied.

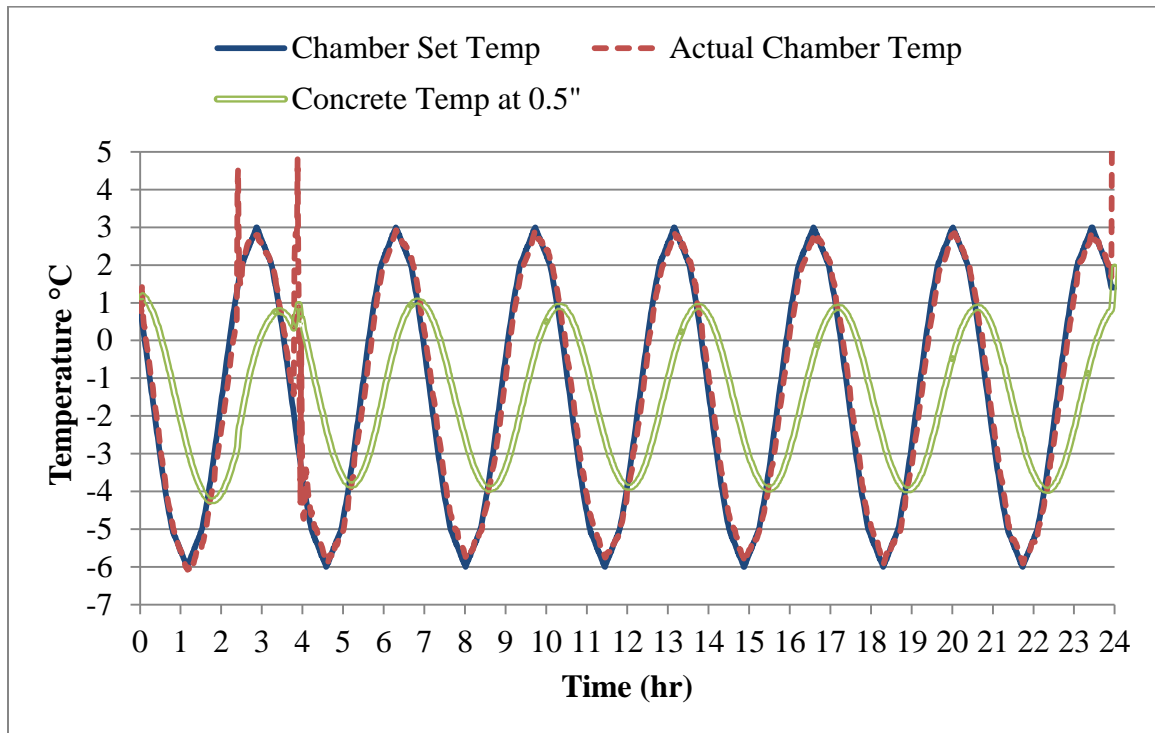


FIGURE 5.10: Overview of temperature readings of one cycle

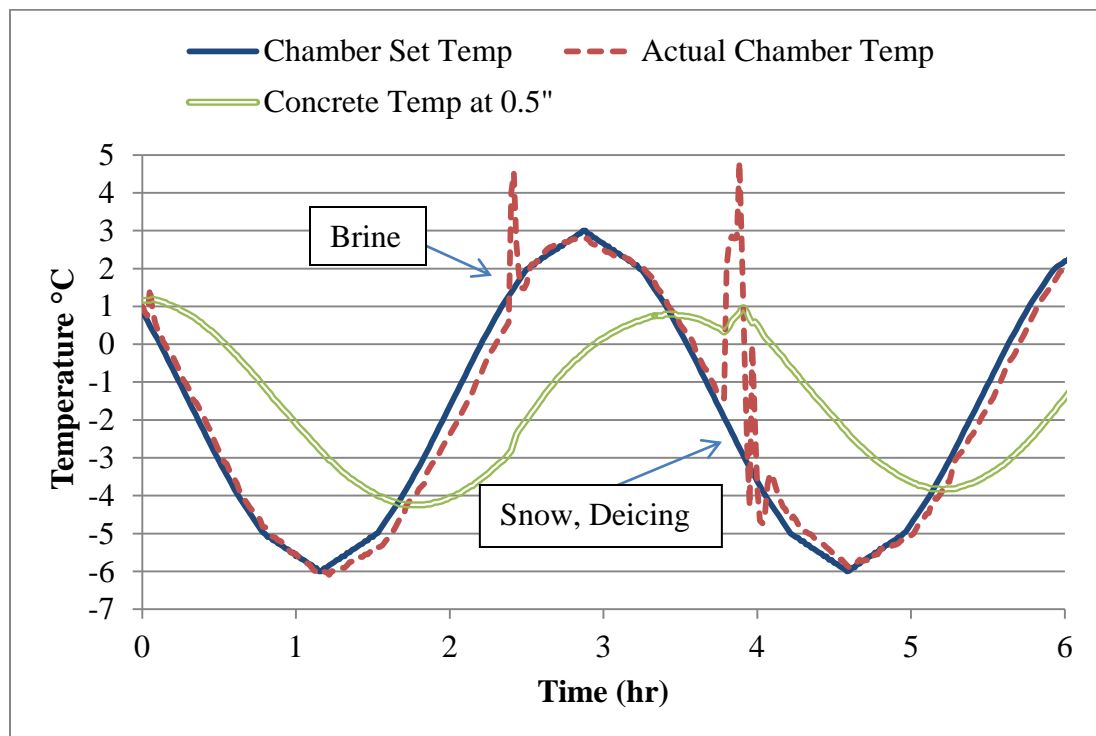


FIGURE 5.11: Temperature readings at brine, snow, and deicing application

The figures indicate that chamber temperatures were well maintained to the set temperatures at specific times. A deviation from the actual and set temperature occurs when the chamber door was opened to allow for snow and deicing treatments. As shown in FIGURE 5.11, the first deviation of the measured temperature from the set-point occurs two hours and 30 minutes into the cycle, when brine was applied. The second deviation occurs at four hours into the cycle, when snow and granular treatments were applied. Measurements of concrete temperatures at 0.5" depth indicate a lag in temperature change compared to the ambient temperatures. The extreme high and low temperatures were 1.6°C and -4°C as compared to the set temperature at 3°C and -6°C for the chamber environment. The temperatures plot also indicated a lag time of 26 minutes from peak ambient to concrete temperatures.

Cyclic exposures of freeze-thaw, snow, and deicing treatments were ended after 14 weeks. Concrete powder samples were collected from each sample for chloride content measurement. Powder samples were collected by drilling the samples using an electric drill press. Each sampling point was drilled at five increments of 0.2" for a total depth of 1". A total of three sampling points were drilled for each test specimen to reduce uncertainties associated with sampling as well as the potential for uneven application of deicing materials across the surface of each test specimen. To profile the chloride concentration with depth, the Rapid Chloride Test (RCT) was performed on the collected powder. Standard procedures were used for the RCT test with equipment and materials sourced from Germann Instruments. Per manufacturer recommendations, each powder sample was measured to 1.5 gram and placed in an extraction vial. The vials were left to extract chloride ions overnight before measuring the chloride content of the

solution with the ion-selective electrode. Measurements were compared to calibrated curves prepared from solutions of known chloride concentration.

#### 5.4 Results

Voltage measurements obtained across the 100  $\Omega$  resistor for all specimens did not show any changes during the test period used for this experiment. Therefore calculation of integrated macrocell current across the rebar via ASTM G109 was not possible. The half-cell potential after 14 weeks for the 3% NaCl ponding control was measured to be -58.16 mV using a saturated calomel reference electrode. Converting the reading to a copper-copper sulfate reference electrode, the voltage measurement is equivalent to -135.16 mV. As per ASTM C876, Standard Test Method for Corrosion Potentials of Uncoated Reinforcing Steel in Concrete (ASTM 2009), a voltage potential that is more positive than -200 mV using a copper-copper sulfate reference electrode have a 90% probability that no corrosion is occurring. The 3% ponding specimen was expected to be exposed to the highest chloride level; this reinforces indications that no corrosion potential was measured across the rebar or corrosion has yet to initiate for the other specimens.

Chloride concentrations at each depth for multiple sampling points were averaged together for each test specimen. The results for each test specimen are shown in TABLE 5.4. The full set of results is shown in APPENDIX 5.3. Plots of the chloride concentration at increasing depths within the samples are shown in FIGURE 5.12.

TABLE 5.4: RCT results at 0.2" depth increments

Depth (in.)	Chloride Percent (Cl%)				
	Snow Ctrl	3% Ponding	Brine	Granular	Sand-Mix
0.20	0.064	0.394	0.329	0.341	0.293
0.40	0.050	0.272	0.230	0.229	0.204
0.60	0.040	0.160	0.100	0.115	0.089
0.80	0.040	0.065	0.044	0.052	0.048
1.00	0.039	0.050	0.041	0.042	0.046

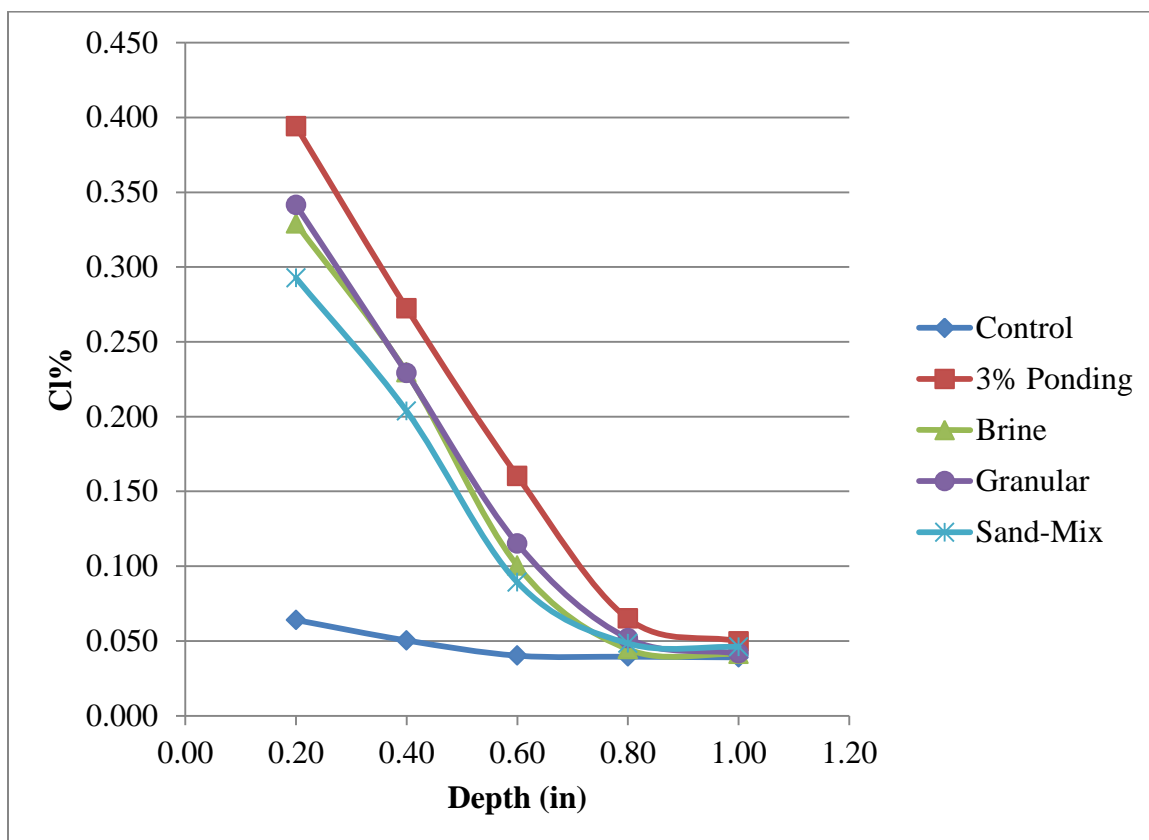


FIGURE 5.12: Chloride concentrations at drilled depth for each treatment type



The greatest chloride concentration was found in the specimen that was ponded with 3% solution. This specimen had much greater exposure to the chloride solution than those with only intermittent dosing. Granular salt treatment and brine treatment show similar concentrations at each depth while salt-sand mix was slightly lower. The control specimen represents the background chloride content of the concrete mixture. The plot indicates that no additional chloride was introduced during the test program at the 1” depth for all specimens where reinforced rebar is located. TABLE 5.5 shows the actual mass of salt that was contained in each of the deicing applications applied in one cycle. The quantity of salt contained in one treatment of brine and one treatment of salt-sand mix are very similar. Solution concentrations of salt and snow used for each application were determined from the mass of salt applied and the 100 mL of snow used. The melted 100 mL of snow was equivalent to 55 mL of water. The solution concentrations are shown in TABLE 5.6, assuming snow is fully melted.

TABLE 5.5: Calculated mass of salt for each treatment type and control

Salt/application (g)	
Snow Ctrl	0
Sand-Mix	0.201
Brine	0.205
Granular	0.402
3% Ponding	12.20

TABLE 5.6: Calculated salt concentration for each treatment type and control

Concentration of salt solution (%)	
Snow Ctrl	0
Sand-Mix	0.364
Brine	0.367
Granular	0.726
3% Ponding	3.00

Plots of the salt solution concentrations versus chloride percent for each depth are shown in FIGURE 5.13. The plot indicates that the chloride level of the powder sample is not directly related to the amount of salt used for the treatment. Brine and sand-mix treatments both contained similar amounts of salt, yet the concrete chloride percent is significantly higher. For brine application results indicate that the difference is also greater at shallower depths. The differences in chloride percent are 0.036%, 0.026%, and 0.011% at 0.2", 0.4", and 0.6", respectively. Brine is initially in solution form that is saturated with salt and can immediately ingress into the concrete at very high concentration once applied. On the other hand, application of granular salt is applied on top of the snow and only reaches the surface once the snow is melted and the salt is significantly diluted in solution. An additional difference is in the wetness of the concrete surface during application, where during brine application the surface is visually dry. Initial water absorption of the surface during snow melt can influence the amount of chloride ingress for granular salt and salt-sand mix application.

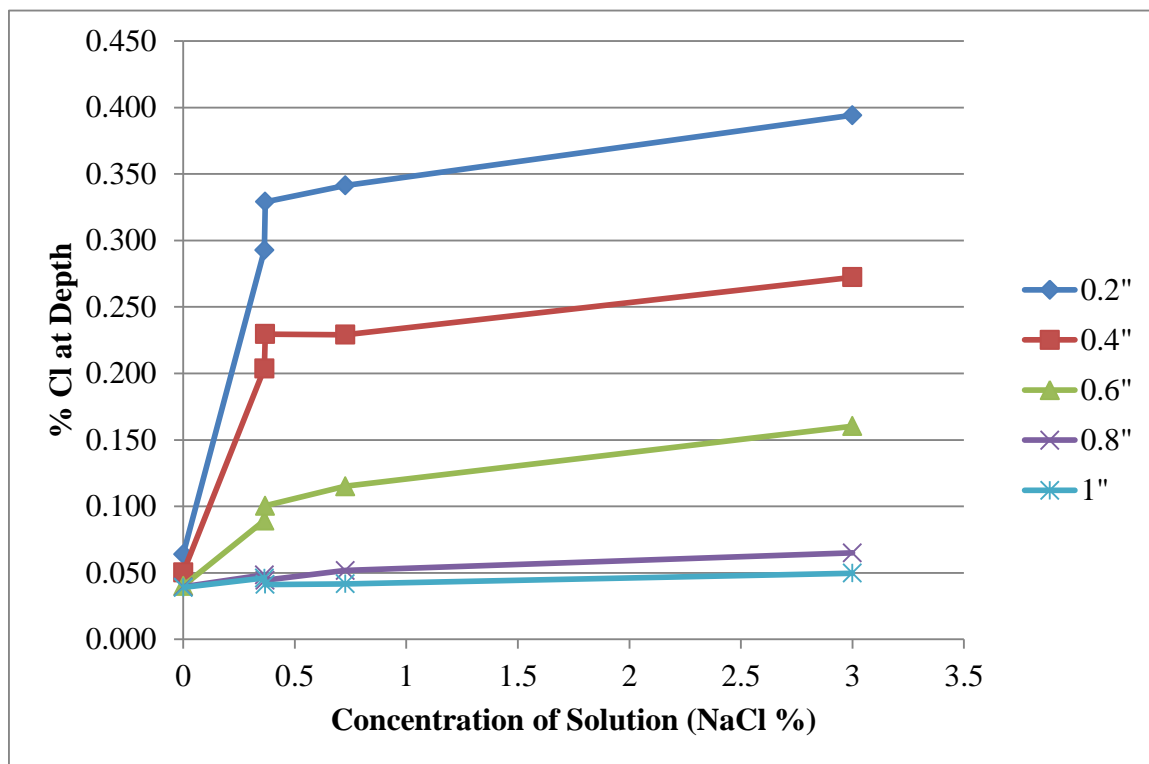


FIGURE 5.13: Plot of surface solution concentration and RCT chloride percent

To generalize the amount of chloride contribution to the number of applications at a certain application rate for the three treatment types, a plot of chloride percent per application at 0.2" depth were plotted versus the application rate for brine, granular, and salt-sand mix (FIGURE 5.14). Application rate for brine is applied in gallons per lane-mile and granular salt is applied in pounds per lane-mile. The chloride percent results were based on three times the application rate of 35 gallons per lane-mile and 150 pounds per lane-mile for granular salt and salt-sand mix at 1:1 ratio for this study. The plot assumes a linear relationship for application rate and chloride percent found at 0.2" depth of concrete surface.

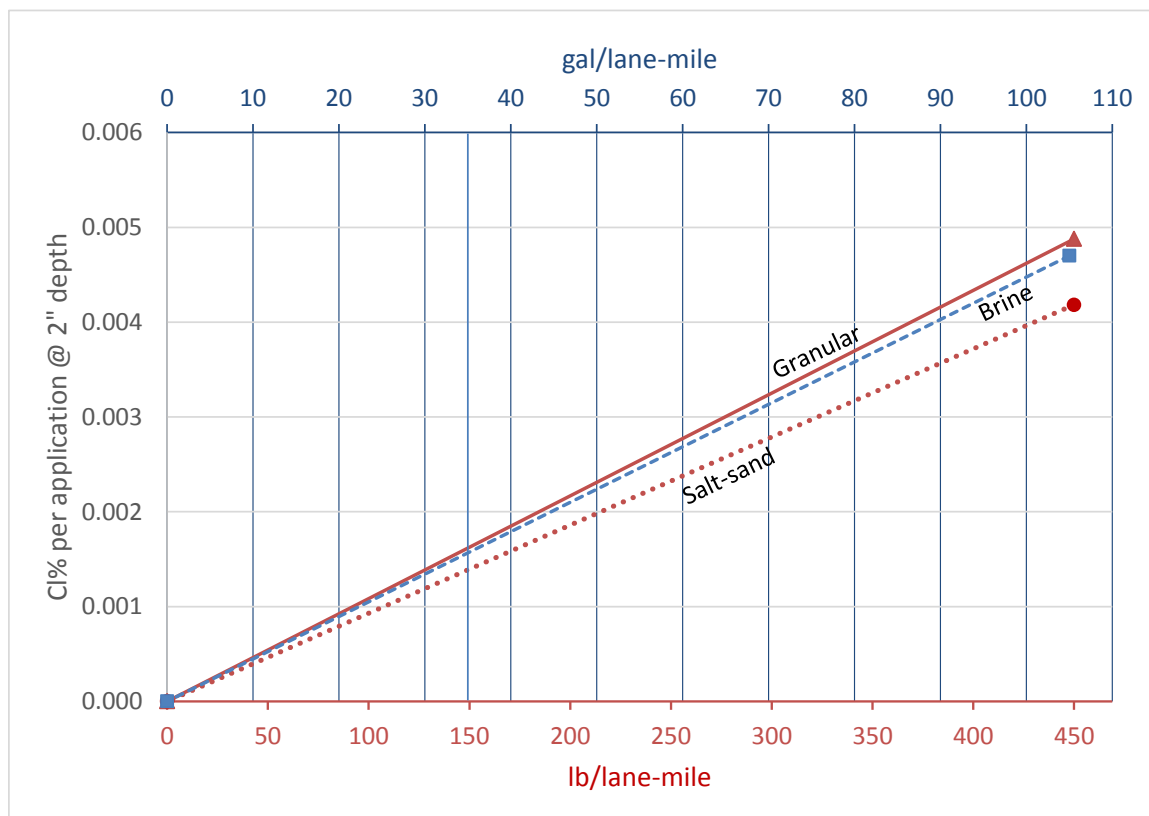


FIGURE 5.14: Plot of Cl% per application at 0.2" depth vs application rate

## 5.5 Conclusion

Results indicate that there is a difference between chloride ingress observed for anti-icing brine treatments and granular deicing treatments on reinforced concrete specimens. A similar chloride profile was observed for brine and granular specimens although each application of granular salt contained about twice the amount of salt as used in the brine application. The difference can be explained due to differences in the time characteristics of the surface concentrations. Brined specimens received solutions of initially high salt concentration applied directly to the dry surface while granular specimens received granular salt treatment after snow was deposited. The greater amount of chloride ingress observed in the brined specimens is attributed to high rates of initial

absorption of the higher sodium chloride concentrations at the dry surface of the concrete. In contrast, the surface of specimens treated with granular applications was initially exposed to melted snow prior to the applications of the treatment. The presence of the winter precipitation both works to saturate the pores at the surface of the concrete to reduce absorption rates and also dilutes the concentration of the granular salts applied to the surface. These findings are consistent with a field study conducted by Prah-Ennin (2013), which found higher initial chloride concentrations for deck subjected to brine application compared to granular applications. Average surface chloride measurements were also found to remain higher for the brine treatment until flushing of the surface by rain. The results also indicated that chloride ingress for granular deicing treatments are not proportional to the amount of salt applied. This was observed in the current study, where the granular salt applications, which contained twice the amount of salt compared to salt-sand mix, exhibited an increase of 1.16 times the chloride content at the 0.2" depth relative to the salt-sand applications.

## CHAPTER 6: SUMMARY

### 6.1 Concluding Remarks

Test methods for corrosive evaluation of bare steel show limitation in fully immersed specimens at high concentration. Cyclic wet/dry corrosive evaluation of bare steel indicated that A36 steel show slightly less corrosive loss compared to A572 and A588 steel while A572 and A588 showed comparable corrosive loss across 3%, 5%, and 23% sodium chloride concentration. A36 steel and A588 steel showed increase in corrosion rate for 3% to 5% salt concentration while A572 steel showed similar corrosion rates at the two concentrations. Specimens exposed to 23% salt concentration in cyclic test showed half the corrosive mass loss compared to those exposed to 3% and 5% salt concentration at the end of the eight week test period for all steel types.

Scribed coating test indicated that painted specimens show better performance for both blistering and corrosion creepage over epoxy coated specimens. Epoxy coated A588 steel demonstrated the poorest performance compared to epoxy coated A572 and painted A572. For galvanized specimens, corrosion was observed to take place mainly on the galvanized coating with little to no corrosion observed on the base metal outside of the scribed line.

The study of field sampling of corrosive loss on bridge girders indicated that the highest mass losses occurred on Asheville bridges, this was expected since these bridges received double the number of deicing treatments compared to Greensboro bridges.

Results from all samples indicated that the bottom flange on girders experience about 1.5 times the corrosion mass loss than web components. Regression analysis of the mass loss results and deicing treatment types shows that granular application has the largest contribution to mass loss followed by salt-sand then brine. Other statistically significant factors contributing to corrosive mass loss include bridge age, average daily traffic, and girder location.

Results from laboratory simulation of the effect of anti-icing and deicing treatment on reinforced concrete samples indicate that there is a significant difference on the amount of chloride ingress for anti-icing brine treatments and granular deicing treatments. A similar chloride profile was observed for brine and granular specimens while the amount of salt for brine application is much less than granular application. The difference can be explained due to the treatment effects. The greater amount of chloride ingress is due to initial absorption of the dry concrete surface and higher surface concentration observed for brine application. The result also indicates that for granular deicing treatments the amount of chloride ingress is not proportional to the amount of salt applied.

## 6.2 Future Work

The study provides experimental evidence quantifying the corrosive effects of anti-icing and deicing salt on highway bridge components. However, the results are limited and future work should be conducted to independently verify and extend these results. Suggestions for future work are enumerated as follows:

- Corrosion of bare steel was expected due to exposure to various levels of salt concentrations. The study was limited in assuming 3%, 5%, and 23%

salt solution concentration exposures. Further study on verifying actual steel surface exposure in the field is recommended. A longer testing period (more than 8 weeks) is recommended to verify the ability of weathering steel to form a protective rust layer that can significantly reduce the corrosion process in the long term.

- Statistical regression analysis on field sampling was performed on a small set of data. Larger, more representative sampling data is needed to avoid bias and the ability to eliminate possible outliers. Contributing factors in the regression analysis such as age should be more carefully considered in the sample.
- Investigation of the effect of both anti-icing and deicing application on a set of specimen to verify the possibility of superposition of separate treatment type. The assumption that chloride content and application rate for a specific treatment is linear should be verified since the laboratory test used 3 times the standard application rate for anti-icing and deicing.



## REFERENCES

- Albrecht, P, and T. Hall. "Atmospheric Corrosion Resistance of Stuctural Steels." *Journal of Materials in Civil Engineering*, 2003.
- American Concrete Institute. *Building Code Requirements for Structural Concrete (ACI 318-11) and Commentary*. 2011.
- American Iron and Steel Institute. *Performance of Weathering Steel in Highway Bridges*. 1995.
- Angst, U., and Ø Vennesland. *Critical chloride content in reinforced concrete-State of the art*. London: Taylor & Francis Group, 2009.
- ASTM. *C876-09, Standard Test Method for Corrosion Potentials of Uncoated Reinforcing Steel in Concrete*. WEST Conshohocken, PA: ASTM International, 2009.
- ASTM. *D1654-08, Standard Test Method for Evaluation of Painted or Coated Specimens Subjected to Corrosive Environments*. West Conshohocken, PA: ASTM International, 2008.
- ASTM. *D7087-05, Standard Test Method for An Imaging Technique to Measure Rust Creepage at Scribe on Coated Test Panels Subjected to Corrosive Environments*. West Conshohocken, PA: ASTM International, 2005.
- ASTM. *D714-02(2009), Standard Test Method for Evaluating Degree of Blistering of Paints*. West Conshohocken, PA: ASTM International, 2009.
- ASTM. *G1-03, Standard Practice for Preparing, Cleaning, and Evaluating Corrosion Test Specimens*. West Conshohocken, PA: ASTM International, 2003.
- ASTM. *G109-07, Determining Effects of Chemical Admixtures on Corrosion of Embedded Steel Reinforcement in Concrete Exposed to Chloride Enviroments*. West Conshohocken, PA: ASTM International, 2007.
- ASTM. *G31-72(2004), Standard Practice for Laboratory Immersion Corrosion Testing of Metals*. West Conshohocken, PA: ASTM International, 2004.
- ASTM. *G50-10, Standard Practice for Conducting Atmospheric Corrosion Tests on Metals*. West Conshohocken, PA: ASTM International, 2010.
- ASTM International. *Steel Standards*. 2014. <http://www.astm.org/Standards/steel-standards.html> (accessed 2014).

- Bioubakhsh, S. "The Penetration of Chloride in Concrete subject to Wetting and Drying." Doctoral Thesis, University College London, 2011.
- Boatman, Brandon. *Epoxy Coated Rebar Bridge Decks: Expected Service Life*. 2010.
- El-Shazly, A.H., and A.A. Wazzan. "Using Polypyrrole Coating for Improving the Corrosion Resistance of Steel Buried in Corrosive Mediums." *International Journal of Electrochemical Science*, 2012.
- Federal Highway Administration Technical Advisory. *Uncoated Weathering Steel in Structures, T5140.22*. 1989.
- Gergely, Janos, Joshua Bledsoe, Brett Tempest, and Iosif Szabo. "Concrete Diffusion Coefficients and Existing Chloride Exposure in North Carolina." Research Project, Department of Civil Engineering, University of North Carolina at Charlotte, 2006.
- Guthrie, Jeffrey, Brigittle Battaat, and Chris Grethlein. "Accelerated Corrosion Testing." *The AMPTIAC Quarterly* 6, no. 3 (2002).
- Imperatore, S., and Z. Rinaldi. "Mechanical behavior of corroded rebars and influence on the structural response of R/C elements." Thesis, 2009.
- ISO. *11130, Corrosion of metals and alloys - Alternate immersion test in salt solution*. 2010.
- ISO. *9226, Corrosion of Metals and Alloys - Corrosivity of Atmospheres - Determination of Corrosion Rate of Standard Specimens for the Evaluation of Corrosivity*. 2012.
- Kline, E.S. "Steel Bridge: Corrosion Protection for 100 Years." *Journal of Protective Coatings and Linings*, 2008: 22-31.
- Koch, G.H, Brongers M.P., N.G. Thompson, Y.P. Virmani, and J.H. Payer. *Corrosion Costs and Preventive Strategies in the United States*. Washington, D.C.: FHWA, 2002.
- Kogler, Robert. *Steel Bridge Design Handbook: Corrosion Protection of Steel Bridges*. FHWA Report No. FHWA-IF-12-052, Federal Highway Administration, 2012.
- Levelton Consultants Ltd. *Guidelines for the selection of snow and ice control materials to mitigate environmental impacts. NCHRP REPORT 577*. Washington, D.C.: National Research Council, 2007.
- Mailvaganam, N.P., and P.G. Collins. "Effective Installation of Membranes on Parking Garage Decks." *Construction Technology Updates* (Institute for Research in Construction), 1999.

- MatWeb. *MatWeb Material Property Data*. 2011. <http://www.matweb.com> (accessed 2014).
- Mindess, Sidney, J. Francis Young, and David Darwin. *Concrete*. 2nd. New Jersey: Prentice Hall, 2002.
- Morcillo, M., B. Chico, I. Diaz, Cano H., and D. de la Fuente. "Atmospheric corrosion data of weathering steels. A review." *Corrosion Science*, 2013.
- National Cooperative Highway Research Program. *Synthesis 425, Waterproofing Membranes for Concrete Bridge Decks*. WASHINGTON, D.C, 2012.
- Nixon, Wilfrid, George Kochumman, Lin Qiu, Ju Qiu, and Jing Xiong. "Evaluation of Deicing Materials and Corrosion Reducing Treatments for Deicing Salts." Technical Report, College of Engineering, The University of Iowa, 2007.
- North Carolina Department of Transportation. *Safety Tips List*. 2013. <http://www.ncdot.gov/travel/safetytips/> (accessed 2014).
- Nuclear Energy Agency. "Electrochemical Techniques to Detect Corrosion in Concrete Structure in Nuclear Installations." Technical Note, 2002.
- Pacific Northwest Snowfighter. "Snow and ice control chemical products specifications and test protocols for the PNS association of British Columbia, Idaho, Montana, Oregon and Washington ." 2010.
- Pitroda, J. *Evaluation of Sorptivity and Water Absorption of Concrete with Partial Replacement of Cement by Thermal Industrial Waste (Fly Ash)*. International Journal of Engineering and Innovative Technology, 2013.
- Prah-Ennin, Papa Kwesi. "Quantifying Corrosive Potential of De-icing and Anti-icing Solutions to Steel and Concrete Bridge Components." Thesis, 2013.
- Q-Lab Corporation. *Introduction to Cyclic Corrosion Testing*. 2009.
- SAE International. "Cosmetic corrosion lab test." SAE J2334, 1998.
- SHRP. *Handbook of Test Methods for Evaluating Chemical Deicers*. Washington, DC: Strategic Highway Research Program, 1992.
- Smith, Jeffrey, and Yash Virmani. *Performance of Epoxy-Coated Rebars in Bridge Decks*. 1996.
- Trejo, D., C. Halmen, and K. Reinschmidt. *Corrosion Performance Tests for Reinforcing Steel in Concrete*. Report No. FHWA/TX-09/0-4825-1 , FHWA, 2009.

Vitro Minerals. "Portland Cement and Pozzolans." Technical Report, 2006.

Weather Underground. *Weather Underground*. 2013. <http://www.wunderground.com/> (accessed 2013).

Yao, Yuan, Pradeep Kodumuri, and Seung-Kyoung Lee. *Performance Evaluation of One-Coat Systems for New Steel Bridges*. FHWA Report No. FHWA-HRT-11-046, Federal Highway Administration, 2011.

## APPENDIX 3.1: MASS DATA FROM CYCLIC TEST

<b>1 Week</b>	<b>Weight Loss After Cleaning (mg)</b>			
	0%	3%	5%	23%
A36	23.4	213.4	289.2	158.5
A572	142.9	292.2	293	160.1
A588	25	177	301.1	214.9
A36 Galv**	N/A	76.7	104.7	36.9
A588 Epoxy	18.7	16.5	13.1	12.9
A572 Epoxy	13.5	10.5	13.7	16.8
A572 Paint	-9	-18.5	-2.1	-12.2
%Galv	NA	3.66%	5.93%	1.82%
<b>1 Week</b>	<b>Weight Loss After Sand Blasting (mg)</b>			
	0%	3%	5%	23%
A36	26	221.8	383	162.8
A572	151.1	430.7	335.3	164.8
A588	33.4	321.4	454.5	249.1
A36 Galv	NA	199.1	364	86.9

<b>2 Week</b>	<b>Weight Loss After Cleaning (mg)</b>			
	0%	3%	5%	23%
A36	29.8	242	336.7	387.6
A572	51.7	140.6	313.8	493.1
A588	19.1	-169	193.3	421.4
A36 Galv	9.9	181.6	154.1	223.8
A588 Epoxy	20.2	-6.6	-1.8	0.9
A572 Epoxy	21	-8.4	3.1	0.9
A572 Paint	-10.9	-20	-25	-7.9
<b>2 Week</b>	<b>Weight Loss After Sand Blast (mg)</b>			
	0%	3%	5%	23%
A36	37.4	580.7	852.7	416.5
A572	54	796.8	867.9	517.2
A588	28.7	1771	903.7	445.8
A36 Galv	27.4	724.7	908.5	607.2

## APPENDIX 3.1: (CONTINUED)

<b>3 Week</b>	<b>Mass Loss After Cleaning (mg)</b>			
	0%	3%	5%	23%
A36	18.7	745.4	639.4	521.5
A572	25.8	252.9	709.1	675.8
A588	22.3	-78.6	433.2	582.4
A36 Galv	37	313.6	409.1	344.8
A588 Epoxy	17.8	-1.9	15	13.7
A572 Epoxy	18.2	1.2	18.9	18
A572 Paint	-9	-27.4	-2.7	-11.4
<b>3 Week</b>	<b>Mass Loss After Sand Blast (mg)</b>			
	0%	3%	5%	23%
A36	18.7	814.1	1053	523.2
A572	33.2	1253.7	1324.5	691.3
A588	33.2	1191.6	1251.2	596.1
A36 Galv	30.8	941.4	1157.9	962.7

<b>4 Week</b>	<b>Mass Loss After Cleaning (mg)</b>			
	0%	3%	5%	23%
A36	35.5	1073.6	1422.3	715.6
A572	44.7	540.7	1485	1068.5
A588	47.6	361.9	1357.6	897.5
A36 Galv	9.6	345.1	257.3	490.1
A588 Epoxy	14	-6.3	23.7	12.6
A572 Epoxy	13	-8.3	13.4	16.6
A572 Paint	-18.2	-22.4	-7.7	-24.6
<b>4 Week</b>	<b>Mass Loss After Sand Blast (mg)</b>			
	0%	3%	5%	23%
A36	32.2	1231.8	1499.7	734.8
A572	53.8	1616.7	1628.4	1105.6
A588	49.3	1559.4	1754.3	918.5
A36 Galv	52.9	1214.9	1320.7	1081.9

## APPENDIX 3.1: (CONTINUED)

<b>6 Week</b>	<b>Mass Loss After Cleaning (mg)</b>			
6	0%	3%	5%	23%
A36	27.6	725.8	329.6	1112.5
A572	53.05	-600.6	-50.6	1219.9
A588	44.95	-1317.8	-839.55	1139.65
A36 Galv	2.95	283.75	-19.55	534.95
A588 Epoxy	16.2	-91.65	-42.1	-6.75
A572 Epoxy	12.5	-61.85	-31.35	-0.15
A572 Paint	-12.25	-51.3	-34.4	-41
<b>6 Week</b>	<b>Mass Loss After Sand Blast (mg)</b>			
6	0%	3%	5%	23%
A36	32.7	2112.7	2049.75	1137.6
A572	71.75	2179.65	2283.35	1228.9
A588	61.5	2446.1	2294.55	1178.8
A36 Galv	24.9	1536.4	1530.75	1473.1

<b>8 Week</b>	<b>Mass Loss After Cleaning (mg)</b>			
8	0%	3%	5%	23%
A36	40.85	1020.35	1070.85	1298.1
A572	44.05	-331.85	1074.4	1612.95
A588	56.15	-1111.25	-474.15	1518.3
A36 Galv	14.15	373.95	243.15	581.25
A588 Epoxy	6.65	-46.3	-7.3	10.4
A572 Epoxy	7.3	-93.7	-8.35	13.3
A572 Paint	-15.45	-59	-17.15	-20.2
<b>8 Week</b>	<b>Mass Loss After Sand Blast (mg)</b>			
8	0%	3%	5%	23%
A36	42.4	2792.1	2499.75	1323.75
A572	55.9	2745.45	2741.8	1627.1
A588	69.6	3141.45	2633.75	1553.9
A36 Galv	40.75	1345.2	1483.95	1222.95

## APPENDIX 3.1: (CONTINUED)

<b>% Mass Loss of Galvanization After Sand Blasting</b>				
<b>Week</b>	<b>0%</b>	<b>3%</b>	<b>5%</b>	<b>23%</b>
1	NA	9.50%	20.60%	4.29%
2	1.44%	40.51%	45.28%	29.47%
3	1.59%	56.34%	59.57%	46.57%
4	2.58%	69.64%	73.47%	55.25%
6	1.19%	73.54%	77.07%	71.24%
8	2.18%	69.70%	73.71%	59.75%



## APPENDIX 4.1: MINITAB OUTPUT FOR FIRST RUN

## Regression Analysis: First run

Method

Categorical predictor coding (1, 0)

Forward Selection of Terms

Candidate terms: Salt-sand, Brine, Granular, Age(0-19), Age(20-39), Age(40-50), Clear(<16), Clear(16-17), Clear(>17), ADT(0-3k), ADT(>3k-4k), ADT(>4k), Rail T, Joint G, Joint F, Joint P, Traffic Type, Exterior Flange, Exterior Web, Interior Flange, Interior Web

	-----Step 1-----		-----Step 2-----		-----Step 3-----	
	Coef	P	Coef	P	Coef	P
Salt-sand	0.6650	0.000	0.6650	0.000	0.4788	0.000
Rail T			2.436	0.000	1.906	0.000
ADT(0-3k)					2.196	0.004
S	3.02933		2.61076		2.47120	
R-sq	55.23%		67.22%		71.06%	
R-sq(adj)	54.59%		66.27%		69.78%	
R-sq(pred)	53.68%		65.02%		68.19%	
	-----Step 4-----		-----Step 5-----		-----Step 6-----	
	Coef	P	Coef	P	Coef	P
Salt-sand	0.4051	0.000	0.5052	0.000	0.5505	0.000
Rail T	0.279	0.724	0.304	0.687	-0.551	0.500
ADT(0-3k)	3.065	0.000	3.218	0.000	2.883	0.000
Clear(>17)	1.868	0.012	2.396	0.001	2.749	0.000
Interior Web			-1.490	0.008	-1.714	0.002
Joint G					1.528	0.022
S	2.37347		2.26509		2.19119	
R-sq	73.70%		76.40%		78.25%	
R-sq(adj)	72.12%		74.61%		76.24%	
R-sq(pred)	70.63%		72.54%		74.02%	

 $\alpha$  to enter = 0.2

## APPENDIX 4.1: (CONTINUED)

## Analysis of Variance

Source	DF	Adj SS	AdjMS	F-Value	P-Value
Regression	6	1122.76	187.127	38.97	0.000
Salt-sand	1	181.77	181.769	37.86	0.000
Clear(>17)	1	72.57	72.570	15.11	0.000
ADT(0-3k)	1	73.99	73.992	15.41	0.000
Rail T	1	2.21	2.213	0.46	0.500
Joint G	1	26.54	26.536	5.53	0.022
Interior Web	1	49.73	49.731	10.36	0.002
Error	65	312.09	4.801		
Lack-of-Fit	43	214.80	4.995	1.13	0.388
Pure Error	22	97.29	4.422		
Total	71	1434.85			

## Model Summary

S	R-sq	R-sq(adj)	R-sq(pred)
2.19119	78.25%	76.24%	74.02%

## Coefficients

Term	Coef	SECoef	T-Value	P-Value	VIF
Salt-sand	0.5505	0.0895	6.15	0.000	2.99
Clear(>17)					
1	2.749	0.707	3.89	0.000	3.12
ADT(0-3k)					
1	2.883	0.734	3.93	0.000	2.92
Rail T					
1	-0.551	0.811	-0.68	0.500	3.98
Joint G					
1	1.528	0.650	2.35	0.022	1.76
Interior Web					
1	-1.714	0.533	-3.22	0.002	1.89

## Regression Equation

Mass Loss (g) = 0.5505 Salt-sand + 2.749 Clear(>17)\_1 + 2.883 ADT(0-3k)\_1  
 - 0.551 Rail T\_1 + 1.528 Joint G\_1 - 1.714 Interior Web\_1

## Fits and Diagnostics for Unusual Observations

Obs	Mass Loss (g)	Fit	Resid	StdResid	
31	8.320	2.146	6.174	3.05	R
62	12.680	7.288	5.392	2.55	R
70	0.500	5.573	-5.073	-2.38	R

R Large residual

## APPENDIX 4.2: MINITAB OUTPUT FOR SECOND RUN

## Regression Analysis: Second run, Removal of Rail Type

Method

Categorical predictor coding (1, 0)

Forward Selection of Terms

Candidate terms: Salt-sand, Brine, Granular, Age(0-19), Age(20-39), Age(40-50), Clear(<16), Clear(16-17), Clear(>17), ADT(0-3k), ADT(>3k-4k), ADT(>4k), Joint G, Joint F, Joint P, Traffic Type, Exterior Flange, Exterior Web, Interior Flange, Interior Web

-----Step 1-----			-----Step 2-----		-----Step 3-----	
	Coef	P	Coef	P	Coef	P
Salt-sand	0.6650	0.000	0.6650	0.000	0.4807	0.000
Granular			0.624	0.000	0.481	0.000
Age(20-39)					2.172	0.000
Interior Web						
ADT(>4k)						
S		3.02933		2.62983		2.39803
R-sq		55.23%		66.74%		72.75%
R-sq(adj)		54.59%		65.78%		71.54%
R-sq(pred)		53.68%		64.61%		70.20%
-----Step 4-----			-----Step 5-----			
	Coef	P	Coef	P		
Salt-sand	0.5973	0.000	0.6122	0.000		
Granular	0.642	0.000	0.742	0.000		
Age(20-39)	2.221	0.000	2.460	0.000		
Interior Web	-1.590	0.005	-1.532	0.006		
ADT(>4k)			-0.987	0.061		
S		2.27850		2.23512		
R-sq		75.76%		77.02%		
R-sq(adj)		74.31%		75.28%		
R-sq(pred)		72.68%		73.46%		

 $\alpha$  to enter = 0.2

## APPENDIX 4.2: (CONTINUED)

## Analysis of Variance

Source	DF	Adj SS	AdjMS	F-Value	P-Value
Regression	5	1105.13	221.025	44.24	0.000
Salt-sand	1	293.12	293.119	58.67	0.000
Granular	1	146.82	146.824	29.39	0.000
Age(20-39)	1	104.39	104.394	20.90	0.000
ADT(>4k)	1	18.12	18.117	3.63	0.061
Interior Web	1	39.98	39.983	8.00	0.006
Error	66	329.72	4.996		
Lack-of-Fit	44	232.43	5.283	1.19	0.333
Pure Error	22	97.29	4.422		
Total	71	1434.85			

## Model Summary

S	R-sq	R-sq(adj)	R-sq(pred)
2.23512	77.02%	75.28%	73.46%

## Coefficients

Term	Coef	SECoef	T-Value	P-Value	VIF
Salt-sand	0.6122	0.0799	7.66	0.000	2.29
Granular	0.742	0.137	5.42	0.000	1.59
Age(20-39)					
1	2.460	0.538	4.57	0.000	1.91
ADT(>4k)					
1	-0.987	0.519	-1.90	0.061	1.56
Interior Web					
1	-1.532	0.541	-2.83	0.006	1.88

## Regression Equation

Mass Loss (g) = 0.6122 Salt-sand + 0.742 Granular + 2.460 Age(20-39)\_1  
 - 0.987 ADT(>4k)\_1 - 1.532 Interior Web\_1

## Fits and Diagnostics for Unusual Observations

Obs	Mass Loss (g)	Fit	ResidStdResid	
28	7.740	2.956	4.784	2.22 R
31	8.320	1.435	6.885	3.20 R
62	12.680	7.358	5.322	2.47 R
70	0.500	5.826	-5.326	-2.46 R

R Large residual

## APPENDIX 5.1: CONCRETE MIX-DESIGN

Concrete Mix Proportion According to ACI 211

(Tables reproduced from “Concrete” 2<sup>nd</sup> Edition by Mindes, Young, Darwin)

Mix-Design requirements:

From ASTM G109-07:

Water to cement ratio: < 0.5

Slump: 2”

Typical deck mix:

Water to cement ratio: ~0.49

Air content: 6%

Material properties used:

Fineness modulus of sand: 2.4

Specific gravity of coarse aggregate: 2.79

Specific gravity of fine aggregate: 2.6

Specific gravity of cement: 3.5

Max aggregate size: #78, 0.5”

Bulk density: 109lb/ft<sup>3</sup>

Using Table 10.2, for Air-Entrained concrete, 3-4” slump, and max aggregate size of 0.5”

$$\text{Amount of water} = 325 \frac{\text{lb}}{\text{yd}^3}$$

Using Table 10.3, Air-Entrained, ~4,000 psi compressive strength

Water to cement ratio = 0.48

$$\text{Amount of cement} = \frac{325}{0.48} = 677 \frac{\text{lb}}{\text{yd}^3}$$

## APPENDIX 5.1: (CONTINUED)

Using Table 10.8, for fineness modulus of sand = 2.4, max aggregate size = 0.5”

$$\text{Amount of coarse aggregate} = 0.59 \frac{yd^3}{yd^3}$$

$$0.59(27 \frac{yd^3}{yd^3})(109 \frac{lb}{ft^3}) = 1,736 \frac{lb}{yd^3}$$

Calculation of fine aggregate: (one cubic yard of concrete)

$$\text{Volume of FA} = 27 - \left[ \frac{325}{62.4} + \frac{677}{3.5 * 62.4} + \frac{1736}{2.79 * 62.4} + 27 * 0.06 \right]$$

$$\text{Volume of FA} = 7.1 \text{ ft}^3$$

$$\text{Amount of FA} = 7.1 * 2.6 * 62.4 = 1152 \frac{lb}{yd^3}$$

Concrete Mix:            Water = 325 lb

                                 Cement = 277 lb

                                 Coarse Aggregate = 1,736 lb

                                 Fine Aggregate = 1,152 lb

Air-Entrained: MB-AE90

Trial amount to achieve 6% on 0.35 ft<sup>3</sup> of concrete = 6 mL

Estimated for one cubic yard = 463 mL

## APPENDIX 5.2: CALCULATIONS OF APPLICATION RATE FOR REINFORCED CONCRETE TEST

Calculation of Application Rate for Cyclic Test:

NCDOT Practices:

Brine: (23% Concentration) at 35 gallon per lane-mile

Granular: 150 lb per lane-mile

Salt-sand: 150 lb per lane-mile (75 lb salt, 75 lb sand)

Sample Area: 3"x6"=18 in<sup>2</sup>

Snow Depth: 0.31"

Assume Lane Width: 12 ft

$$(One\ lane * mile) \left( \frac{5,280 ft}{mile} \right) \left( \frac{12 ft}{lane} \right) = 63,360 ft^2$$

$$63,360 ft^2 \left( \frac{144 in^2}{ft^2} \right) = 9,123,840 in^2$$

Brine:

$$35 gallons \left( \frac{3,785.41 mL}{gallon} \right) \left( \frac{18 in^2}{9,123,840 in^2} \right) = 0.261 mL$$

Granular:

$$150 lb \left( \frac{453.592 g}{lb} \right) \left( \frac{18 in^2}{9,123,840 in^2} \right) = 0.134 g$$

Salt-sand:

$$\left( \frac{1}{2} \right) (0.134) = 0.067 g$$

Snow:

$$0.31" (3") (6") = 5.58 in^3 \left( \frac{16.387 mL}{in^3} \right) = 91.4 mL$$

3x Scale:

Brine: 3(0.261) = 0.78mL

Granular: 3(0.134) = 0.402g

Salt-sand: 3(0.067) = 0.201g

## APPENDIX 5.3: RCT RESULTS FOR CONCRETE SPECIMENS

C2: 3% Ponding						
Depth (in)	mV(1)	mV(2)	mV(3)	Cl % (1)	Cl % (2)	Cl % (3)
0.2	3.01	2.05	3.95	0.394	0.411	0.378
0.4	11.9	10.59	11.98	0.267	0.283	0.267
0.6	24.61	22.86	23.55	0.154	0.166	0.161
0.8	43.22	45.06	45.03	0.068	0.063	0.063
1	50.73	51.13	49.85	0.049	0.049	0.051

C1: Snow Control						
Depth (in)	mV(1)	mV(2)	mV(3)	Cl % (1)	Cl % (2)	Cl % (3)
0.2	na	na	na	na	na	na
0.4	53.84	49.09	na	0.043	0.053	na
0.6	53.02	56.68	53.33	0.045	0.038	0.044
0.8	56.36	55.81	59.12	0.039	0.040	0.034
1	59.88	58.95	54.3	0.033	0.035	0.042

C3: Snow Control						
Depth (in)	mV(1)	mV(2)	mV(3)	Cl % (1)	Cl % (2)	Cl % (3)
0.2	45.46	45.43	na	0.064	0.064	na
0.4	53.07	49.85	48.24	0.046	0.053	0.057
0.6	57.85	59.1	55.41	0.037	0.035	0.042
0.8	55.36	54.68	56.27	0.042	0.043	0.040
1	53.91	57.83	54.82	0.044	0.037	0.043



## APPENDIX 5.3: (CONTINUED)

B1: Brine						
Depth (in)	mV(1)	mV(2)	mV(3)	Cl % (1)	Cl % (2)	Cl % (3)
0.2	7.57	8.34	6.51	0.331	0.320	0.347
0.4	15.98	17.91	15.75	0.230	0.211	0.232
0.6	35.76	35.14	35.22	0.097	0.100	0.100
0.8	56.19	56.48	58.24	0.040	0.040	0.037
1	52.18	58.81	56.8	0.048	0.036	0.039

B2: Brine						
Depth (in)	mV(1)	mV(2)	mV(3)	Cl % (1)	Cl % (2)	Cl % (3)
0.2	7.19	7.71	na	0.328	0.321	na
0.4	14.3	14.05	15.72	0.247	0.250	0.233
0.6	33.76	34.64	33.04	0.106	0.102	0.110
0.8	51.72	47.49	47.52	0.049	0.059	0.059
1	50.3	51.6	52.12	0.052	0.049	0.048

B3: Brine						
Depth (in)	mV(1)	mV(2)	mV(3)	Cl % (1)	Cl % (2)	Cl % (3)
0.2	6.7	7.74	na	0.335	0.321	na
0.4	16.55	15.84	16.52	0.218	0.225	0.219
0.6	36.01	35.66	34.74	0.094	0.095	0.099
0.8	56.27	55.46	56.21	0.039	0.040	0.039
1	61.78	57.45	60.5	0.031	0.037	0.032

## APPENDIX 5.3: (CONTINUED)

G1: Granular						
Depth (in)	mV(1)	mV(2)	mV(3)	Cl % (1)	Cl % (2)	Cl % (3)
0.2	6.13	7.16	na	0.344	0.329	na
0.4	16.96	15.97	17.34	0.220	0.230	0.217
0.6	30.81	30.25	30.76	0.121	0.124	0.121
0.8	49.24	44.81	46.64	0.054	0.066	0.061
1	54.73	50.78	55.55	0.043	0.051	0.041

G2: Granular						
Depth (in)	mV(1)	mV(2)	mV(3)	Cl % (1)	Cl % (2)	Cl % (3)
0.2	na	na	na	na	na	na
0.4	16.27	16.88	16.74	0.221	0.215	0.217
0.6	30.41	29.69	27.66	0.120	0.123	0.135
0.8	50.45	52.46	50.89	0.050	0.046	0.049
1	57.27	54.89	55.64	0.037	0.041	0.040

G3: Granular						
Depth (in)	mV(1)	mV(2)	mV(3)	Cl % (1)	Cl % (2)	Cl % (3)
0.2	6.54	6.51	na	0.346	0.347	na
0.4	14.96	13.1	14.92	0.240	0.261	0.241
0.6	35.15	36.29	35.88	0.100	0.095	0.097
0.8	53.18	53.07	51.77	0.046	0.046	0.049
1	56.41	54.94	56.31	0.040	0.042	0.040

## APPENDIX 5.3: (CONTINUED)

S1: Sand-mix						
Depth (in)	mV(1)	mV(2)	mV(3)	Cl % (1)	Cl % (2)	Cl % (3)
0.2	9.68	10.35	10.22	0.295	0.286	0.288
0.4	18.13	17.41	19.22	0.204	0.210	0.195
0.6	40.09	41.23	40.29	0.078	0.075	0.078
0.8	56.13	55.3	56.17	0.039	0.040	0.039
1	59.15	56.38	59.46	0.034	0.039	0.034

S2: Sand-mix						
Depth (in)	mV(1)	mV(2)	mV(3)	Cl % (1)	Cl % (2)	Cl % (3)
0.2	10.58	9.64	na	0.283	0.295	na
0.4	18.68	19.36	19.67	0.205	0.199	0.196
0.6	43.52	40.04	34.61	0.070	0.081	0.102
0.8	51.82	53.64	54.63	0.049	0.045	0.043
1	55.64	54.8	54.82	0.041	0.043	0.043

S3: Sand-mix						
Depth (in)	mV(1)	mV(2)	mV(3)	Cl % (1)	Cl % (2)	Cl % (3)
0.2	9.44	10.69	9.81	0.305	0.289	0.300
0.4	18.98	19.25	16.6	0.202	0.200	0.224
0.6	35.85	33.76	31.67	0.097	0.106	0.116
0.8	49.02	47.83	43.97	0.055	0.058	0.068
1	46.34	45.26	48.71	0.062	0.065	0.056